THEORETICAL STUDIES OF UT-3 THERMOCHEMICAL HYDROGEN PRODUCTION CYCLE AND DEVELOPMENT OF CALCIUM OXIDE REACTANT FOR UT-3 CYCLE AND CARBON DIOXIDE CAPTURE

By

MAN SU LEE

A DISSERTATION PRESENTED TO THE GRADUATE SCHOOL
OF THE UNIVERSITY OF FLORIDA IN PARTIAL FULFILLMENT
OF THE REQUIREMENTS FOR THE DEGREE OF
DOCTOR OF PHILOSOPHY

UNIVERSITY OF FLORIDA

2008

To my loving wife, Sam Jung; daughter Alicia, and my parents

ACKNOWLEDGMENTS

I would like to sincerely thank my advisor, Dr. D. Yogi Goswami for all the advice and guidance he has always so generously provided. He has been a great mentor and teacher. I also express appreciation to my committee, Dr. Skip Ingley, Dr. William Lear, Dr. S. A. Sherif, and Dr. Samim Anghaie for their advice and support for the progress of my research.

I would like to thank all the former members and colleagues of the Solar Energy and Energy Conversion Laboratory at University of Florida for their assistance and friendship. Specially, I thank Dr. Deepak Deshpande, Dr. Sanjay Vijayaraghavan and Dr. Nikhil Kothurkar for their valuable advice and effort. I have great appreciation for Chuck Garretson for his practical and critical support to help me pursue my experimental research in the laboratory. Also I would like to thank Dr. Elias K. Stefanakos and all the staff members (specially Barbara Graham, Ginny Cosmides, Dr. Sesha Srinivasan and Dr. Nikolai Kislov) and also appreciate the friendship and cooperation of Mohammad Abutayeh, Huijaun Chen, Omatoyo Kofi Dalrymple, Gokeman Demirkaya, John Feddock, Ricardo Vasquez-Padillo, Paula Algarin-Amaris, Sam Wiejewardane, Drupatie Latchman and Jonathan Mbah in the Clean Energy Research Center at the University of South Florida. I would like to thank Dr. Anghaie and all the staff in INSPI for the use of their facilities and friendly assistance. I also thank all the staff at PERC in UF and NNRC in USF who helped and trained me to use their equipments. I would also like to acknowledge the US Department of Energy for funding my researches on hydrogen production and carbon dioxide capture.

I thank my parents, brother and sister for their constant encouragement and support from South Korea. Lastly, above all I thank my wife, Sam Jung Yang and would like to acknowledge that this doctoral degree would not be possible without her love and support.

TABLE OF CONTENTS

page

LIST OF TABLES

LIST OF FIGURES

LIST OF ABBREVIATIONS

a	activity
E	equilibrium potential or voltage (V)
F	Faraday constant (96, 500 C mol^{-1})
ΔG	change of Gibbs free energy (kJ/mol)
H	enthalpy (kJ/mol)
ΔH	change of enthalpy change (kJ/mol)
HHV	Higher Heating Value (kJ/mol)
HTGR	High Temperature Gas-cooled Reactor
IGCC	Integrated Gasification Combined Cycle
LHV	Lower Heating Value (kJ/mol)
M	molecular weight
n	moles of electrons
N	number of cycle
P	pressure (atm)
R	mole fraction
ΔS	change of entropy change (kJ/mol·K)
SMR	Steam Methane Reforming
T	Temperature (K or °C)
ΔT_{min}	minimum approach temperature
W	weight of sample
W_o	weight of unreacted sample
X	conversion

Subscripts:

a	anode
c	cathode
in	input

Abstract of Dissertation Presented to the Graduate School
of the University of Florida in Partial Fulfillment of the
Requirements for the Degree of Doctor of Philosophy

THEORETICAL STUDIES OF UT-3 THERMOCHEMICAL HYDROGEN PRODUCTION CYCLE AND DEVELOPMENT OF CALCIUM OXIDE REACTANT FOR UT-3 CYCLE AND CARBON DIOXIDE CAPTURE

By

Man Su Lee

August 2008

Chair: D. Yogi Goswami
Major: Mechanical Engineering

Hydrogen can be a viable alternative energy carrier if it can be produced cost effectively from renewable resources. UT-3 thermochemical cycle to produce hydrogen from water is attractive because its temperature requirement is moderate (~700°C) and it can be operated with solar or nuclear energy. There are still several issues that must be resolved before it becomes viable. These issues include developing high reactive surface area solid reactant structures which are able to go through large volume changes in a cycle while maintaining cyclic reactivity and strength of the solid reactants and speeding up of the hydrolysis reaction of calcium bromide, the rate limiting step in the cycle.

In this study, thermodynamic feasibility investigation of the UT-3 process was conducted to determine the optimal operating conditions for high reaction rate as well as high conversion. A new calcium oxide reactant dispersed and immobilized on a yttria fabric was fabricated via an inexpensive and straightforward immobilization process. The performance of the sample was evaluated in cyclic bromination and hydrolysis reactions experimentally using the optimum conditions determined theoretically. The calcium oxide fabric showed continuous higher reactivity in four bromination reactions and the rate of hydrolysis reaction was faster than that of

our calcium oxide pellets and comparable to that of calcium oxide pellets reported in the literature. The thermodynamic efficiency of the UT-3 cycle was estimated considering inert materials and incomplete conversion and heat recovery. It was found that the effects of inert materials and heat recovery on the efficiency were considerable while the influence of incomplete conversion was not significant. With heat recovery, the calculated efficiency for the calcium oxide fabric including inert materials and incomplete conversion was 52.4%.

The use of calcium oxide on fabric was also studied for its application to high temperature carbon dioxide capture. The conventional calcium oxide absorbents could not maintained their performance in cyclic operations due to the reduction of active surface area. On the other hand, the new calcium oxide absorbent on fibrous alumina achieved continuous cyclic carbonation conversion over ten carbonation-calcination cycles under mild calcination condition. However, under the more severe calcination condition, its performance dropped by about eight percent after 12 cycles possibly due to the formation of $Ca_{12}Al_{14}O_{33}$ by the reaction between calcium oxide and alumina. When calcium oxide was applied to yttria fabric, the absorbent maintained its performance for 12 cycles even under the severe calcination condition.

CHAPTER 1
INTRODUCTION

1.1 Hydrogen Facts

Hydrogen is the lightest gas and also the simplest element ever known. It is colorless, odorless, non-toxic and non-corrosive. Hydrogen is considered as a promising energy carrier because it is the most abundant element on earth and can be produced and used without or with little generation of pollution. However, hydrogen must be extracted from water or fossil fuels such as coal, natural gas and petroleum, since hydrogen is not available freely in nature. Hydrogen also represents a promising energy storage means for renewable energy sources which are intermittent (solar radiation and wind) or may not be convenient for some applications (biomass).

Presently about 9 million tons of hydrogen is produced per year in the United States and it is mostly used for chemical industries such as fertilizer and petrochemical industries. About 150 million tons of hydrogen would be needed for fuel-cell vehicles annually by 2040, considering a transition from petroleum to hydrogen as a fuel for transportation (Argonne National Laboratory, 2003).

1.2 Motivation

For hydrogen alternative to become feasible, cost effective and pollution free methods to produce hydrogen must be developed. Currently, there are a number of methods of producing hydrogen which are available commercially or are under research. The processes currently available commercially are steam methane reformation (SMR), water electrolysis, partial oxidation of heavy hydrocarbons (POX) and coal gasification. Additional methods being investigated at the laboratory level include thermochemical cycles, biomass gasification, photoelectrical, photochemical and biological processes. Regardless of the maturity of the

technologies, they all fall under two basic categories: 1. Hydrogen production from carbon based fuels such as fossil fuels. 2. Hydrogen production by splitting water. The second category is more attractive in a long term prospective because it is clean and renewable.

A thermochemical cycle is a clean and efficient hydrogen production method because it splits water into hydrogen and oxygen using heat as the energy source. Among the several hundred thermochemical cycles proposed so far, UT-3 cycle was selected for this study considering its strengths described in the section 3.2.

1.2.1 Issues Concerning the UT-3 Cycle

In order to make the UT-3 cycle practically feasible, there are still several barriers and issues to be investigated and solved, as described below.

1.2.1.1 Preparations of solid reactants

UT-3 cycle is comprised of four heterogeneous reactions. In order to simplify the product separation in the cyclic system and operate the process continuously, the solid reactants and products should remain in the reactors while the gaseous reactants and products move from one reactor to the next. Accelerating the reaction rate, and increasing cyclic life time and durability of the solid reactants are important keys for making the cycle practical. Preparation of the solid reactants with inert structural materials has been introduced and developed (Aihara et al., 1990 and 1992; Amir et al., 1993; Sakurai et al., 1995 and 2006), but the preparation procedures seem rather complicated and expensive and the practicality of the pellet-type reactant is still in doubt. Lemort et al. (2006) also suggested the possibility of decomposition of the inert material, calcium titanate ($CaTiO_3$), in the pellets by HBr.

1.2.1.2 Slow reaction rate

In order to improve the process efficiency, the hydrolysis reaction of hydrogen bromide, which is the slowest and rate limiting step among the four reactions in the cycle, must be

accelerated. The reaction rate can be enhanced by increasing the reaction temperature since the reaction is endothermic. However, the reaction temperature is limited because of the melting point of calcium bromine. The conversion with excess steam and at lower pressures is expected to be higher according to the Le Chatelier's principle. Therefore, optimal process conditions for the hydrolysis reaction must be determined to speed up the reaction rate. The reaction rate may be also enhanced by providing a large surface area between the gas and solid reactant particles with the elimination of diffusion resistances.

1.2.1.3 Volume changes of solid reactants

The hydrolysis reaction of calcium bromide is the kinetically slowest reaction in the UT-3 cycle. Besides, it was found that about 76 percent increase in the molar volume of the solid reactants (Simpson et al., 2007) from calcium oxide to calcium bromide during the bromination reaction, accounted for a significant decrease of porosity of the pellets (Aihara et al., 1990; Lee et al., 2006). This reduction leads to low reactivity and degradation of the pellets. So, in order to overcome these disadvantages, development of a durable porous reactant that maintains cyclic reactivity as well as has an enduring structure in cyclic transformations is required.

1.2.1.4 Separation technology

The difficulty of separation of hydrogen and oxygen from the process stream is one of the major factors affecting the efficiency of the process. In the adiabatic UT-3 cycle, excess steam is used as a heat carrier (Sakurai et al., 1996a) and it was proved that the additional steam improved the hydrolysis process.

Hydrogen and oxygen are produced as mixed with highly corrosive components such as Br_2 and HBr as well as steam at very high temperatures in the process. If hydrogen and oxygen are separated from other gaseous products by a conventional condensation method, it will result in severe energy loss. According to Teo et al. (2005), UT-3 cycle is economically feasible only if

high temperature separation technology is realized without the unwanted energy loss. For that reason, ceramic membranes that have corrosion resistance at high temperatures and other corrosive conditions have been investigated (Ohya et al., 1994; Morooka et al., 1996; Ohya et al., 1997). Separation by membrane is not efficient if the concentrations of hydrogen and oxygen in the stream are low. In order to increase the separation efficiency, either high pressure or high surface area of the membrane is required (T-Raissi, 2005). However, high operating pressure has an adverse effect on the hydrogen yield and increasing the surface area of the membrane is costly.

1.3 Objectives of Present Study

1.3.1 Thermodynamic Approach

First of all, comprehensive theoretical feasibility of each reaction in the UT-3 cycle will be investigated and optimal operating conditions for high conversion and reaction rate will be determined via a thermodynamic analysis. Thermal efficiency of the UT-3 cycle will be evaluated at the optimum conditions.

1.3.2 Improving Performance of Solid Reactants

The life-time of the solid reactants is the most important factor for commercialization of the UT-3 cycle as mentioned earlier. In order to make the cycle practical and cost-effective, the solid reactants must be chemically reactive and physically stable in cyclic operation and the reaction rates must be accelerated. A goal of this research is to develop a calcium oxide reactant with more favorable characteristics such as continuous high cyclic reactivity, high reaction rates and simple reactant preparation step.

1.3.3 Evaluation of Thermal Efficiency

Thermal efficiency of the UT-3 cycle has been evaluated by several authors. But the inert materials in the solid reactants, incomplete conversion and heat recovery were not considered as a major factor in the calculations so far. These factors would have an important effect upon the

efficiency as well as the operational costs since the solid reactants contain considerable amounts of inert materials and the conversions were found to be incomplete through the experiments. In this study, a practical thermodynamic efficiency with and without heat recovery, inclusion of inert materials, and with incomplete conversion will be evaluated at the optimum conditions obtained by theoretical studies, to improve the process performance and reduce the uncertainties.

1.3.4 Calcium Oxide Absorbent for High Temperature Carbon Dioixde Capture

Calcium oxide, an important reactant in the UT-3 cycle, is also a well-known absorbent of carbon dioxide (CO_2), a major greenhouse gas. Carbon dioxide reacts with calcium oxide to form calcium carbonate in the carbonation reaction and the calcium oxide is regenerated and pure carbon dioxide can be obtained through the calcination reaction. However, degradation of its performance due to the loss in active surface area, pore plugging and sintering of the particles must be overcome or minimized for the calcium oxide absorbent to be practical. In this study, the calcium oxide immobilized on a fibrous ceramic fabric for the UT-3 cycle was introduced to enhance the cyclic performance of high temperature carbon dioxide capture. The characteristics and cyclic performance of the proposed immobilized calcium oxide on the fabric were examined and compared with the previous results in the literature.

CHAPTER 2
HYDROGEN PRODUCTION METHODS

2.1 Hydrogen Production from Fossil Fuels

Most of the hydrogen consumed presently in our world is produced from fossil fuels since it is currently the most economical and efficient way. However, fossil fuel resources are limited. Therefore these methods will lose their cost competitiveness in the long run. Additionally, they cause environmental pollution.

2.1.1 Steam Methane Reformation (SMR)

Steam methane reformation (SMR), sometimes referred to as steam reforming of natural gas, is the most commercialized way to produce hydrogen since it is the least expensive means at present. Today, about 95% of the hydrogen produced in the U.S. is made through SMR (U. S. DOE, 2002). Basic SMR process is composed of two chemical reactions involving methane, water, and a catalyst along with heat supply (Casper, 1978), as shown below:.

Reformation of Methane

$$CH_4 + H_2O + heat \longleftrightarrow CO + 3H_2 \qquad (2\text{-}1)$$

Water-Gas Shift reaction

$$CO + H_2O \longleftrightarrow CO_2 + H_2 + heat \qquad (2\text{-}2)$$

Mixture of methane and steam at high temperature (1000K~1300K) is catalytically converted into carbon monoxide and hydrogen at the first step (steam reforming reaction (2-1)). The product gases are then reacted on a packed bed of catalyst to produce carbon dioxide and more hydrogen by the water-gas shift reaction (2-2). Approximately 71-75 mol % hydrogen with other gases such as carbon dioxide, carbon monoxide, and methane is obtained through these two steps. This mixture is purified by condensation and pressure swing adsorption at high purity level.

Overall energy and exergy efficiencies of the SMR process that produces 97 wt % hydrogen were determined to be about 86% and 78%, respectively (Rosen, 1996).

A simplified schematic for SMR using natural gas as a methane source is outlined in Figure 2-1.

More than 80% of the hydrogen used around the world is currently produced by SMR (National Research Council and National Academy of Engineering, 2004). The cost of hydrogen production from the SMR process strongly depends on the cost of natural gas, a major methane source (Goel et al., 2003). Moreover, generation of carbon dioxide and release of methane during conversion are inevitable. In order to reduce the emission of CO_2, the CO_2 could be sequestered with about 25-30% additional capital and operational costs (Goel et al., 2003).

2.1.2 Partial Oxidation of Hydrocarbons (POX)

Partial oxidation (POX) is analogous to SMR while the addition of a partial oxidation reaction of hydrocarbons. Therefore, the POX process includes three steps shown below (Goel et al., 2003).

Partial Oxidation of Hydrocarbon

$$C_nH_m + nO_2 \longleftrightarrow nCO + \frac{m}{2}H_2 + heat \tag{2-3}$$

Reformation of Hydrocarbon

$$C_nH_m + nH_2O + heat \longleftrightarrow nCO + \left(\frac{2n+m}{2}\right)H_2 \tag{2-4}$$

Water-Gas Shift reaction

$$CO + H_2O \longleftrightarrow CO_2 + H_2 + heat \tag{2-5}$$

Hydrocarbons are partially burned with less than the stoichiometric amount of oxygen and are converted into carbon monoxide and hydrogen in a partial oxidation reaction (2-3) with heat rejection. The remaining hydrocarbons with steam are catalytically converted into carbon

monoxide and hydrogen at the steam reforming step using thermal energy from the partial oxidation.

Air separation units would be needed to avoid NOx which would be generated from the fuel combustion in air. Therefore the hydrogen production cost from POX is higher than that from the SMR process due to this additional capital cost for the separation (Goel et al., 2003).

2.1.3 Coal and Biomass Gasification

Gasification of coal and biomass is considered as one of best methods for hydrogen production because of its environmental performance, high efficiency and abundant resource available.

Coal and biomass gasification for hydrogen production are very similar to partial oxidation except for the operating temperature needed and the types of feedstock. Gasification requires much higher temperature (1100°C -1300°C) and uses various types of solid-based feedstocks such as coal, petroleum coke and biomass rather than liquid or gaseous hydrocarbon.

Primary reactions of coal and biomass gasification for hydrogen production are identical to the reactions, (2-3) ~ (2-5), for POX. Coal gasification was to produce 93% hydrogen with about 59% and 49% of overall energy and exergy efficiencies, respectively (Rosen, 1996).

The synthesis gas, a mixture of carbon monoxide and hydrogen, generated by the reactions, (2-3) and (2-4), can be used to generate electricity through integrated gasification combined cycle (IGCC) or reacted with steam to increase the H_2 yield by water-gas shift reaction (2-5). A schematic diagram of the process to generate both electricity and hydrogen in one gasification-based system is illustrated in Figure 2-2.

In addition to the capital cost reduction and efficiency improvement, research on the coal and biomass gasification is also focused on the development of carbon dioxide capture and

sequestration technologies and the membranes for hydrogen separation from other gases (National Research Council and National Academy of Engineering, 2004).

2.2 Hydrogen Production from Water

In order to make the "hydrogen economy" feasible or at least make hydrogen an attractive energy carrier for some applications, hydrogen must be produced ultimately from water via economical and environment-friendly ways since fossils fuels are limited and generate carbon dioxide.

Hydrogen production from water, however, is still in the research and development stage except water electrolysis while most of hydrogen production technologies from fossil fuels are commercialized today.

2.2.1 Water Electrolysis

Water electrolysis is a developed technology for hydrogen production. However, it has not been used widely because the energy source, electric energy, is expensive. This electrolysis technique may become more viable in the future when electricity is generated from renewable energy.

Hydrogen and oxygen are produced by electrolysis at the cathode and anode, respectively. The two reactions at the cathode and anode are as under (Wendt, 1990):

Cathode: $$2H_2O + 2e^- \longrightarrow H_2 + 2OH^- \quad (2\text{-}6)$$

Anode: $$2OH^- \longrightarrow \frac{1}{2}O_2 + H_2O + 2e^- \quad (2\text{-}7)$$

Overall net reaction is represented as:

Overall: $$H_2O + Energy(Electricity) \longrightarrow H_2 + \frac{1}{2}O_2 \quad (2\text{-}8)$$

The equilibrium potentials at the cathode, E_c, and anode, E_a, at 25°C are described as (Ohta, 1979):

$$E_c = -0.828 - 0.059 \log a_{OH^-} \quad (2\text{-}9)$$

$$E_a = 0.401 - 0.059 \log a_{OH^-} \quad (2\text{-}10)$$

where a is the activity. Using these relations, the lowest electric voltage, E_a-E_c, called the reversible voltage at 25°C is 1.229V. Therefore, the required minimum electrical energy for the water electrolysis is calculated to be 237.18kJ by the following equation:

$$\Delta G = -nFE \quad (2\text{-}11)$$

where n is moles of electrons, F the Faraday constant (96, 500 C mol^{-1}) and E voltage in volts (V).

The changes in total energy and electrical energy demands for the water electrolysis are approximately displayed with temperature in Figure 2-3. The deference between the total energy demand (ΔH) and the minimum electrical energy demand (ΔG) is the required heat energy ($T\Delta S$) for the electrolysis with the minimum electrical energy. As shown in Figure 2-3, the minimum electric energy demand decreases with temperature. Therefore, efficiency of the electrolysis can be improved by increasing the temperature because inexpensive thermal energy can replace a part of the costly electric energy. However, the improvement is limited due to the corrosion problems of the materials and the evaporation of water (Cox and Williamson, 1977). As a result, the development of high temperature electrolysis (solid oxide electrolyzer operated at 700 to 1000°C) is underway to improve the performance by replacing the electric energy with thermal energy (Riis et al., 2006).

Main types of electrolyzers are alkaline, solid polymer (SPE) and solid oxide electrolyzers which are named after the electrolytes. Current research on water electrolysis is focused on cost reduction and performance improvement.

2.2.2 Thermochemical Hydrogen Production

In principle a thermochemical hydrogen production cycle is similar to high temperature thermal cracking in that it requires only water as the raw material and heat as the energy source. The cycle contains a combination of at least two recurring chemical reactions operated while high temperature thermal cracking has one direct decomposition reaction. By this approach, water can be separated into hydrogen and oxygen at comparatively lower temperatures than thermal cracking and in separate steps, while the sum of the reactions results in the decomposition of water.

Thermochemical processes for hydrogen production were suggested in the 1960's to produce hydrogen from water as a more efficient or cheaper method as compared to electrolysis (Funk and Reinstrom, 1966).

The concept can be simply described (Beghi, 1986) as shown in Figure 2-4. Water is supplied with heat into the system which controls a combination of thermochemical reactions. Hydrogen and oxygen are produced separately through the process. All chemicals involved except water, hydrogen and oxygen are recycled in the process.

In view of the fact that a thermochemical process does not create any pollution and may be coupled with thermal energy sources like solar energy, nuclear power or waste heat, it appears to be the most attractive method to produce hydrogen. Some of the thermochemical cycles under study will be discussed later in this chapter.

2.2.3 Photo-biological Hydrogen Production

Photo-biological process for hydrogen production consists of the following two reactions, photosynthesis and hydrogen production (Riis et al., 2006):

Photosynthesis $$2H_2O \longrightarrow 4H^+ + 4e^- + O_2 \quad (2\text{-}12)$$

Hydrogen Production $$4H^+ + 4e^- \longrightarrow 2H_2 \quad (2\text{-}13)$$

The process uses microbes such as green algae and cyanobacteria to promote the reaction in the presence of sunlight and water. Through the natural organic processes, hydrogen and oxygen are produced. A schematic diagram of the photo-biological hydrogen production process is displayed in Figure 2-5.

Photo-biological hydrogen production requires low initial investment and low energy, however, the process is still under development (Goel et al., 2003).

2.3 Thermochemical Cycles for Hydrogen Production

Several hundred thermochemical cycles for hydrogen production have been proposed and approximately eight hundred publications have been released through 1999 (Funk, 2001) since the concept was introduced by Funk and Reinstrom (1964 and 1966). In the following section and chapter, several historically important and commercially potential thermochemical cycles will be discussed.

2.3.1 Ispra Mark Processes

Mark 1 cycle was developed at the Joint Research Center, Ispra based on preliminary studies on the thermochemical hydrogen production performed through thermodynamic calculations. The reactions in the Mark 1 cycle are shown below:

$$CaBr_2 + 2H_2O \xrightarrow{1050K} Ca(OH)_2 + 2HBr \quad (2\text{-}14)$$

$$2HBr + Hg \xrightarrow{450K} HgBr_2 + H_2 \quad (2\text{-}15)$$

$$HgBr_2 + Ca(OH)_2 \xrightarrow{450K} CaBr_2 + HgO + H_2O \quad (2\text{-}16)$$

$$HgO \xrightarrow{900K} Hg + \frac{1}{2}O_2 \quad (2\text{-}17)$$

Both experimental kinetics studies of the reactions in Mark 1 and corrosion tests for material selections were carried out thoroughly and the results showed that the cycle was feasible. However research on this process was abandoned because of mercury use in the process. Subsequently, Mark 2, 3 and 6 cycles without mercury were introduced and evaluated, but it was found that they were not promising (Beghi, 1986).

During early 1970s, Mark 7, 9, 14 and 15 cycles involving iron and chlorine were developed. Among them, Mark 15 cycle shown below was extensively studied and evaluated in detail.

Mark 15 cycle

$$3FeCl_2 + 4H_2O \xrightarrow{923-973K} Fe_3O_4 + 6HCl + H_2 \quad (2\text{-}18)$$

$$Fe_3O_4 + 8HCl \xrightarrow{473-573K} FeCl_2 + 2FeCl_3 + 4H_2O \quad (2\text{-}19)$$

$$2FeCl_3 \xrightarrow{553-593K} 2FeCl_2 + Cl_2 \quad (2\text{-}20)$$

$$Cl_2 + H_2O \xrightarrow{873-973K} 2HCl + \frac{1}{2}O_2 \quad (2\text{-}21)$$

Through comprehensive experiments and analyses, the cycle was proved to be feasible while the calculated thermal efficiency was somewhat low, about 20%, and highly corrosive chlorine was considered to be a problem. Nevertheless, research on the Mark 15 process was stopped since technical problems on the scale-up of the hydrolysis reaction of ferrous chloride ($FeCl_2$) and chemically unfavorable thermal decomposition of ferric chloride ($FeCl_3$) were not solved (Beghi, 1986).

Sulfur based cycles for hydrogen production such as Mark 11, 13, and 16 were also widely investigated at the Joint Research Center.

The Mark 11 cycle shown below includes an electrochemical reaction for the production of sulfuric acid (Brecher et al., 1977)

Mark 11 cycle

$$H_2SO_4 \xrightarrow{1123K} H_2O + SO_2 + \frac{1}{2}O_2 \quad (2\text{-}22)$$

$$SO_2 + 2H_2O \xrightarrow{353-393K} H_2SO_4 + H_2 \quad \text{(Electrochemical step)} \quad (2\text{-}23)$$

This two-step hybrid sulfur process is also known as the Westinghouse sulfur cycle and GA-22. The cycle was successfully operated at a bench scale and a pilot scale by Westinghouse Electric Corporation and Joint Research Center, respectively (Brown et al., 2003). The calculated overall process efficiency was about 41% (Beghi, 1986). However, in order to make the cycle practical, scale-up problems on the electrochemical process still need to be solved (Brown et al., 2003).

A variation of the above cycle is Mark 13 (Velzen et al., 1980) which is given below:

$$H_2SO_4 \xrightarrow{1000-1100K} H_2O + SO_2 + \frac{1}{2}O_2 \quad (2\text{-}24)$$

$$2H_2O + Br_2 + SO_2 \xrightarrow{320-370K} H_2SO_4 + 2HBr \quad (2\text{-}25)$$

$$2HBr \xrightarrow{350K} H_2 + Br_2 \quad \text{(Electrochemical step)} \quad (2\text{-}26)$$

The process was proposed by Schültz and Fiebelmann in 1974 and experimental studies including bench-scale operation were successfully conducted by the Joint Research Center and the overall process efficiency was estimated to be about 39% (Beghi, 1986). The overall efficiency of the Mark 13-V2 process coupled with a central solar receiver system was about 21% (Bilgen and Joels, 1985). However, it was found that this hybrid cycle also had scale-up problems on the electrode system engaged in thin membranes (Brown et al., 2003).

Mark 16 cycle uses iodine instead of bromine in the Mark 14 cycle. This cycle is also known as Sulfur-Iodine or Iodine-Sulfur cycle (IS cycle) which was investigated at the General Atomic (GA) Corp. The detailed history of the IS cycle will be discussed in the next section.

2.3.2 Iodine-Sulfur (IS) Cycle

Unlike other sulfur family cycles such as Mark 11 and 13, IS cycle does not require electricity for the reactions shown below.

$$H_2SO_4 \xrightarrow{1123K} H_2O + SO_2 + \frac{1}{2}O_2 \qquad (2\text{-}27)$$

$$2H_2O + I_2 + SO_2 \xrightarrow{393K} H_2SO_4 + 2HI \quad \text{(Bunsen Reaction)} \qquad (2\text{-}28)$$

$$2HI \xrightarrow{723K} H_2 + I_2 \qquad (2\text{-}29)$$

The system for the cycle consists of three parts, Bunsen reaction system, H_2SO_4 decomposition system, and HI decomposition system (Figure 2-6) (Ogawa and Nishihara, 2004).

The IS cycle has been studied at the General Atomic (GA) Corp. and Japan Atomic Energy Research Institute (JAERI) since being proposed by GA in the 1970's. At JAERI, High Temperature Gas-cooled Reactor (HTGR) was developed for hydrogen production and the HTGR technology capable providing high temperature heat of around 950°C was attained in 2004 (Onuki et al., 2005). Also, a continuous hydrogen production closed loop test for 20 hours was conducted in 2003 (Ogawa and Nishihara, 2004). The IS cycle and the adiabatic UT-3 cycle (Sakurai et al., 1996) were selected as the two promising cycles by GA for hydrogen generation using nuclear power (Brown et al., 2003).

All reactions of the IS cycle were demonstrated experimentally as well as investigated theoretically and the overall process efficiency was estimated to be high, about 47% (Funk, 2001). However, there are still some challenges to be considered and solved for commercialization. The issues are: 1) difficulty in HI decomposition due to excess steam for

enhancing the Bunsen reaction, 2) material selection for the corrosive chemicals, 3) high temperature of more than 900°C, 4) relatively expensive material, I_2, which accounts for $45M capital cost estimated for 600MW hydrogen production plant and 5) uncertain economics (Onuki et al., 2005; T-Raissi, 2005; Vitart et al., 2008).

2.3.3 ZnO/Zn Cycle

One of the most well-known two-step metal oxide reduction-oxidation (redox) reactions for hydrogen production is solar thermal based ZnO/Zn cycle (Steinfeld, 2002). The ZnO process powered by concentrated solar thermal energy is illustrated in Figure 2-7. As shown in the figure, the process consists of two reactions, a high endothermic thermal decomposition reaction of ZnO and an exothermic hydrolysis reaction of zinc. Since the decomposition of ZnO requires very high temperature, a concentrating solar chemical reactor was specially designed by Haueter et al. (1999) and the experimental tests and developments on the reactor are ongoing.

2.4 Fresh Water Demands for Hydrogen Production

Shortage of fresh water is one of the greatest problems facing the world today. If "hydrogen economy" is realized in the future, it will be on the basis of hydrogen production from water. Only fresh water can be used as the feedstock to produce hydrogen although saline water can be used as the cooling water (Webber, 2007). Thus, desalination of water may be necessary, which is very energy intensive. Water consumption was estimated for hydrogen production by electrolysis and SMR and compared to that for refining petroleum by Webber (Webber, 2007). It was estimated that water electrolysis consumes about 2.38 gallons of fresh water as a feedstock to produce 1kg of hydrogen while SMR requires 1.19 gallons of fresh water as a feedstock and an additional 3.5 gallons of fresh water for excess steam (Spath and Mann, 2001). Webber (2007) estimated that direct water consumption for hydrogen production via electrolysis is comparable to that for refining an equivalent amount of gasoline. Seawater electrolysis was

investigated for the reduction of the fresh water consumption (Bockris, 1975; Williams, 1975; Bennett, 1980), however, corrosion and contamination on the electrodes due to the undesirable gas product, chlorine, and impurities and the release of the chlorine gas must be overcome.

Like water electrolysis, the thermochemical hydrogen production process also uses water as the raw material to produce hydrogen. However, high temperature steam is needed for the thermochemical process instead of liquid water. Thus, fresh water may not be necessary for the thermochemical process since the saline water can be heated to supply pure steam to the process from an additional distiller.

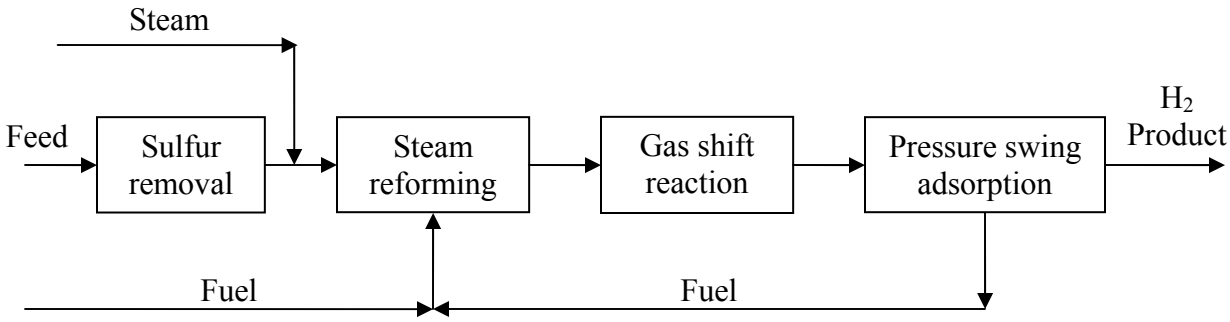

Figure 2-1. Natural gas steam reforming. Adapted from National Research Council and National Academy of Engineering, 2004. *The Hydrogen Economy: Opportunities, Costs, Barriers, and R&D Needs*, The National Academies Press. (Figure G-1, page 199).

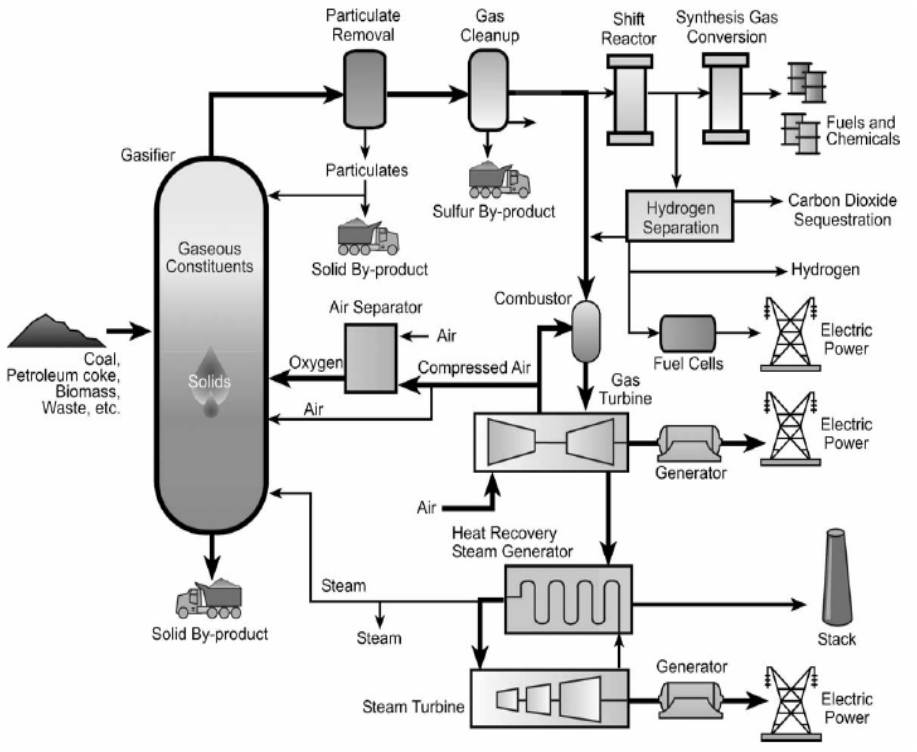

Figure 2-2. Gasification-based energy conversion system. Adapted from Stiegel, G. J., Ramezan, M., 2006. Hydrogen from coal gasification: an economical pathway to a sustainable energy future. International Journal of Coal Geology 65, 173-190 (Figure 2, page 177).

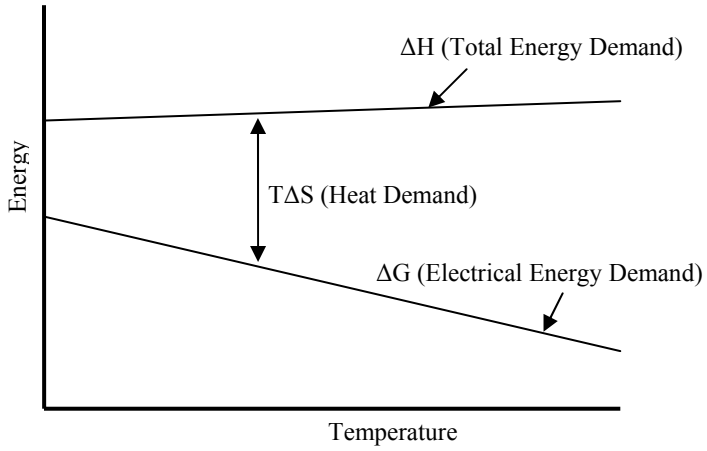

Figure 2-3. Energy demands for water electrolysis. Adapted from Ohta, T., ed., 1979. *Solar-Hydrogen Energy Systems*, Oxford and New York, Pergamon Press.

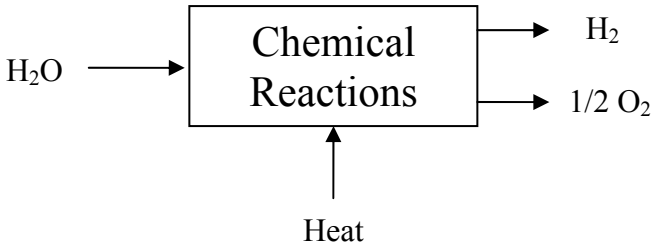

Figure 2-4. Simplified model of thermochemical cycle for hydrogen production

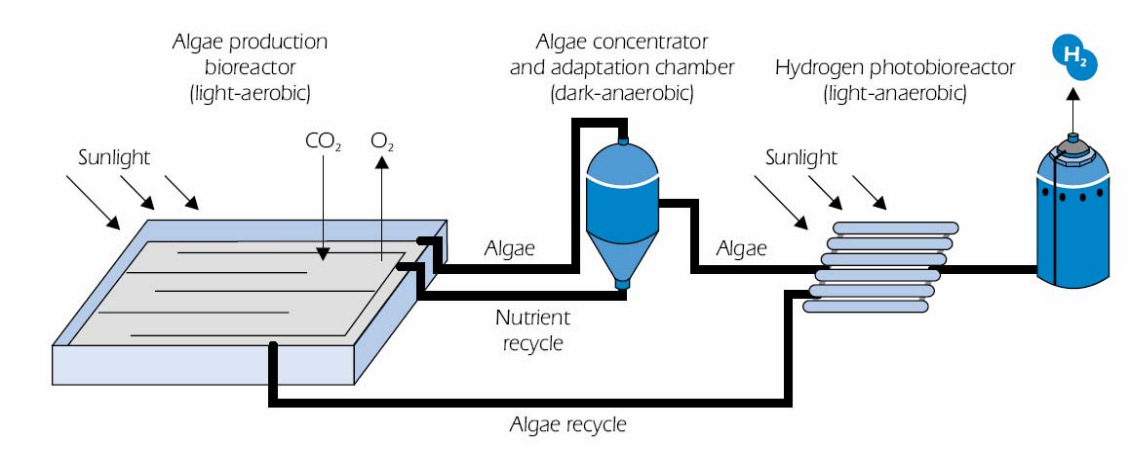

Figure 2-5. Photo-biological hydrogen production. Adapted from Riis, T., Hagen, E. F., Vie, P. J. S., Ulleberg, O., 2006. Hydrogen production R&D: priorities and gaps. International Energy Agency (IEA). (Figure 6, page 13).

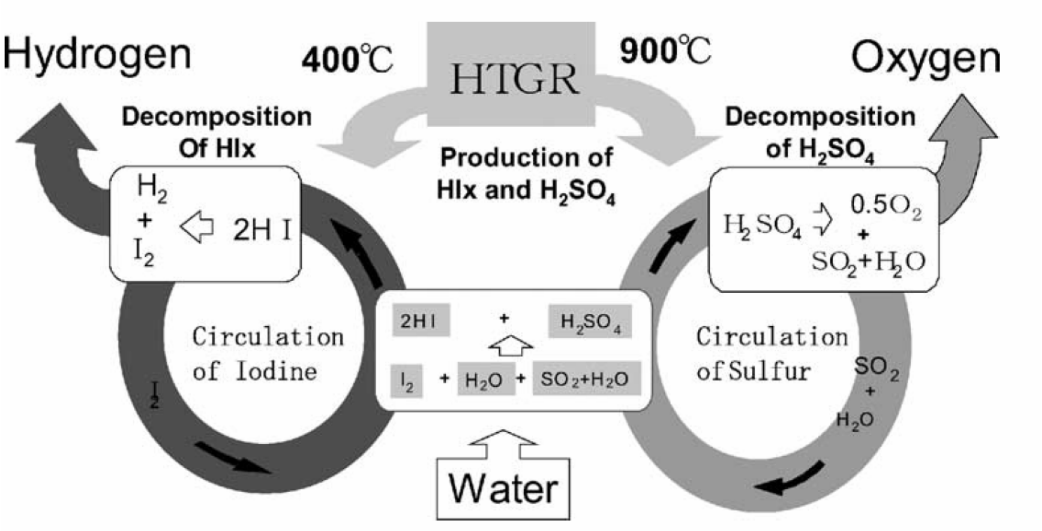

Figure 2-6. The IS thermochemical cycle. Adapted from Ogawa, M., Nishihara, T., 2004. Present status of energy in Japan and HTTR project. Nuclear Engineering and Design 233, 5-10 (Figure 6, page 9).

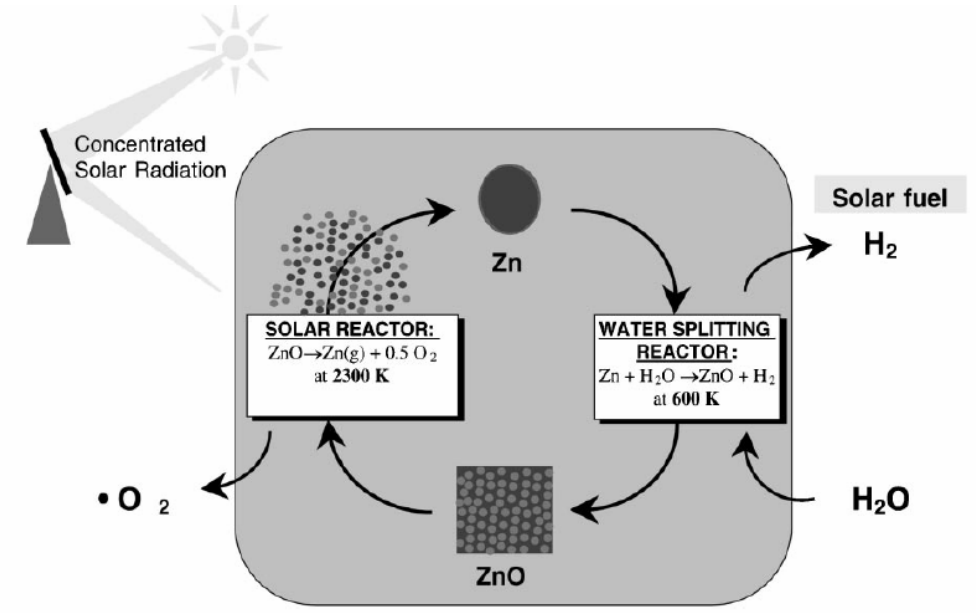

Figure 2-7. The ZnO/Zn cycle for hydrogen production. Adapted from Weidenkaff, A., Reller, A. W., Wokaun, A., Steinfeld, A., 2000. Thermogravimetric analysis of the ZnO/Zn water splitting cycle**.** Thermochimica Acta 359, 69-75 (Figure 1, page 70).

CHAPTER 3
THE UT-3 THERMOCHEMICAL CYCLE FOR HYDROGEN PRODUCTION

UT-3 cycle is one of the very few thermochemical cycles that have been studied, both theoretically and experimentally, since being proposed in 1978 (Kameyama and Yoshida, 1978). This cycle requires a relatively lower maximum temperature, 730°C, than the other cycles. Thus, concentrated solar thermal energy as well as nuclear power can drive the process.

The cycle is comprised of four gas-solid reactions, two of which involve calcium compounds and the remaining two, iron compounds as shown below.

$$CaO(s) + Br_2(g) \xrightarrow{600^\circ C} CaBr_2(s) + \frac{1}{2}O_2(g) \quad (3\text{-}1)$$

$$CaBr_2(s) + H_2O(g) \xrightarrow{730^\circ C} CaO(s) + 2HBr(g) \quad (3\text{-}2)$$

$$Fe_3O_4(s) + 8HBr(g) \xrightarrow{210^\circ C} 3FeBr_2(s) + 4H_2O(g) + Br_2(g) \quad (3\text{-}3)$$

$$3FeBr_2(s) + 4H_2O(g) \xrightarrow{560^\circ C} Fe_3O_4(s) + 6HBr(g) + H_2(g) \quad (3\text{-}4)$$

Each of four reactions occurs in a separate reactor that contains a solid reactant. Solid products produced remain in the reactor for the next reaction which simplifies the separation steps. Only the gaseous reactants and products move through the reactors. Reactions, (3-1) and (3-2), involving calcium compounds, have been extensively investigated since the hydrolysis of calcium bromide, reaction (3-2), is the kinetically slowest reaction and the rate-limiting step (T-Raissi, 2005) as well as the highest-temperature reaction. Moreover, repetitive substantial volume changes of the solid reactants as they cycle between oxide and bromide forms adversely affect the physical stability and chemical reactivity of the solid reactants.

A bench scale plant, named MASCOT (Model Apparatus for the Study of Cyclic Operation in Tokyo), was constructed and operated with continuous hydrogen production during several test runs (Nakayama et al., 1984). Adiabatic UT-3 cycle shown in Figure 3-1 (Sakurai et

al., 1996) was selected together with the IS cycle as one of the two final cycles by General Atomics (GA) Corp. for hydrogen generation using nuclear power (Brown et al., 2003). There are still several technical issues to be resolved even though extensive research on the process has already been done. These issues were outlined in chapter 1.

3.1 Historical Survey of UT-3 Thermochemical Cycle

3.1.1 Studies of UT-3 processes and System

Kameyama and Yoshida (1978) introduced the UT-3 cycle in 1978 based on the Gibbs free energy change as a function of the reaction temperature. Experimental kinetic studies using the apparatus in Figure 3-2 showed very low conversions in the hydrolysis reactions of calcium bromide and iron bromide, (3-2) and (3-4) while bromination reactions of calcium oxide and iron oxide, (3-1) and (3-3) were completed. Separation techniques of oxygen and hydrogen using condensation were mentioned and thermal efficiency of the cycle was estimated to be 36.8% on the basis of the HHV of hydrogen.

A first conceptual plant design of the UT-3 cycle coupled with a high temperature nuclear power plant was suggested by Kameyama and Yoshida (1981). Figure 3-3 describes the conceptual plant design which consists of three parts: a calcium tower, an iron tower and a heat exchanger tower. A honeycomb shaped solid reactant was made with an inert material and packed in a tubular reactor. This approach was chosen to make it easy to select the reactor material since the outside part of the honeycomb would remain in as oxide while the inside part would cycle between the bromide and the oxide forms.

The solid reactant was mixed with inert binding materials to increase its strength. Fe_3O_4 pellets were fabricated by mixing magnetite powder with silicasol, gelling by adding ammonium carbonate, molding, drying and sintering. A kinetic study of bromination of the iron oxide pellets was conducted, and a simulation was performed to evaluate the reactor performance using the

experimental data. It was found through the simulation studies that the honeycomb-shaped solid reactant was feasible for the process.

In 1984, a bench-scale UT-3 plant named MASCOT (Model Apparatus for Studying Cyclic Operation in Tokyo) was built to produce 3 L/hr of hydrogen continuously as shown in Figure 3-4. In several test runs, 2L/hr of hydrogen was continuously produced (Nakayama et al., 1984).

Aochi et al. (1989) designed a commercial size plant (20,000 Nm^3/h of H_2) of the UT-3 cycle conceptually and estimated the thermal efficiency of the plant to be about 40%, provided the efficiency of power generation from recovered heat was more than 25%.

A new flow scheme shown in Figure 3-5 was suggested by Kameyama et al. (1989). The system consists of four reactors in series with two separators. At first, all four solid reactants are placed in each reactor. Steam is introduced into the reactor (1) which contains calcium bromide. Hydrolysis of the calcium bromide with water produces calcium oxide in solid form, which remains in the reactor while the gaseous product, HBr, and the residual gases move to the reactor (4). From the reactor (4), hydrogen is separated from the other gases. Bromine and water produced in the reactor (3) flow into the reactor (2).

Sakurai et al. (1992) reported continuous operation for 11 cycles, generating H_2 and O_2 in the ratio of 2:1. As illustrated in Figure 3-6, the experimental set-up was composed of Ca and Fe packed reactors. New Fe pellets showed improved performance by changing the inert materials and the mixing ratio of the reactant to the inert compounds.

An adiabatic UT-3 Cycle was suggested by Sakurai et al. (1996a) and a flowsheet of the cycle using a nuclear reactor is shown in Figure 3-1. The system would use excess steam and nitrogen as the heat carriers between adiabatic reactors and a gas stream including the excess

steam, nitrogen and reactant gases was cooled or heated through a heat exchange before entering each adiabatic reactor. Hydrogen and oxygen would be separated by a zirconium-silica membrane at high temperature. A computer simulation with ASPEN-PLUS was conducted and the first and second law efficiencies were found to be 48.9% and 53.2%, respectively. The adiabatic cycle has the following advantages. 1) Enhanced efficiency, 2) Reduced total heat duty of the heat exchanger, 3) Reduced power consumption and 4) mitigated criteria of material selection for the reactor.

Furthermore, the adiabatic UT-3 cycle was coupled with a solar heat source (Sakurai et al., 1996b). A continuous operation concept was considered using thermal storage for night operation. The overall thermal efficiency was estimated to be 49.5% and the exergy efficiency was estimated to be 52.9% by ASPEN-PLUS.

Teo et al. (2005) conducted a critical evaluation on the efficiency of UT-3 process considering solar energy and other high temperature heat as energy sources (Figure 3-7) and compared the efficiencies with that of water electrolysis.

As shown in Figure 3-7, instead of the HHV based efficiency (49.5%) previously reported, a LHV based efficiency of 42% was used for the calculations. They conducted detailed calculations considering equipment efficiencies (compressors, heat exchangers), separation membranes and associated pressure losses, incomplete conversions for the reactions and the impracticality of isothermal operation in the reactors (Teo et al., 2005). They reported the upper efficiency of UT-3 cycle based on a high temperature heat to be around 13 %, which is much lower than the previous estimates (Sakurai et al., 1996a and 1996b).

3.1.2 Development of Solid Reactant

The development of superior solid reactant has been regarded as one of the most important keys for the practicality of the UT-3 cycle. Even in the first proposal of the UT-3 process

(Kameyama and Yoshida, 1978) the importance of developing durable solid reactants was emphasized. The following attempts on the iron and calcium reactants have been tried to improve the performance of the solid reactants.

3.1.2.1 Development of Fe-pellets

In the first study of the UT-3 cycle (Kameyama and Yoshida, 1978), three types of iron pellets using glass beads, bentonite and kaolin as supporting materials were prepared by mixing, molding, drying and sintering. Each pellet was tested in order to find out a durable and reliable supporting method for the iron solid reactant. Among them, the iron pellets supported by bentonite showed the best cyclic reactivity.

In 1981, Fe_3O_4 pellets with a different inert material were also fabricated (Kameyama and Yoshida, 1981). A mixture of Fe_3O_4 powder and the inert binding material, silicasol (Cataloid-S-3OH), was gelled by adding a saturated ammonia carbonate solution. The mixture was then formed into a sphere of 1.0 cm diameter and dried at 80°C. Next, the sphere was sintered at 900 °C. For the bromination reaction of the prepared iron oxide pellets, gaseous HBr and steam were supplied into the reactor where the pellets were placed in. Using the experimental results, a simulation study of the performance of the newly introduced honeycomb-shaped solid reactant was carried out.

Figure 3-8 shows the fabrication process of the CaO and Fe_2O_3 pellets used by Yoshida et al. (1990). Using the pellets thus fabricated, they experimentally evaluated the reaction rates of all the four reactions. Their experimental set-up is shown in Figure 3-9.

In order to make the pellets porous, Amir et al. (1992) mixed the magnetite powder with graphite powder and cellulose along with the inert materials such as zirconia and silica. They measured the pore volumes of the pellets with various graphite contents using mercury porosimeter. Figure 3-10 shows the relationship of pore volume and the graphite contents. Based

on the plots, the total cumulative pore volume was found to increase linearly with the graphite content.

Figure 3-11 shows the effects of the graphite addition on the bromination and hydrolysis conversion of the Fe_2O_3 pellets. It was observed that the conversion of pellets with 20% graphite was more than 45% in 2 hours. However, the conversion was decreased in the cyclic operations.

In order to develop iron reactant pellets strong enough to overcome the cyclic volume change between oxide and bromide form, Amir et al. (1993) prepared and evaluated the iron reactants. The results such as chemical composition, hardness, porosity, and reactivity of the pellets are shown in Table 3-1.

Through the studies on the cyclic reactivity, it was found that degradation of reactivity occurred over a number of cycles due to sublimation of $FeBr_2$, aggregation of Fe_3O_4 and formation of inert compounds by reaction between the reactant and the support materials.

Nakajima et al. (2000) fabricated Fe-pellets by an alkoxide method. The Fe-pellets contained reactant particles, Fe_2O_3, dispersed between the inert binder materials, Fe_2TiO_3. The actual reactant, Fe_3O_4, was generated first by the following reactions.

$$3Fe_2O_3 + 18HBr \xrightarrow{473-573K} 6FeBr_2 + 9H_2O + 3Br_2 \quad (3\text{-}5)$$

$$6FeBr_2 + 8H_2O \xrightarrow{823-873K} 2Fe_3O_4 + 12HBr + 2H_2 \quad (3\text{-}6)$$

Figure 3-12 shows the improvement on the initial conversion by adapting the alkoxide method for the preparation of Fe-pellets instead of the old powder mixing method. It was observed that the rates of bromination and hydrolysis reactions of the iron reactant were accelerated at least twice as fast.

Recently, Sakurai et al. (2006) published more detailed experimental studies on the Fe-pellets. Their pelletization procedure is shown in Figure 3-13. The figure shows the conversion trend of

the bromination of iron pellets prepared by the alkoxide method and the conventional powder mixing method. It can be seen that the conversion of the pellet by the alkoxide method was well maintained in 10 cycles while the pellets using powder mixing method degraded significantly.

3.1.2.2 Development of Ca-pellets

Compared to the preparation step of Fe-pellets, the alkoxide chemistry for Ca-pellets was introduced comparatively early. In 1990, Aihara et al. (1990) suggested the pelletization process using the alkoxide method (Figure 3-15). Through the new method, they achieved significant improvement in both bromination and hydrolysis reaction rates of Ca-pellets.

Figure 3-16 shows a comparison between the new pellets by the alkoxide chemistry and the old type pellets by a conventional powder mixing method. It was observed from this figure that the pellets by the new method had a much higher reaction rate than the ones by the conventional preparation step. The time to maximum conversion was reduced significantly, and degradation was not observed in 6 cycles.

In order to further improve the hydrolysis rate, Sakurai et al. (1995) synthesized the CaO and $CaTiO_3$ separately and then mixed the two compounds to form the final product (Figure 3-17). Through the new process, the CaO agglomerates were smaller than those produced from the previous method. Lauric acid was used as a pore foaming agent in this preparation to make CaO agglomerates finer and increase the surface area.

From Figure 3-18(A), the volume of micropores (pores with diameter less than 0.5 micrometers) was almost the same but the volume of macropores (pores with diameter greater than 0.5 micrometers) was increased around 4 times by applying the new method. So, one can conclude from the figure that the macropores were significantly increased by the lauric acid addition and the separated process chain and as a result, the rate of hydrolysis was approximately three times faster (Figure 3-18(B)).

3.2 Strengths and Weaknesses of UT-3 Cycle

3.2.1 Strengths

- It is attractive because the UT-3 cycle is composed of only gas-solid reactions, which would simplify the separation of gaseous products from solid products.

- The process requires relatively low temperatures for the process which can be achieved through solar concentrators or nuclear reactors.

- The chemistry and kinetics of each reaction in the cycle have been studied extensively and well documented.

- The UT-3 cycle is one of a few processes which were operated at a bench-scale plant.

- Involved elements such as calcium, iron, and bromine are inexpensive and abundant and no precious metals are needed in this cycle. (Average price of bromine was $2/kg, while average price of iodine for IS cycle was about $20/kg in 2007 (Bromine Statistics and Information, 2008; Iodine Statistics and Information, 2008)

3.2.2 Weaknesses

There are weaknesses of the UT-3 cycle as well.

- For the process to be feasible, the solid reactants must be physically stable and chemically active while cycling between oxide and bromide forms.

- The excess steam needed for thermal energy and the hydrolysis reaction would decrease the performance of membrane separation.

- Hydrolysis reaction of calcium bromide is thermodynamically unfavorable reaction which means the conversion would be low at equilibrium state. However, the ultimate conversion efficiency would be higher since the gaseous product, HBr, is removed immediately from the reactor by the gaseous stream as soon as it is produced. This assumption would be verified in the chapter 4 and 5.

- Bromine and hydrogen bromide are circulated in the system at high temperature, so special materials of construction are required.

- Teo et al. (2005) predicted a much lower efficiency of less than 13% for the UT-3 cycle although this prediction was based on some assumptions which may not be correct.

3.3 Modification of UT-3 Cycle

Recently, in order to simplify or overcome some barriers in the UT-3 cycle, a few modifications of the UT-3 cycle were suggested and investigated.

Doctor et al. (2002) proposed a modified 3-stage UT-3 cycle named Ca-Br cycle to simplify the process. The Ca-Br process uses a single-stage HBr dissociation by a commercial HBr electrolyzer or plasma dissociation instead of the two-steps HBr dissociation involving iron oxide and iron bromide. From the data in the Figure 3-19, HBr electrolysis was expected to require about 48% lower electricity than water electrolysis.

In 2006, instead of the packed bed reactor, a fluidized bed reactor for the gas-solid reaction was proposed by Lemort et al. (2006) in order to improve the reaction kinetics and avoid the expensive preparation steps. The process efficiency was estimated to be 22.5%, provided the membrane technology for high temperature separation was developed. The conceptual design is shown in Figure 3-20.

Simpson et al. (2007) suggested an innovative concept (Figure 3-21) based on molten calcium bromide with melted calcium oxide and conducted preliminary experiments to support the idea.

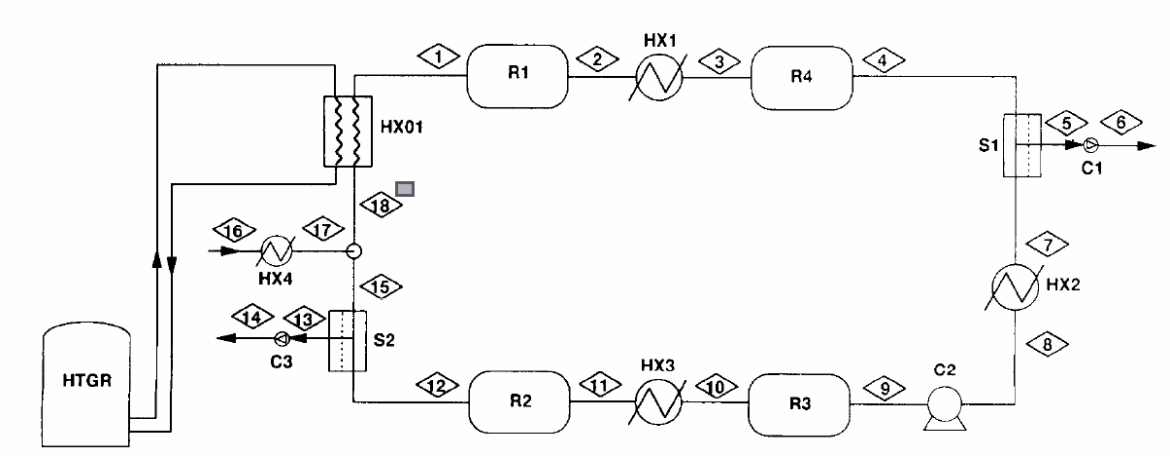

Figure 3-1. Flowsheet of the adiabatic UT-3 thermochemical cycle. Adapted from Sakurai, M., Bilgen, E., Tsutsumi, A., Yoshida, K., 1996a. Adiabatic UT-3 thermochemical process for hydrogen production. International Journal of Hydrogen Energy 21, 865-870 (Figure 1, page 866).

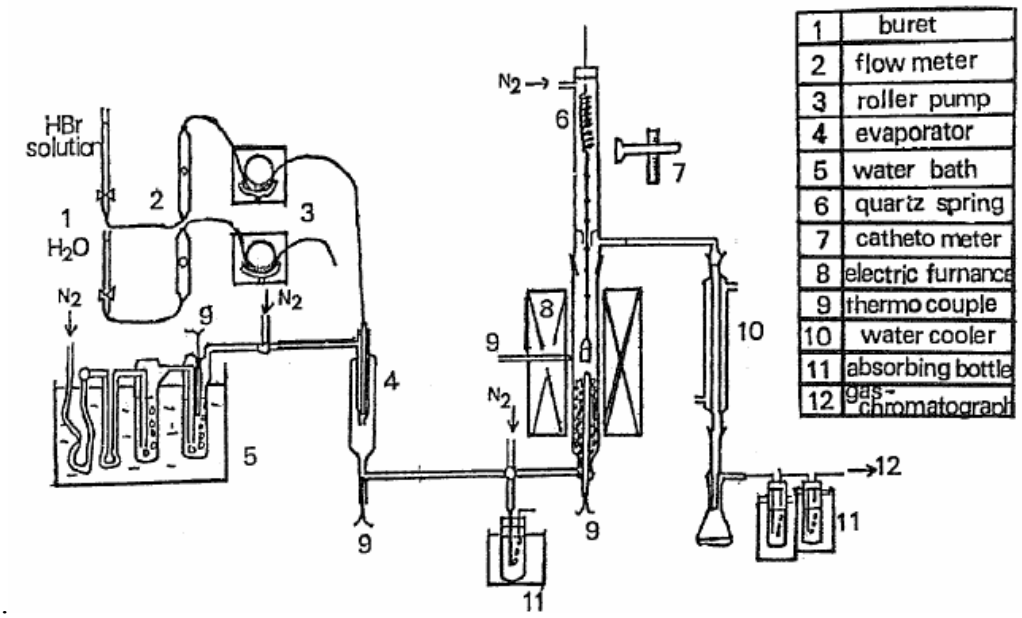

Figure 3-2. Experimental apparatus for kinetic studies. Adapted from Kameyama, H., Yoshida, K., 1978. Br-Ca-Fe water-decomposition cycles for hydrogen production. Proc. of the 2nd World Hydrogen Energy Conf., Zurich, Switzerland, 829-850 (Figure 2, page 840).

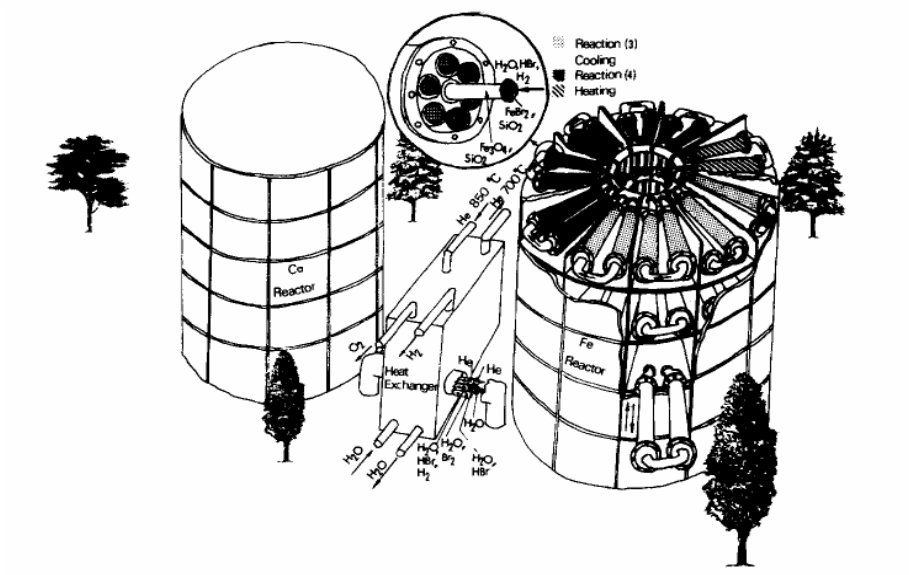

Figure 3-3. Conceptual plant design for UT-3 cycle. Adapted from Kameyama, H., Yoshida, K., 1981. Reactor design for the UT-3 thermochemical hydrogen production process. International Journal of Hydrogen Energy 6, 567-575 (Figure 1, page 569).

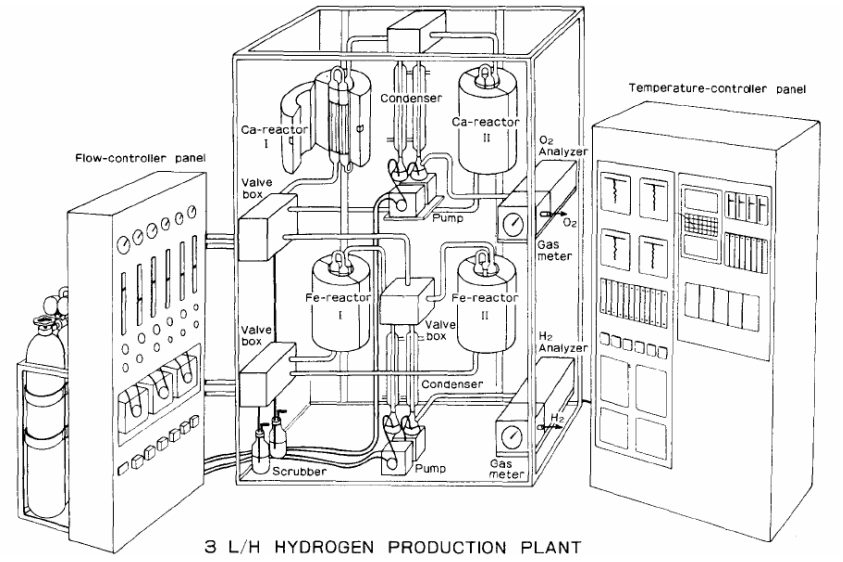

Figure 3-4. The MASCOT plant. Adapted from Nakayama, T., Yoshioka, H., Furutani, H., Kameyama, H., Yoshida, K., 1984. MASCOT- a bench-scale plant for producing hydrogen by the UT-3 thermochemical decomposition cycle. International Journal of Hydrogen Energy 9, 187-190 (Figure 1, page 188).

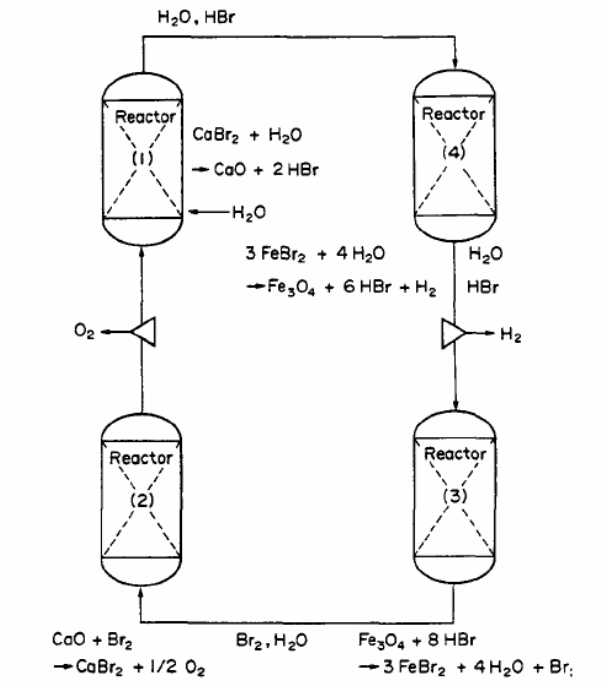

Figure 3-5. New flow scheme for the UT-3 process. Adapted from Kameyama, H., Tomino,Y., Sato, T., Amir, R., Orihara, A., Aihara, M., Yoshida, K., 1989. Process simulation of "MASCOT" plant using the UT-3 thermochemical cycle for hydrogen production. International Journal of Hydrogen Energy 14, 323-330 (Figure 1, page 324).

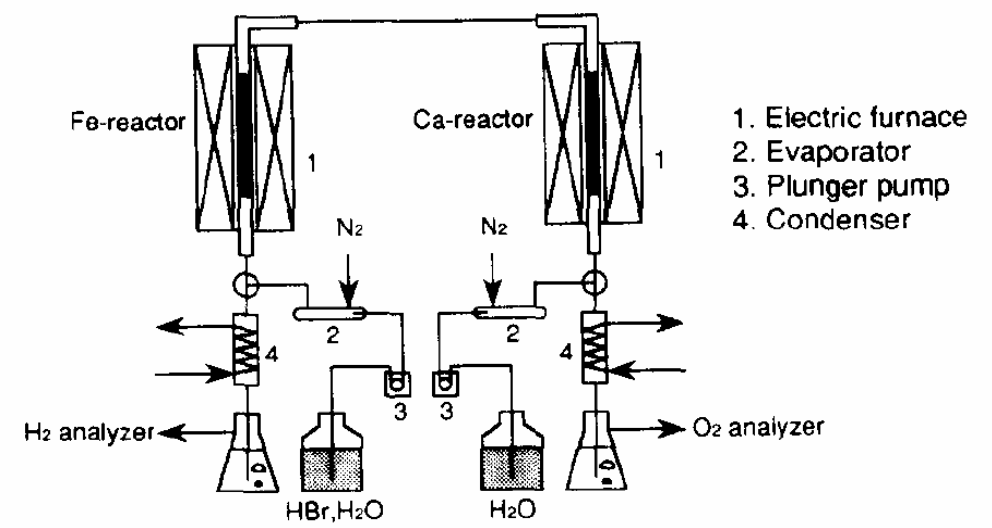

Figure 3-6. Experimental set-up for MASCOT plant. Adapted from Sakurai, M., Aihara, M., Miyake, N., Tsutsumi, A., Yoshida, K., 1992. Test of one-loop flow scheme for the UT-3 thermochemical hydrogen production process. International Journal of Hydrogen Energy 17, 587-592 (Figure 13, page 591).

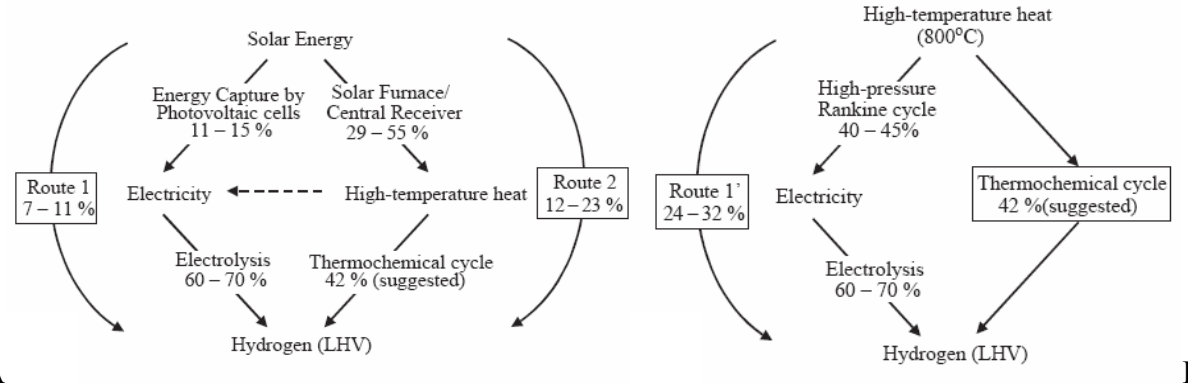

A B

Figure 3-7. Pathway efficiencies. A) Solar energy to hydrogen. B) High temperature heat to hydrogen. Adapted from Teo, E. D., Brandon, N. P., Vos, E., Kramer, G. J., 2005. A critical pathway energy efficiency analysis of the thermochemical UT-3 cycle. International Journal of Hydrogen Energy 30, 559-564 (Figure 2, page 561).

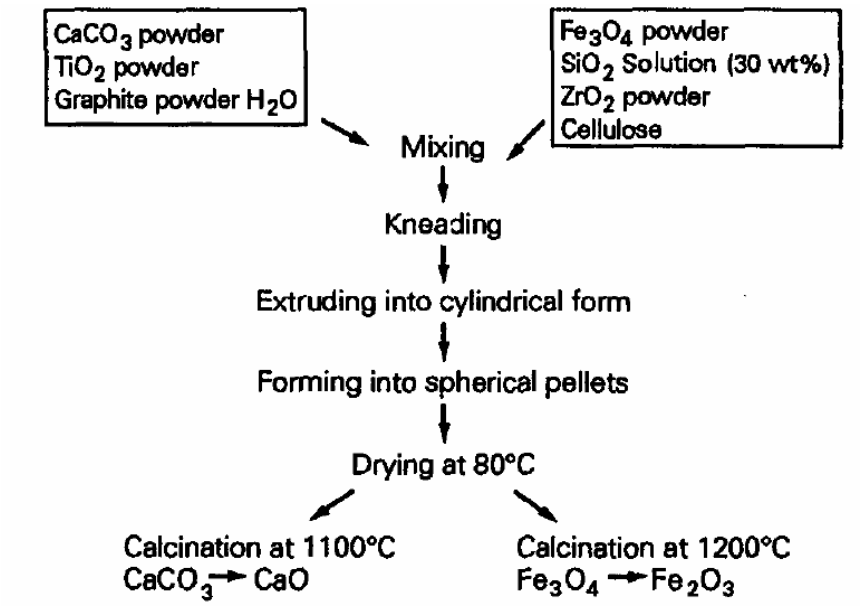

Figure 3-8. Pelletization process for the solid reactant pellets. Aadapted from Yoshida, K., Kameyama, H., Aochi, T., Nobue, M., Aihara, M., Amir, R., Kondo, H., Sato, T., Tadokoro, Y., Yamaguchi, T., Sakai, N., 1990. A simulation study of the UT-3 thermochemical hydrogen production process. International Journal of Hydrogen Energy 15, 171-178 (Figure 3, page 172).

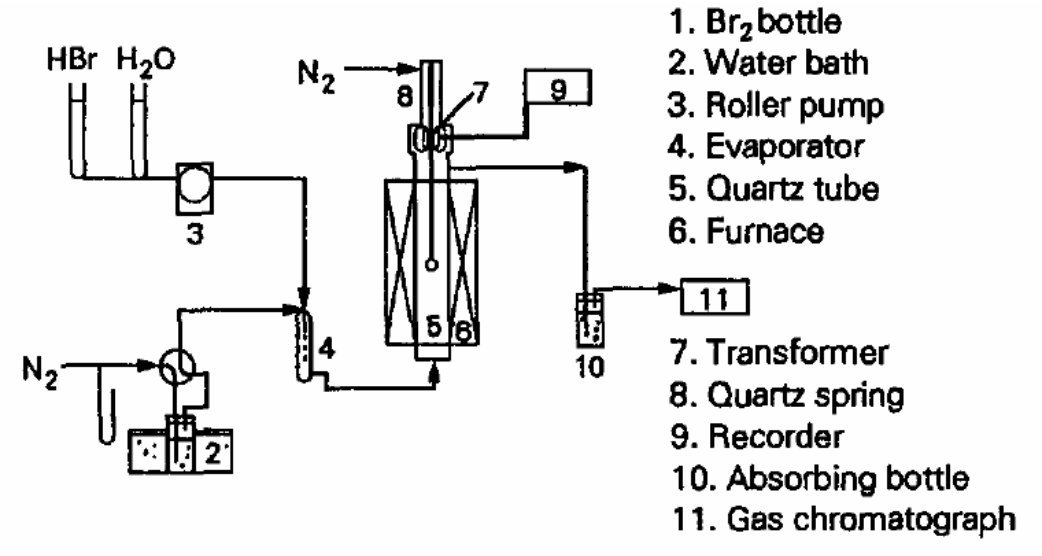

Figure 3-9. Experimental apparatus for the kinetic tests of pellets. Adapted from Yoshida, K., Kameyama, H., Aochi, T., Nobue, M., Aihara, M., Amir, R., Kondo, H., Sato, T., Tadokoro, Y., Yamaguchi, T., Sakai, N., 1990. A simulation study of the UT-3 thermochemical hydrogen production process. International Journal of Hydrogen Energy 15, 171-178 (Figure 2, page 172).

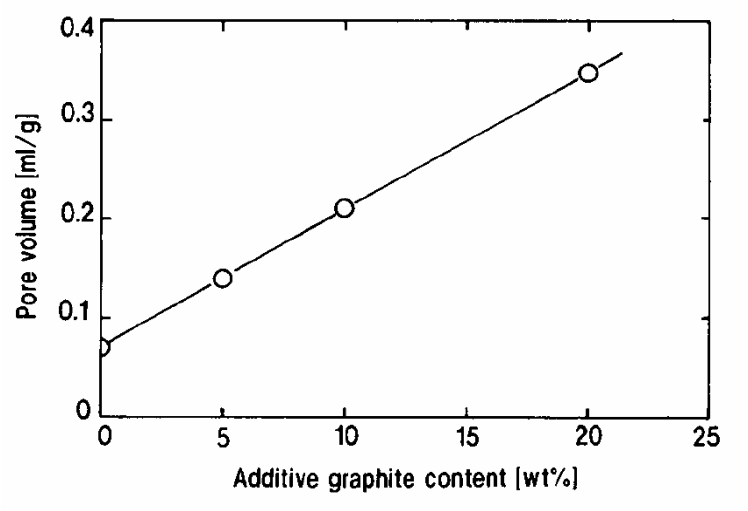

Figure 3-10. Experimental apparatus for the kinetic tests of pellets. Aadapted from Amir, R., Sato, T., Yoko Yamamoto, K., Kabe, T., Kameyama, H., 1992. Design of solid reactants and reaction kinetics concerning the iron compounds in the UT-3 thermochemical cycle. International Journal of Hydrogen Energy 17, 783-788 (Figure 2, page 785).

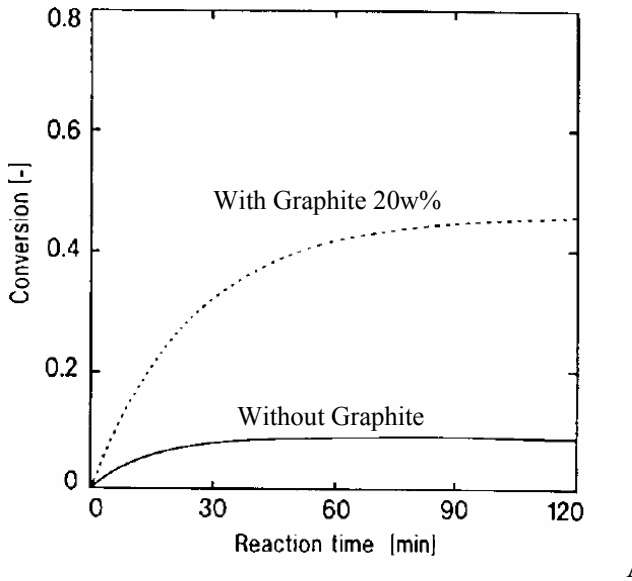

A

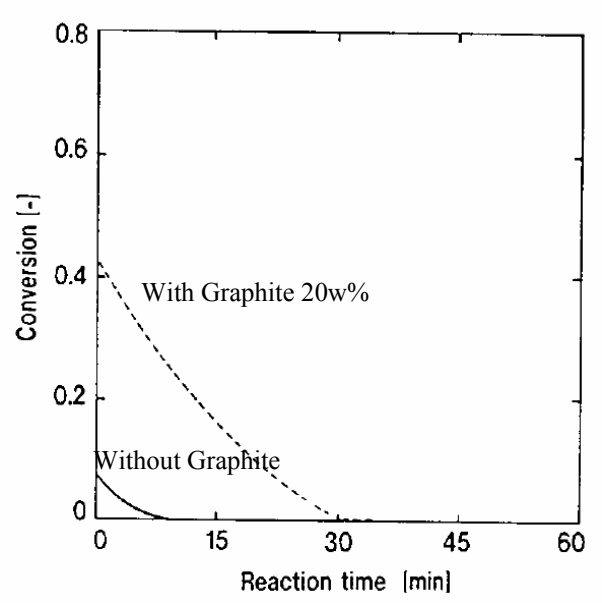

B

Figure 3-11. Bromination and hydrolysis conversion of the Fe_2O_3 pellets. A) Bromination. B) Hydrolysis of the Fe_2O_3 pellets by adding graphite. Adapted from Amir, R., Sato, T., Yoko Yamamoto, K., Kabe, T., Kameyama, H., 1992. Design of solid reactants and reaction kinetics concerning the iron compounds in the UT-3 thermochemical cycle. International Journal of Hydrogen Energy 17, 783-788 (Figure 3 and 4, page 785).

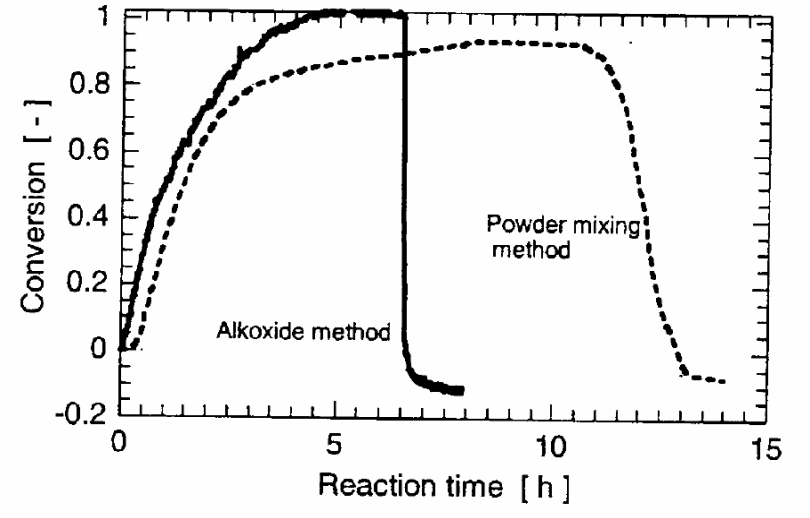

Figure 3-12. Initial conversion profile of Fe-pellets. Adapted from Nakajima, R., Kikuchi, R., Tsutsumi, A., 2000. Improvement of the Fe-pellet reactivity in the UT-3 thermochemical hydrogen production cycle. Hydrogen energy progress XIII: Proceedings of the 13th World Hydrogen Energy Conference, Beijing, China.303-307 (Figure 8, page 307).

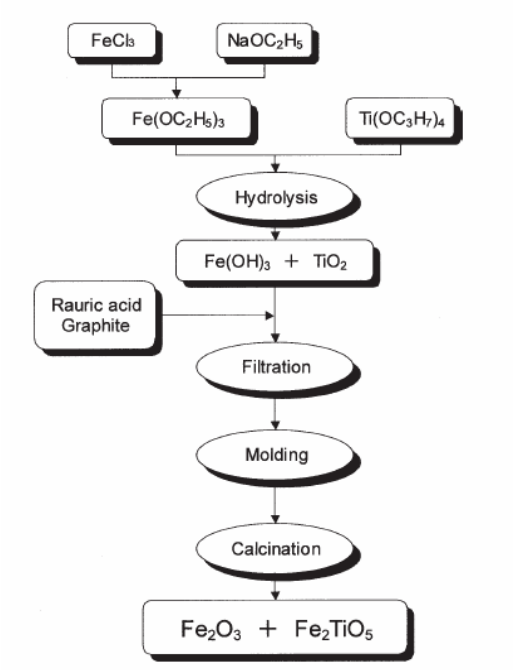

Figure 3-13. Flowsheet for the preparation of Fe-pellets. Adapted from Sakurai, M., Ogiwara, J., Kameyama, H., 2006. Reactivity improvement of Fe-compounds for the UT-3 thermochemical hydrogen production process. Journal of Chemical Engineering of Japan 39, 553-558 (Figure 1, page 554).

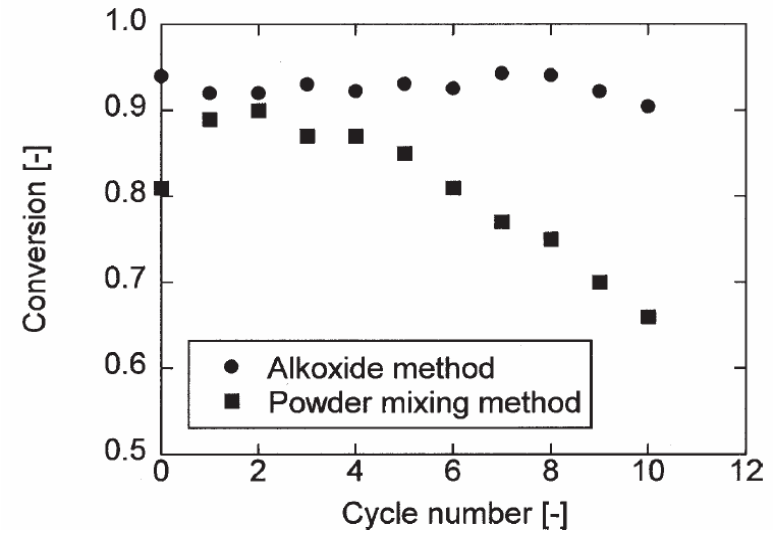

Figure 3-14. Conversions of the bromination in cyclic operation. Adapted from Sakurai, M., Ogiwara, J., Kameyama, H., 2006. Reactivity improvement of Fe-compounds for the UT-3 thermochemical hydrogen production process. Journal of Chemical Engineering of Japan 39, 553-558 (Figure 6, page 556).

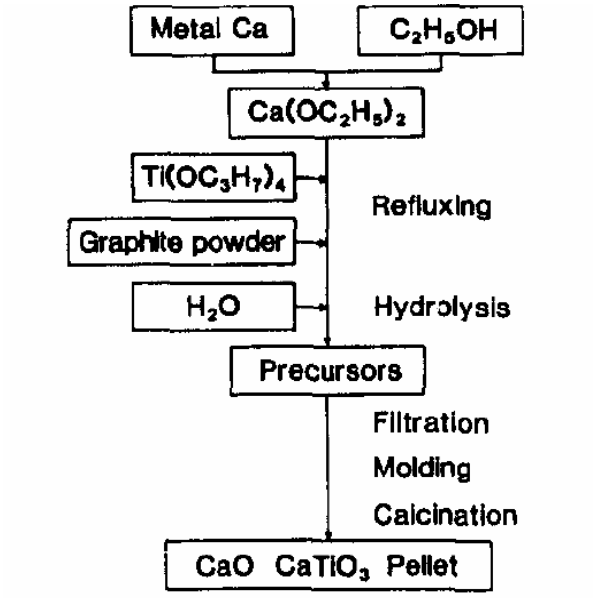

Figure 3-15. Preparation steps of Ca-pellets. Adapted from Aihara, M., Umida, H., Tsutsumi, A., Yoshida, K., 1990. Kinetic study of UT-3 thermochemical hydrogen production process. International Journal of Hydrogen Energy 15, 7-11 (Figure 8, page 9).

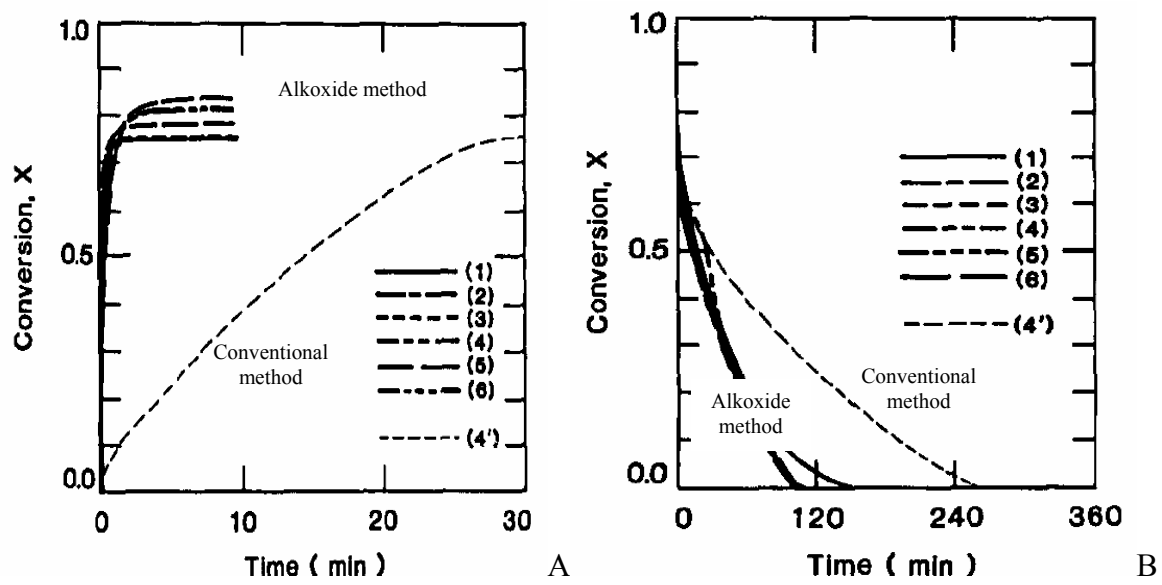

Figure 3-16. Conversion profiles of Ca-pellets. A) Bromination. B) Hydrolysis of Ca-pellets. Adapted from Aihara, M., Umida, H., Tsutsumi, A., Yoshida, K., 1990. Kinetic study of UT-3 thermochemical hydrogen production process. International Journal of Hydrogen Energy 15, 7-11 (Figure 10 and 11, page 10).

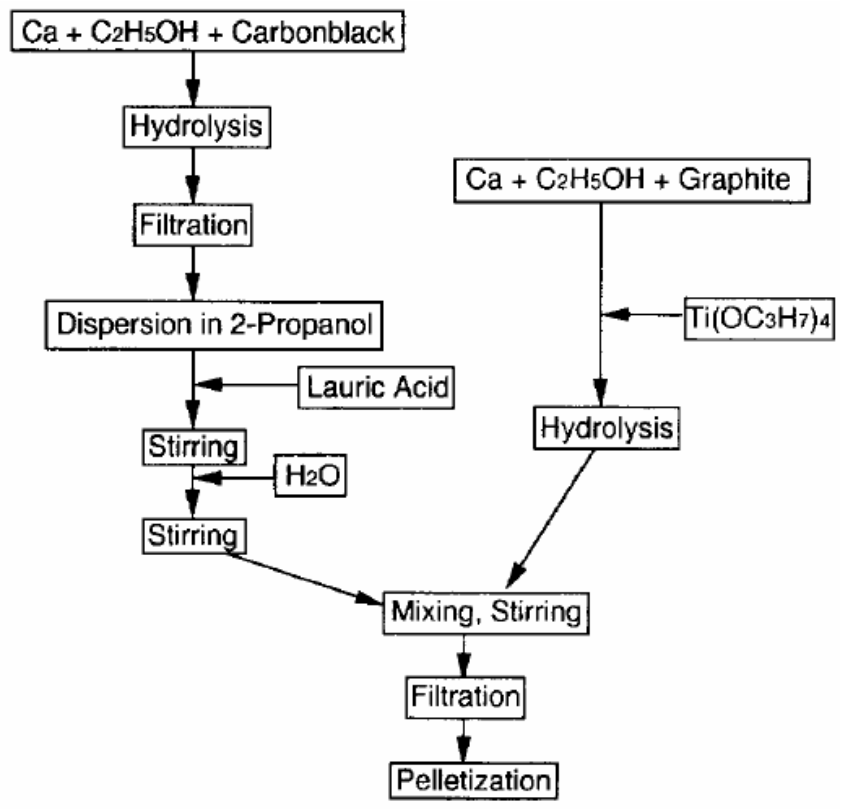

Figure 3-17. New preparation method for Ca-pellets. Adapted from Sakurai, M., Tsutsumi, A., Yoshida, K., 1995. Improvement of Ca-pellet reactivity in UT-3 thermo-chemical hydrogen production cycle. International Journal of Hydrogen Energy 20, 297-301 (Figure 6, page 299).

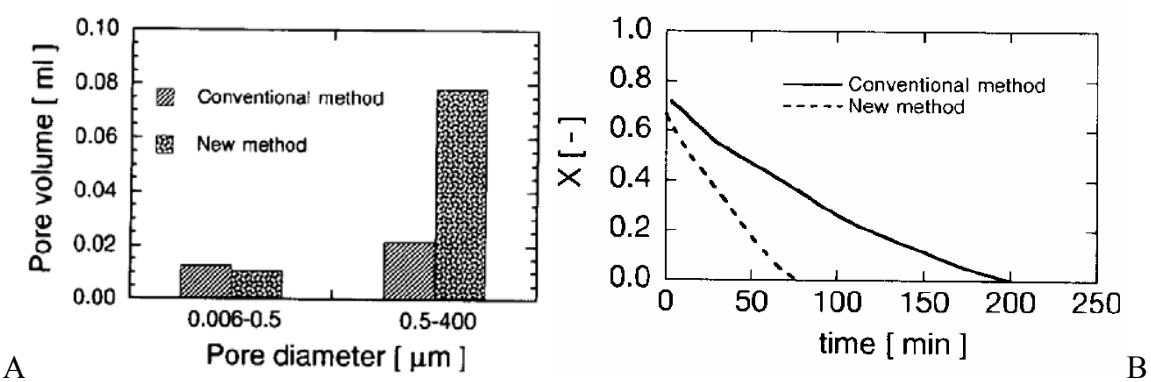

A B

Figure 3-18. Comparison of the pellets by the conventional and new modified method. A) Pore volume. B) Hydrolysis rate. Adapted from Sakurai, M., Tsutsumi, A., Yoshida, K., 1995. Improvement of Ca-pellet reactivity in UT-3 thermo-chemical hydrogen production cycle. International Journal of Hydrogen Energy 20, 297-301 (Figure 7 and 11, page 299 and 301).

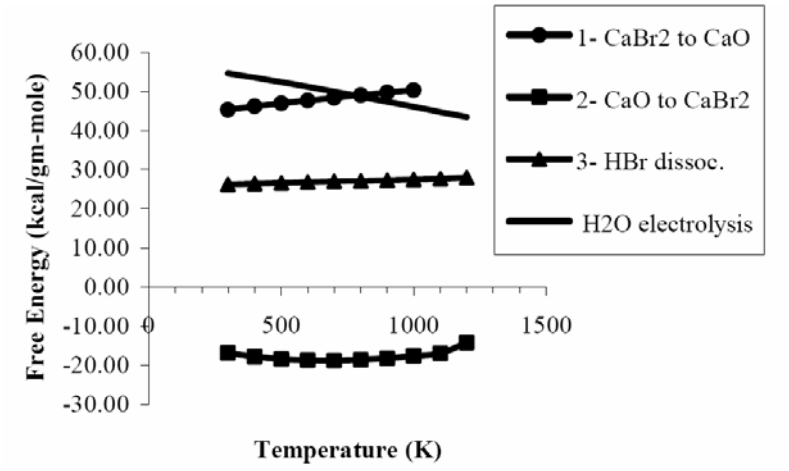

Figure 3-19. Change of Gibbs free energy vs. temperature for the Ca-Br cycle and water electrolysis. Adapted from Doctor, R. D., Marshall, C. L., Wade, D. C., 2002. Hydrogen cycle employing calcium-bromine and electrolysis. ACS Division of Fuel Chemistry, Preprints 47, 755-756.

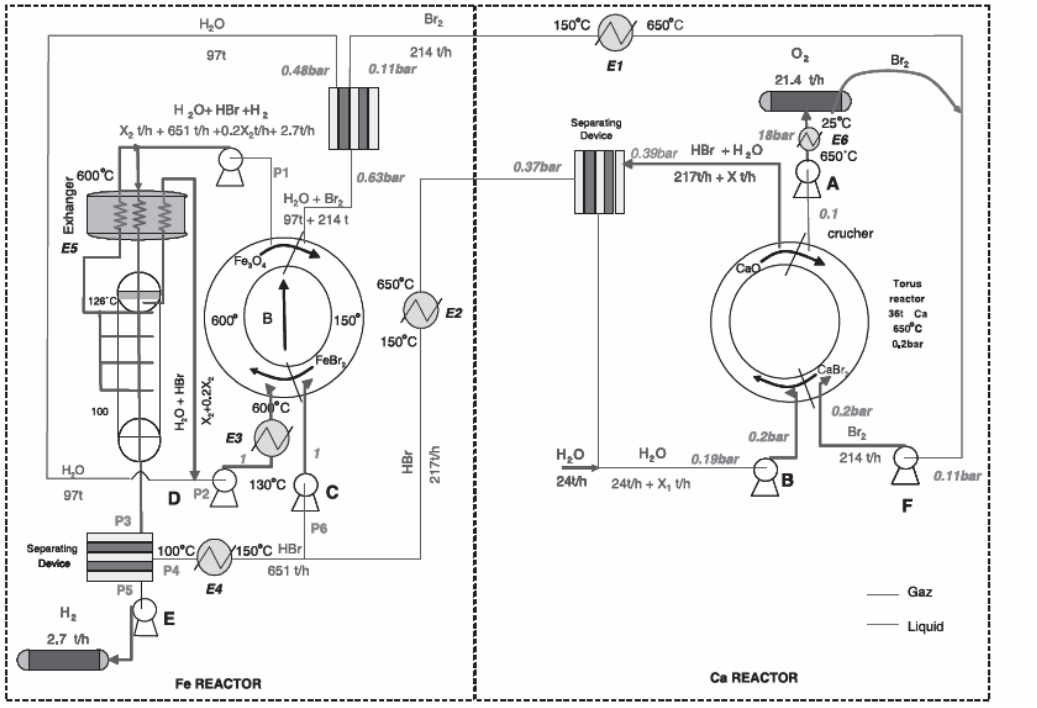

Figure 3-20. Conceptual design of a fluidized bed for UT-3 cycle. Adapted from Lemort, F., Lafon, C., Dedryvère, R., Gonbeau, D., 2006. Physicochemical and thermodynamic investigation of the UT-3 hydrogen production cycle: A new technological assessment. International Journal of Hydrogen Energy 31, 906-918 (Figure 8, page 914).

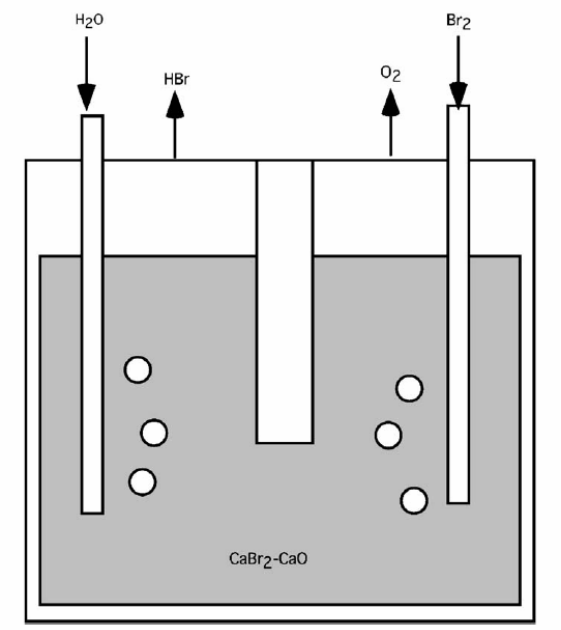

Figure 3-21. Conceptual molten salt-based reactor for hydrolysis/bromination in the Ca–Br cycle. Adapted from Simpson, M. F., Utgikar, V., Sachdev, P., McGrady, C., 2007. A novel method for producing hydrogen based on the Ca–Br cycle. International Journal of Hydrogen Energy 32, 505-509 (Figure 1, page 506).

Table 3-1. Properties of iron solid reactant pellets.

Pellet	Raw material: Reactant	Raw material: Support	Mole ratio Fe:(Zr:Si)/(TZ−Y)	Density (kg m^{-3})	Iron content (mol m^{-3} $pellet^{-1}$)	Hardness (kg mm^{-2})	Pore volume (ml g^{-1})
1	Fe_3O_4	SiO_2 + ZrO_2	1:4.2:4.2	1.8×10^3	5.4×10^3	8	0.45
2	Fe_3O_4	$ZrSiO_4$	1:4.2	1.8×10^3	5.4×10^3	8	0.35
3	Fe_3O_4	TZ−3Y	1:4	3.7×10^3	15.2×10^3	11	0.12
4	Fe_3O_4	TZ−8Y	1:4	3.6×10^3	14.3×10^3	17	0.12
5	Fe_3O_4(UFP)	TZ−3Y	1:4	1.7×10^3	6.9×10^3	9	—
6	$FeC_4H_2O_4$	TZ−3Y	1:4	1.6×10^3	6.5×10^3	<1	—
7	$FeC_{15}H_{21}O_6$	TZ−3Y	1:4	8.9×10^2	3.6×10^3	<1	—
8	$FeC_6H_{18}O_{15}N_3$	TZ−3Y	1:4	1.3×10^3	5.6×10^3	<1	—

Adapted from Amir, R., Shiizaki, Yamamoto, K., Kabe, T., Kameyama, H., 1993. Design development of iron solid reactants in the UT-3 water decomposition cycle based on ceramic support materials. International Journal of Hydrogen Energy 18, 283-286 (Table 2, page 285).

CHAPTER 4
THEORETICAL FEASIBILITY INVESTIGATIONS OF UT-3 CYCLE

Experimental feasibility studies of UT-3 cycle have been conducted and documented well, but rarely using a thermodynamic analysis approach except for one paper recently published by Lemort et al. (2006). In this chapter, the thermodynamic conditions for each reaction in the cycle were comprehensively examined and discussed. This thermodynamic feasibility analysis will contribute to the determination of the optimal operating conditions for high conversion and reaction rate to improve the process efficiency.

4.1 Thermodynamic Analysis of UT-3 Cycle

As introduced in the previous chapter, the UT-3 cycle consists of the following four heterogeneous reactions.

$$\text{(R1)} \quad CaO(s) + Br_2(g) \xrightarrow{600^\circ C} CaBr_2(s) + \frac{1}{2}O_2(g) \tag{4-1}$$

$$\text{(R2)} \quad CaBr_2(s) + H_2O(g) \xrightarrow{730^\circ C} CaO(s) + 2HBr(g) \tag{4-2}$$

$$\text{(R3)} \quad Fe_3O_4(s) + 8HBr(g) \xrightarrow{210^\circ C} 3FeBr_2(s) + 4H_2O(g) + Br_2(g) \tag{4-3}$$

$$\text{(R4)} \quad 3FeBr_2(s) + 4H_2O(g) \xrightarrow{560^\circ C} Fe_3O_4(s) + 6HBr(g) + H_2(g) \tag{4-4}$$

A reaction is spontaneous for negative values of ΔG, while it is non-spontaneous with positive values. It is useful to find favorable conditions, though the spontaneity is not related to the reaction rate (Meites, 1981). In order to check whether the reactions in the cycle will occur spontaneously, the changes of Gibbs free energy as a function of reaction temperature were calculated and are plotted in Figure 4-1. The thermodynamic properties in the JANAF Tables (Chase et al., 1995) were used for the computation.

Based on the Figure 4-1, the bromination reactions of calcium oxide and iron oxide, R1 and R3, are spontaneous, while the hydrolysis reactions of calcium bromide and iron bromide,

R2 and R4, are non-spontaneous. The hydrolysis reactions are advantageous at high temperature but it is limited by the melting points of the bromide forms. Thus, various parameters were considered to find the optimal operating conditions for the reactions. Detailed calculations conducted via an equilibrium module which uses the Gibbs energy minimization algorithm in FactSage thermochemical software and databases (FactSage, Web version) and analysis are described separately for each reaction below. In these results, minor products were neglected.

4.1.1 Reaction 1: Bromination Reaction of Calcium Oxide

$$\text{(R1)} \quad CaO(s) + Br_2(g) \xrightarrow{600^\circ C} CaBr_2(s) + \frac{1}{2}O_2(g) \tag{4-1}$$

Based on the changes of free energy as a function of temperature (Figure 4-1), bromination reaction of calcium oxide is very favorable. This was confirmed by the experimental results of Aihara et al. (1992) and Sakurai et al. (1995). However, the earlier researches also found that the bromination process was terminated with roughly 70% conversion, mainly due to pore plugging in less than 5 minutes. Therefore, a high porous reactant with high surface area free from pore plugging must be developed in order to increase the bromination conversion.

Aihara et al. (1992) investigated the effects of steam concentration on the bromination reaction of calcium oxide pellets experimentally. They reported that the bromination conversion was well maintained in the presence of approximately thirty times excess steam per hydrogen. However, according to Sakurai et al. (1996b), at least one hundred times of steam per hydrogen yield should be used to operate the adiabatic process without any other external heat input to the reactors.

Therefore, in this study, the effect of steam concentration on the bromination reaction of calcium oxide was evaluated up to five hundred times the hydrogen using FactSage thermochemical software and databases (FactSage, Web version). The simulation results are

illustrated in Figure 4-2. As shown in Figure 4-2, only small adverse effect of excess steam up to one hundred times excess supply on the bromination reaction was observed.

With one hundred times excess steam, the effects of temperature and pressure on the reaction progress were also calculated and are displayed in Figure 4-3 and Figure 4-4, respectively.

Based on Figure 4-3, high conversion was achieved at temperatures in the range 600-900K. The influence of temperature on the reaction was slight in the range. However, Aihara et al. (1992) observed the degradation at 823K in their experimental study due to the formation of hydrates of calcium bromide while the reactivity was maintained at 873K without the formation of hydrates.

The effect of operation pressure on the reaction progress is illustrated in Figure 4-4. High pressure did not enhance conversion much, as expected according to the Le Chatelier's principle. Moreover, formation of calcium hydroxide ($Ca(OH)_2$) was observed at high pressures over 5 atm due to the reaction of calcium oxide and steam. Under low pressure, the conversion decreased dramatically.

The theoretical analysis of the bromination reaction of calcium oxide is summarized here.

- In theory, the bromination reaction of calcium oxide is spontaneous and can be completed thermodynamically if there is no barrier.
- Very subtle adverse effect of excess steam up to one hundred times on the bromination was observed in the simulation study.
- Influence of temperature on the conversion of the reaction was insignificant in the range 600-900K.
- The conversion was decreased noticeably under vacuum pressure while it was not much enhanced with pressure over 2 atm.

Based on our theoretical analysis and experimental data from the literature optimum conditions for the bromination of calcium oxide were determined and are presented in Table 4-1.

4.1.2 Reaction 2: Hydrolysis Reaction of Calcium Bromide

$$\text{(R2)} \quad CaBr_2(s) + H_2O(g) \xrightarrow{730^{\circ}C} CaO(s) + 2HBr(g) \tag{4-2}$$

Figure 4-1 tells us that the hydrolysis reaction of calcium bromide (R2) is thermodynamically unfavorable. Actually, this reaction is the slowest and the rate limiting step. Therefore, speeding up this reaction is the key to improve the performance of the cycle. Several experimental (Aihara et al., 1990; Sakurai et al., 1995; Lee et al., 2006 and 2007) and theoretically studies (Lemort et al., 2006) to accelerate the reaction rate have been reported in the literature.

Conversion seems to increase with elevating temperature, since the reaction is endothermic. Besides, the conversion with excess steam and at lower pressures is expected to be higher according to the Le Chatelier's principle.

The effect of excess steam on hydrolysis reaction of calcium bromide at 1000K and 1 atm is shown in Figure 4-5. The hydrolysis reaction was effected significantly by the excess steam and the conversion was increased with the addition of excess steam as expected according to the Le Chatelier's principle. From figure 4-5, only 9.5 percent conversion was expected with 100 times excess steam at atmospheric pressure. This conversion is very close to the value (9.45%) reported by Lemort et al. (2006).

The effect of temperature on the hydrolysis reaction of calcium bromide with one hundred times excess steam was estimated and is displayed in Figure 4-6. The conversion was significantly increased with the elevation of temperature; however, the reaction temperature is limited by the melting point of calcium bromide at about 1000K as shown in the plot.

The influence of pressure was also calculated and the result is displayed in Figure 4-7.

Based on the computation, the conversion was highly dependant on the operation pressure as suggested before (Lemort et al., 2006). If the pressure reduces to 0.01 atm, about 96 percent conversion can be achieved even though the low pressure condition may be impractical as well as inefficient for mass production of hydrogen.

Considering the operation principle of packed-bed reactor involving gas-solid heterogeneous reaction, however, the ultimate conversion efficiency may be higher even at atmospheric pressure since the gaseous products are removed immediately from the reactor by the gaseous stream as soon as they are produced. This assumption was verified by calculating the effect of consecutive hydrogen bromide (HBr) removal from the equilibrium conditions.

As shown in Figure 4-8, it was observed that the conversion could be completed theoretically by removing the product gas, HBr, from each equilibrium state. The hypothesis will be verified by means of the experimental tests in chapter 5. Therefore, considering the advantage of the gas-solid reaction in the packed bed system, atmospheric pressure rather than 0.01 atm is more practical for this reaction.

The theoretical analysis of the hydrolysis reaction of calcium bromide is summarized here.

- Thermodynamically, the hydrolysis reaction of calcium bromide is unfavorable.
- The hydrolysis of calcium bromide is enhanced with the addition of excess steam significantly.
- High temperature and low pressure favors higher conversion though the temperature is constrained due to the melting point of calcium bromide.
- 96 percent conversion is expected with excess steam, $100H_2O/H_2$, at 1000K and 0.01 atm even though the low pressure condition is not feasible for the practical application.
- The conversion is expected to be completed by removing the product gas, HBr, from each equilibrium state even at atmospheric pressure.
- Based on the gas-solid reaction advantage in packed bed system and economic performance, 1 atm rather than 0.01 atm is more practical pressure condition for the reaction.

Through theoretical analysis, optimum conditions for the hydrolysis of calcium bromide are presented in Table 4-2.

4.1.3 Reaction 3: Bromination Reaction of Iron Oxide

$$\text{(R3)} \quad Fe_3O_4(s) + 8HBr(g) \xrightarrow{210^\circ C} 3FeBr_2(s) + 4H_2O(g) + Br_2(g) \qquad (4\text{-}3)$$

The bromination reaction of iron oxide seems to be favorable only at low temperature range (Figure 4-1).

The effect of temperature on the bromination of iron oxide was computed. One hundred times excess steam per hydrogen was included in the reactant gases in the calculation. The results are plotted in Figure 4-9. The figure shows that the conversion increases as the temperature decreases and an undesirable substance, Fe_2O_3, is formed between 400K and 800K. So, 400K was selected as the optimal temperature as suggested by Lemort et al. (2006).

The effect of pressure on the bromination of iron oxide is illustrated in Figure 4-10. Judging from this plot, conversion can be reached almost completely by promoting the bromination of Fe_2O_3 by HBr at pressures slightly above 3 atm.

The theoretical analysis of the bromination reaction of iron oxide is summarized here.

- In theory, the bromination of iron oxide is favorable at low temperature
- Almost complete conversion is reached at a pressure of 3 atm.

All things considered, optimum conditions for the bromination of iron oxide are presented in Table 4-3.

4.1.4 Reaction 4: Hydrolysis Reaction of Iron Bromide

$$\text{(R4)} \quad 3FeBr_2(s) + 4H_2O(g) \xrightarrow{560^\circ C} Fe_3O_4(s) + 6HBr(g) + H_2(g) \qquad (4\text{-}4)$$

R4, hydrolysis of iron bromide, is thermodynamically unfavorable similar to the hydrolysis of calcium bromide. High temperature, excess steam and low pressure seem to be effective in

improving the conversion according to the change of Gibbs free energy versus temperature and the Le Chatelier's principle.

The influence of temperature on the hydrolysis of iron bromide was calculated and is plotted in Figure 4-11. As expected, the conversion is strongly dependant on the temperature in the temperature range below 800K. Above 900K, however, the conversion was decreased gradually as the temperature increased due to the sublimation of iron bromide as reported in the literature (Amir et al., 1993).

Figure 4-12 shows the effect of excess steam on the reaction and it is observed that supplying excess steam is very effective in increasing the conversion.

The theoretical analysis of the hydrolysis reaction of iron bromide is summarized here.

- Thermodynamically, the hydrolysis reaction of iron bromide is unfavorable.
- The highest conversion was achieved at 800K without the sublimation of iron bromide
- The excess steam enhanced the reaction significantly.

Through theoretical analysis, the optimum conditions for the hydrolysis of iron bromide are presented in Table 4-4.

4.2 Optimum Conditions for UT-3 Cycle

Considering excess steam and other thermodynamic parameters, the determined optimum conditions and expected conversions of each reaction in UT-3 cycle are summarized in Table 4-5 subject to no physical barrier of the reactions such as reduction of active surface area and diffusion resistance due to sintering of reactant granules and encapsulation by solid product.

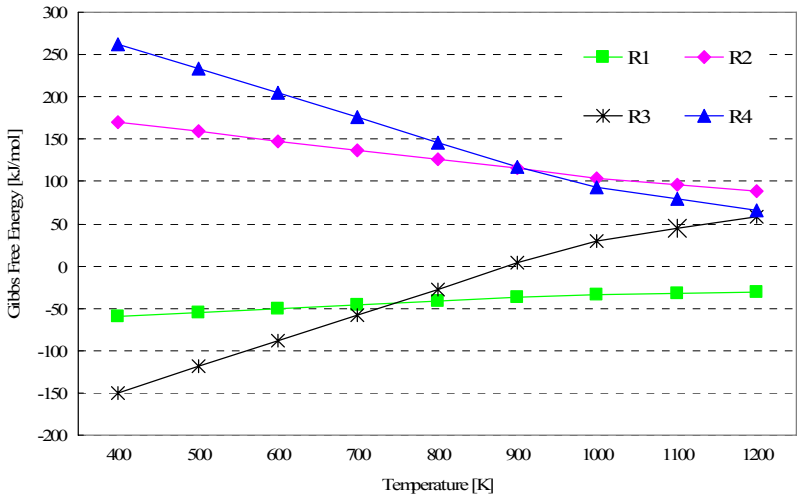

Figure 4-1. Changes of Gibbs free energy of reactions as a function of reaction temperature

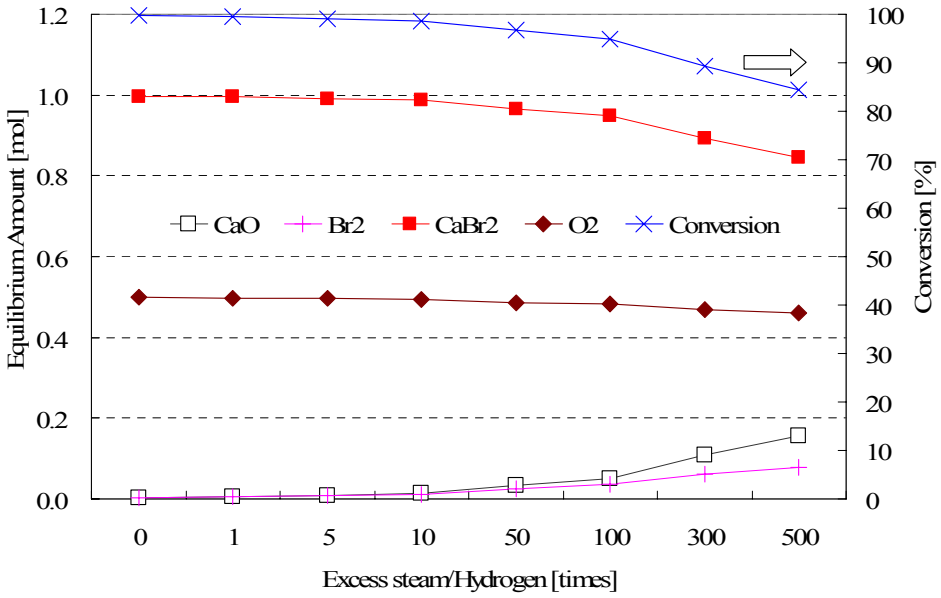

Figure 4-2. Effect of excess steam on bromination reaction of calcium oxide at 873K and 1 atm

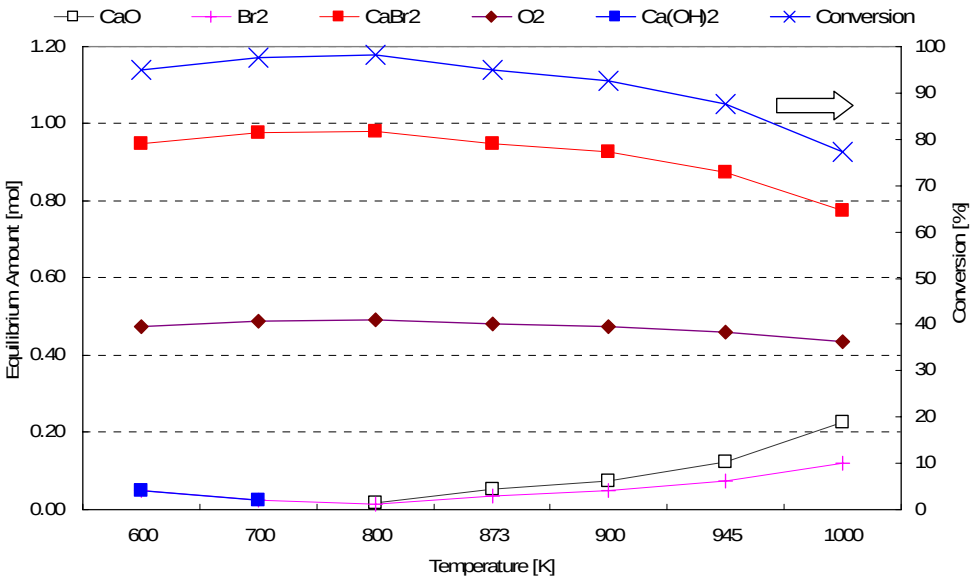

Figure 4-3. Effect of operation temperature on bromination reaction of calcium oxide at 1 atm with $100H_2O/H_2$

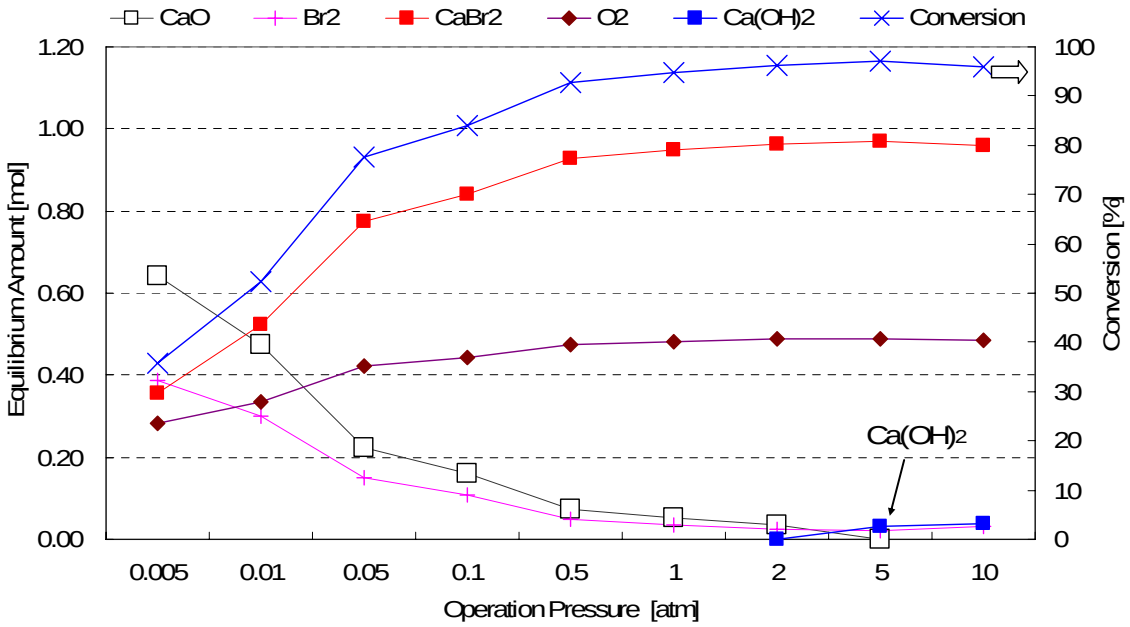

Figure 4-4. Effect of operation pressure on bromination reaction of calcium oxide at 873K with $100H_2O/H_2$

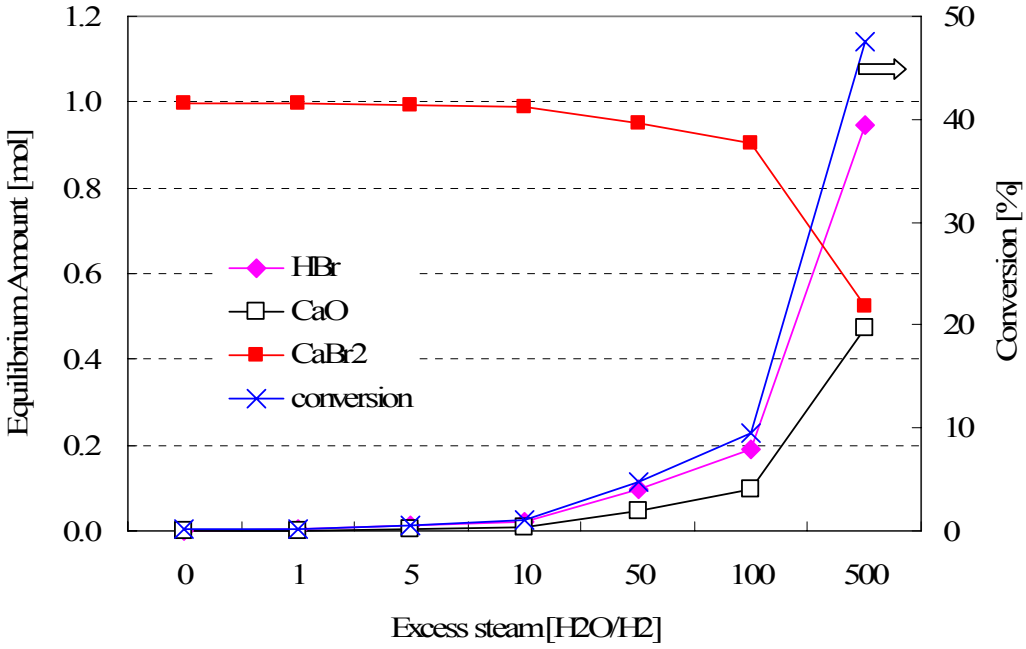

Figure 4-5. Effects of excess steam on hydrolysis of calcium bromide at 1000K and 1 atm

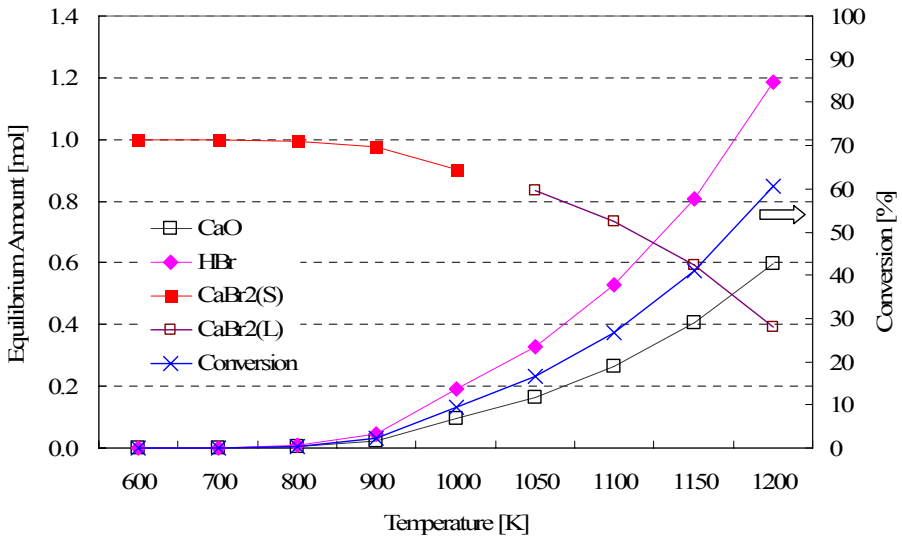

Figure 4-6. Effect of temperature on hydrolysis reaction of calcium bromide with $100H_2O/H_2$ at 1 atm

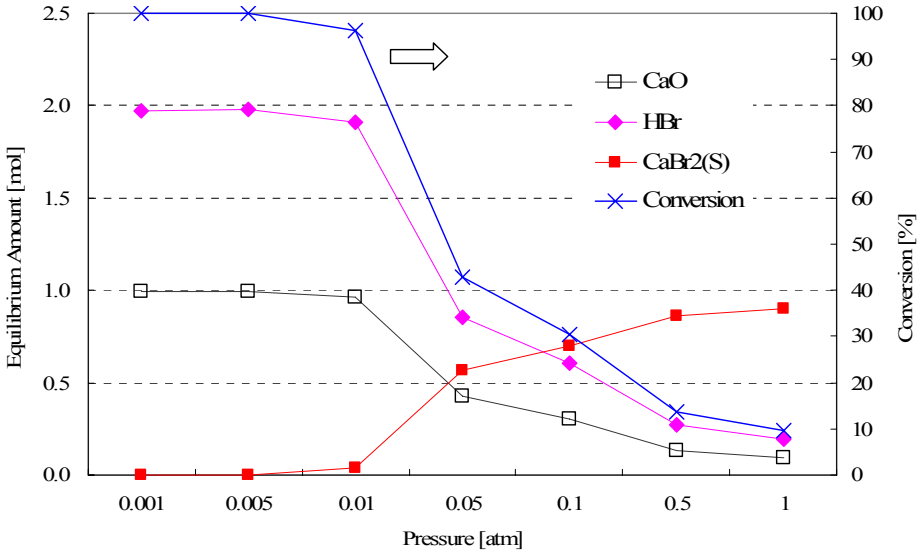

Figure 4-7. Effect of pressure on hydrolysis reaction of calcium bromide with $100H_2O/H_2$ at 1000K

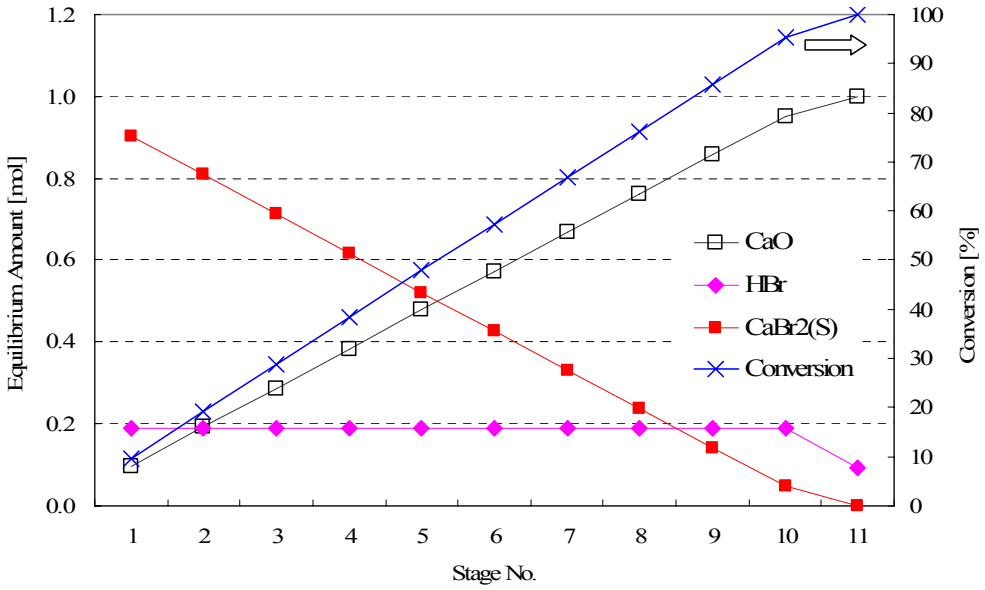

Figure 4-8. Effect of HBr removal from equilibrium states with $100H_2O/H_2$ at 1000K and 1 atm

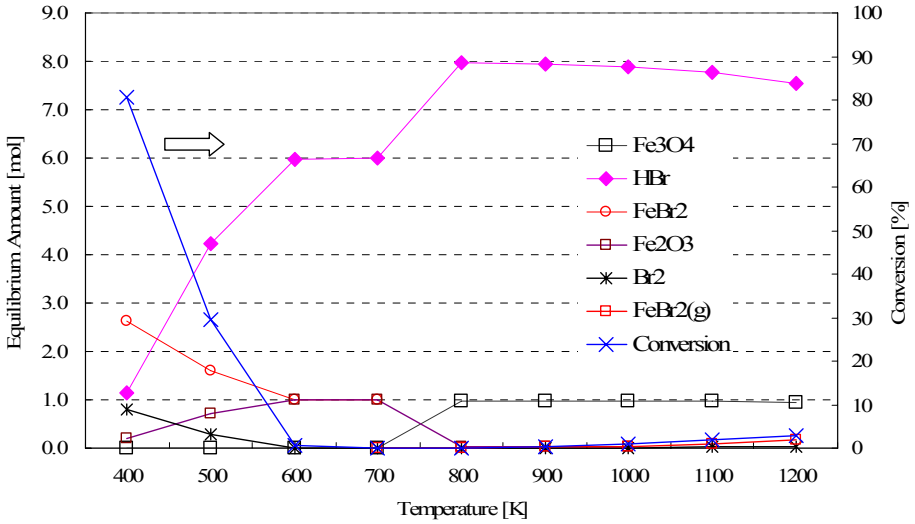

Figure 4-9. Effect of temperature on bromination reaction of iron oxide with $100H_2O/H_2$ at 1 atm

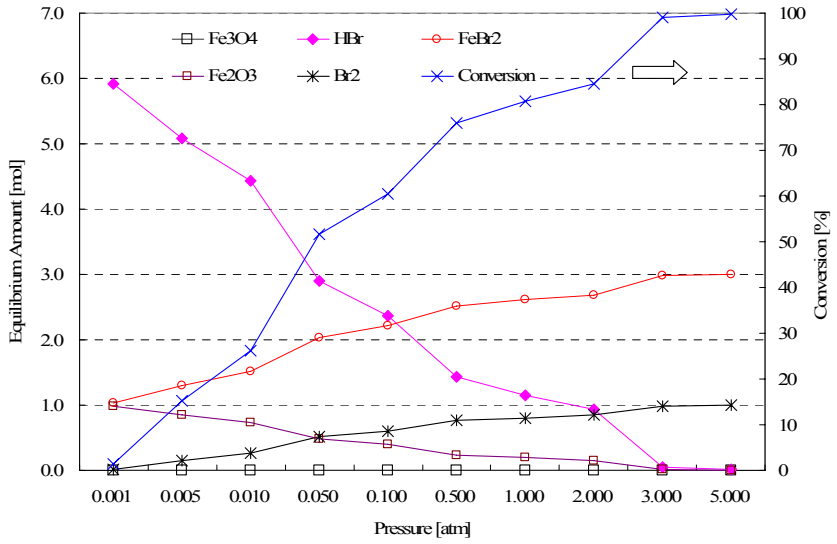

Figure 4-10. Effect of operation pressure on the bromination reaction of iron oxide at 400K with $100H_2O/H_2$

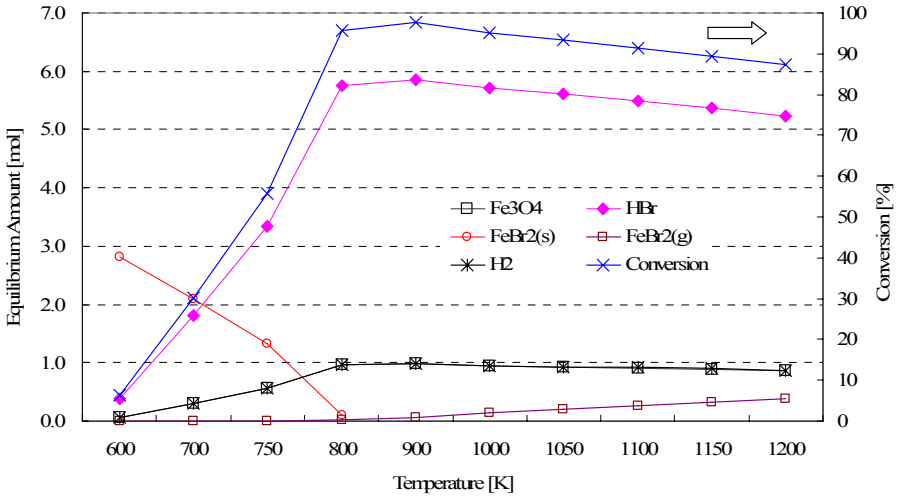

Figure 4-11. Effect of temperature on hydrolysis reaction of iron bromide at 1 atm with $100H_2O/H_2$

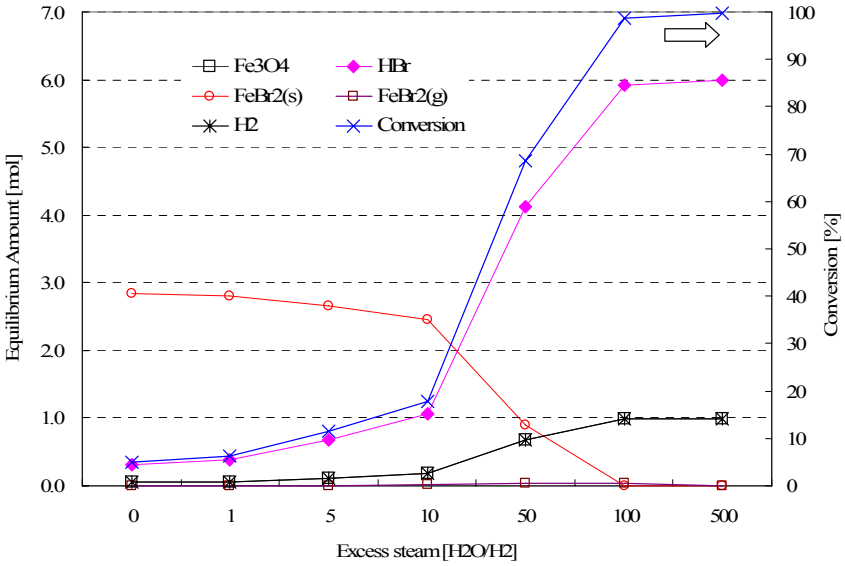

Figure 4-12. Effect of excess steam on hydrolysis reaction of iron bromide at 800K and 1 atm

Table 4-1. Optimum conditions for the bromination of calcium oxide

Reaction Conditions	Optimum value
Excess Steam Quantity	$100H_2O/H_2$
Temperature	873K
Pressure	1 atm

Table 4-2. Optimum conditions for the hydrolysis of calcium bromide

Reaction Conditions	Optimum value
Excess Steam Quantity	$100H_2O/H_2$
Temperature	1000K
Pressure	1 atm

Table 4-3. Optimum conditions for the bromination of iron oxide

Reaction Conditions	Optimum value
Excess Steam Quantity	$100H_2O/H_2$
Temperature	400K
Pressure	3 atm

Table 4-4. Optimum conditions for the hydrolysis of iron bromide

Reaction Conditions	Optimum value
Excess Steam Quantity	$100H_2O/H_2$
Temperature	800K
Pressure	1 atm

Table 4-5. Optimal conditions and expected conversions of the reactions in UT-3 cycle with $100H_2O/H2$

No.	Reaction	Temperature [K]	Pressure [atm]	Expected Conversion
R1	$CaO(s) + Br_2(g) \rightarrow CaBr_2(s) + 0.5O_2(g)$	873	1	94.8 %
R2	$CaBr_2(s) + H_2O(g) \rightarrow CaO(s) + 2HBr(g)$	1000	1	Completed*
R3	$Fe_3O_4(s) + 8HBr(g) \rightarrow 3FeBr_2(s) + Br_2(g) + 4H_2O(g)$	400	3	99.0 %
R4	$3FeBr_2(s) + 4H_2O(g) \rightarrow Fe_3O_4(s) + 6HBr(g) + H_2(g)$	800	1	95.7 %

* The conversion was expected to be completed by removing the product gas according to the Le Chatelier's principle.

CHAPTER 5
PREPARATION AND EVALUATION OF CALCIUM OXIDE REACTANT FOR UT-3 CYCLE

Calcium oxide is involved in two of the four gas-solid reactions in UT-3 cycle. It is converted to calcium bromide by bromination reaction with bromine, and the produced calcium bromide is reconverted into the original calcium oxide during hydrolysis reaction with water. The cyclic reactions must be continuously maintained at high conversion and rates for the UT-3 cycle to be practically viable. Aihara et al. (1990) proposed and made calcium oxide pellets that contain calcium oxide particles dispersed and immobilized in an inert matrix of calcium titanate ($CaTiO_3$) through a procedure based on alkoxide chemistry and sol-gel process. Then they evaluated the pellets in cyclic bromination-hydrolysis reactions and found that the performance was enhanced considerably. However the preparation procedures seem rather complicated and expensive and the practicality of the pellet-type reactant is still in doubt in the long operation. Moreover, Lemort et al. (2006) suggested the possibility of decomposition of the inert material, calcium titanate ($CaTiO_3$) in the pellets by HBr.

In this study, conventional calcium oxide pellets and new developed calcium oxide fabric in which calcium oxide dispersed and immobilized on a yttria fabric were fabricated and evaluated experimentally.

5.1 Calcium Oxide Pellets

The procedure for conventional pellets was developed based on the alkoxide chemistry and sol-gel process of Aihara et al. (1990 and 1992) and Sakurai et al. (1995). The calcium oxide pellets contain calcium oxide reactant dispersed and immobilized in an inert material, calcium titanate ($CaTiO_3$). In this study, pellets were fabricated and their characteristics and performance were evaluated.

5.1.1 Preparation of Calcium Oxide Pellets

A precursor of CaO and $CaTiO_3$ with a mole ratio of 1:2 was synthesized using alkoxide process followed by Sol-Gel technique described by Aihara et al. (1990). Then, predetermined amounts of corn starch, stearic acid, and graphite powders were added into the solution as pore forming agents to increase the porosity in this study while graphite powder and lauric acid were used previously (Sakurai et al., 1995). The amounts of various pore forming agents added are listed in Table 5-1. The slurry was dried via natural evaporation at room temperature for 12h. The resultant powder was crushed, screened and compressed into a specially fabricated cylindrical shaped mold via a uni-axial hydraulic press. The fabricated pellets were then sintered in a furnace in order to strengthen them and burn out the pore forming agents. Heating schedule for the sintering was controlled to ensure mild de-binding of the pore forming agents since rapid burning of additives is a cause of breakage of powder compacts. TG analysis was performed in air by Perkin-Elmer TGA-7 TG Analyzer in order to determine controlled sintering step.

The particle sizes and shape of pore forming agents can be observed with SEM images in Figure 5-1. Based on the micrographs, corn starch and stearic acid are sphere-shaped particles which have approximately 10μm and 200μm in diameter, respectively, while graphite has arbitrary shape.

Figure 5-2 shows a TGA curve of a non-sintered calcium oxide pellet at a heating rate of 10°C /min in air. In the TGA curve, it was observed that residual ethanol and moisture were removed in the first step (60-250°C) and additives were burnt out in the second (250-400°C) and third steps (650-700°C). Considering auto-ignition or thermal decomposition temperature of the additives, it is possible to tell that corn starch, stearic acid and graphite were decomposed during the forepart of the second step, the late stage of second step and the third step, respectively.

On the basis of the TGA result shown in Figure 5-3, the heating profile for sintering was determined. The furnace temperature was slowly increased in the range of burning of additives to decrease the adverse effect of the thermal decomposition of the additives on the final strength of the pellets.

The cylindrical shaped calcium oxide pellets approximately 4mm in diameter and 10mm long were obtained after sintering. A brief procedure of the Ca-pellets preparation is shown in Figure 5-4.

5.1.2 Characterization

The fabricated pellets were subsequently characterized using XRD experiments and Mercury porosimeter.

The composition of the pellets was investigated by XRD experiments to verify the presence of both calcium oxide, CaO, and calcium titanate, $CaTiO_3$. XRD peaks shown in Figure 5-5 indicate the presence of calcium oxide and calcium titanate in the pellet.

The pore size distributions of the pellets were measured by Quantachrome Autoscan 60 Mercury porosimeter from Quantachrome instruments. The pore size distributions of each sample are shown in Figure 5-6. A definite increase of total pore volume was observed by adding pore forming agents. Addition of stearic acid increased the pores greater than 5μm while the addition of graphite and corn starch contributed to the formation of pores less than 5μm. On the surface of the pellets with added stearic acid (samples 3 and 4), macroscopic pores were detected. On the other hand, it was found that the addition of the pore forming agents decreased the strength of the pellets. From the pore size distributions shown in Figure 5-6, it was ascertained that the pore size distribution of pellets was strongly influenced by the type of additives used.

5.1.3 Kinetic Measurements

The bromination and hydrolysis reactions of the selected Ca-pellets were conducted using laboratory experimental set-up shown in Figure 5-7. The schematic diagram of the facility is shown in Figure 5-8.

A CaO reactant-pellet was placed in a platinum basket that was hung from a self-constructed precision spring balance which was purged with nitrogen. The reactor temperature was controlled by a K-type thermocouple installed right under the basket. Bromine and steam were supplied as gases and nitrogen was used as a carrier gas. The weight change of the pellet during the reaction is proportional to the spring deflection, which was detected by a microscope.

The conversion, a measure of the progress of a reaction, is defined as the moles of a species that have reacted over the moles of the same species initially present. Therefore, it is represented as follows (Aihara et al., 1990);

$$X = \frac{M_{CaO}(W - W_o)}{W_o R_{CaO}(M_{CaBr_2} - M_{CaO})} \tag{5-1}$$

where M is molecular weight, W is weight of the sample during reaction, W_0 is weight of a fresh sintered sample, and R_{CaO} is weight fraction of calcium oxide in the fresh sample. The weight change of the sample, $W-W_0$, was determined using the spring constant and deflection of the spring measured by a microscope.

Table 5-2 gives the characteristics measured by the porosimeter and the experimental data by the kinetic measurements. Sample 1 had the largest surface area since small pores account for the surface area. The hydrolysis rate was accelerated by increasing the pore volume greater than 5μm since these pores contribute to the diffusion characteristics inside the pellet. However, our measured rate was still slower than the best result reported by Sakurai et al. (1995).

Cyclic experimental tests were conducted using one of the samples with excellent characteristics in order to see the practical feasibility of the pellets. The temperatures for bromination and hydrolysis reaction were selected as 600°C and 700°C, respectively, based on the thermodynamic analysis and previous studies. For the bromination reaction, bromine and water were supplied while only steam was supplied for hydrolysis reaction. The bromine concentration for bromination and water concentration for hydrolysis were 2.6 mol % and 90 mol %, respectively. The feed for the bromination reaction contained approximately 27 times excess steam per mole of hydrogen production. Nitrogen was used as a carrier gas and a purge gas of the spring balance.

Figure 5-9 shows two cyclic conversion profiles of the bromination and hydrolysis reactions. It took less than ten minutes to reach the maximum conversion in the bromination reaction. The hydrolysis reaction was much slower as compared to bromination reaction. Degradation was observed during the cyclic operations. 70% conversion was attained in the first cycle, while about 50% conversion was achieved in the second. It was also observed that the hydrolysis rate was retarded in the second cycle.

In order to investigate the mechanism of degradation, the changes in the pore size distributions after bromination and hydrolysis processes were measured using a Mercury porosimeter. As shown in Figure 5-10 and Figure 5-11, the pore volume was reduced by almost half in the process of bromination possibly due to expansion of the solid reactant. The pores greater than 5μm were decreased by about 35% after bromination and were regenerated about 20% after hydrolysis. The pores less than 5μm were much more seriously affected by the reactions. The pores less than 5μm were decreased by about 55% after bromination and only 9 % were recovered after hydrolysis. From the changes in the pore volume distribution, it was

ascertained that a reduction in the pore volume leads to the degradation of the chemical reactivity in the cyclic operation.

5.2 Calcium Oxide Fabrics

The concerns about attrition and degradation of the pellets are still present and a simpler and inexpensive preparation step of the reactant is preferable, if possible. Further, the pellet-type reactant is inherently unfavorable for the gas-solid reaction including significant volume change because it increases mass transfer resistances. Hence, a new type of calcium oxide reactant was fabricated on a fibrous yttria fabric via a comparatively straightforward and inexpensive immobilization process.

In the beginning, several ceramic materials such as alumina (Al_2O_3), silica (SiO_2), zirconia (ZrO_2) and yttria (Y_2O_3) were considered as a substrate. But the preliminary experiments showed that the performance of all of these materials except yttria severely degraded at the second cycle possibly due to the formation of inert materials such as calcium aluminate, calcium silicate and calcium zirconate due to reactions between calcium oxide and the substrate materials. The experimental results using alumina, silica and zirconia are given in Appendix A. According to the changes of Gibbs free energy of reactions between calcium oxide and the ceramic materials in Figure 5-12, the formation of the inert materials is very feasible. Hence, yttria was selected as the substrate material for the fabric.

5.2.1 Immobilization of Calcium Oxide on a Fibrous Yttria Fabric

A new procedure for the immobilization of calcium oxide on a fibrous yttria fabric was developed by modifying the process presented earlier (Lee et al., 2007) and is shown in Figure 5-13. The nano-sized precipitated calcium carbonate (PCC; average particle size = 70 nm) surface treated with stearic acid to enhance dispersibility was selected as the starting material. The PCC was blended with ethyl alcohol by mechanical stirring for 10 minutes and ultrasonicated for

another 10 minutes to reduce agglomeration. The suspension was dropped onto a dried yttria fabric (YF-50 from Zircar Zirconia, Inc., USA) using a transfer pipette. Then the fabric was dried at 100°C for 30 minutes and subsequently sintered at 900°C for 20 hours in air. During sintering, the PCC on the yttria fabric was converted into calcium oxide. The size of the sintered fabric sample was roughly 30mm (L) x 10mm (W) x 1.27 mm (T).

5.2.2 Characterization

The calcium oxide particles attached well on the yttria fiber in the fresh sintered sample since no particles fell off from shaking or slight impact.

The chemical compositions of the calcium oxide fabric samples were examined by XRD using Philips MRD X'Pert System. The X-ray diffraction patterns of the fresh and brominated samples are shown in Figure 5-14. According to the XRD data, it was confirmed that all of the calcium carbonate was converted to calcium oxide during the sintering and most of the calcium oxide reacted with bromine to form calcium bromide through the bromination reaction.

5.2.3 Cyclic Reaction Experiments

The cyclic reactions, bromination and hydrolysis reactions, were conducted using the experimental set-up illustrated in Figure 5-7. The prepared sample was suspended from a self-constructed precision spring balance in the reactor whose temperature was controlled by a thermocouple installed right under the sample. The bromination and hydrolysis reaction were conducted at 600°C and 700°C, respectively similar to the earlier experiments with pellets. The feed compositions were also same. Bromine and water were supplied for the bromination reaction, while only steam was supplied for the hydrolysis reaction. The bromine concentration was 2.6 mol %, which included a corresponding water of 27 times excess steam, for bromination. Water concentration for hydrolysis was 90 mol %. Nitrogen was also supplied as a carrier gas of the reactant gases and a purge gas of the spring balance.

The cyclic conversion profile of bromination and hydrolysis reactions is shown in Figure 5-15. About 85 percent conversion of the bromination reaction was obtained in 10 minutes, and it was maintained at the same level through the fourth cycle. This conversion was approximately 5% higher than that obtained from the pellets in the earlier studies (Lee et al., 2006; Sakurai et al., 1995). The hydrolysis rate was about 20 percent higher as compared with that of pellets in our studies (Lee et al., 2006) and comparable to that of the pellets in the literature (Sakurai et al., 1995).

The structure of calcium oxide fabric samples was examined by SEM using Hitachi S-800. SEM images of the bare yttria fabric, fresh calcium oxide fabric sample, and brominated sample are displayed in Figure 5-16. The diameter of the yttria fibers on the original fabric is in the range of approximately 8 to 10 μm (Figure 5-16(A)). As illustrated in the Figure 5-16(B), the surface of the yttria fiber in a fresh sample was tightly covered by interconnected calcium oxide particles with a few hundred nanometer diameter. The changes in the structure of the sample by the bromination reaction were very noticeable, as shown in Figure 5-16(C). After bromination, it was observed that the volume of the particles increased from calcium oxide to calcium bromide and the brominated particles were merged or overlapped.

The amount of calcium oxide in the fresh fabric sample was about 11 wt %, which is almost half of the quantity in the calcium oxide pellet. Lesser inert material is preferable as long as there is no adverse effect on the performance of the reactant in order to reduce the preparation cost and operational energy. For this reason, an attempt was made to increase the calcium oxide content through repetitive impregnation steps. The impregnation steps resulted in a much higher calcium oxide content in the sample (22 wt %). Cyclic performance of the samples thus prepared was examined for the first cycle. The results for the samples with various calcium oxide contents

(8.7, 10.7, 11.9, 22 wt %) are compared in Figure 5-17. As shown in the figure, the hydrolysis rate was retarded by nearly a factor of two as the content increased by two times, while the maximum bromination conversion was not affected much.

5.2.4 Error Analysis

The resolution of the balance to determine the weight fraction of calcium oxide in the sample is 0.1 mg. The spring rate of the spring hung in the balance was measured to be 13.30 ± 0.03 mm/g through repeated microscopic measurements using standard masses. Hence, the uncertainty in measurement of the spring deflection by the microscope was 0.03 mm which is approximately equivalent to 2.2 mg. The combined uncertainties of each measurement in cyclic reactions were graphically represented as the error bar in figures.

5.3 Conclusion and Summary

Porous Ca-pellets for UT-3 thermochemical cycle were prepared and characterized. A set of Ca-pellet samples with different amounts of pore forming agents was fabricated and compared with one another with respect to pore size distribution, conversion and reaction rate. From the characterization and kinetic studies, it was ascertained that the amount and type of additives have an important effect on the pore volume, and increasing the volume of pores greater than 5μm speeds up the hydrolysis rate of the Ca-pellets. Degradation of the bromination reaction was observed during the cyclic experiment. 70% conversion in the first cycle dropped to 50% in the second. It was also observed that the hydrolysis rate was retarded in the second cycle. The degradation in the cyclic operation was found to be caused by a reduction in the pore volume based on the changes in the pore volume distribution.

An inexpensive and straightforward calcium oxide immobilization process on a yttria fabric was developed. Based on the experimental results in the cyclic reactions, the calcium oxide reactant on the yttria fabric had continuous higher reactivity (~ 85%) in the bromination

reaction during four cycles, and the rate of hydrolysis reaction was comparable to that of calcium oxide pellets.

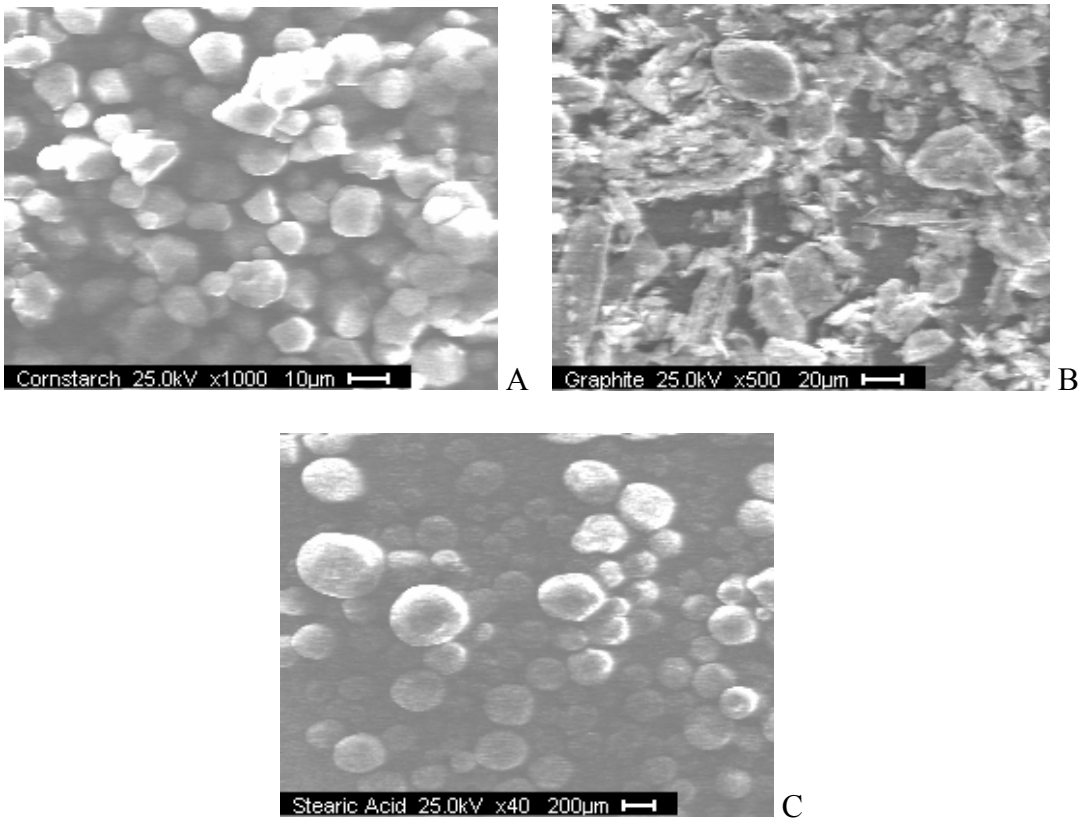

Figure 5-1. The SEM images of pore forming agents. A) Corn starch. B) Graphite. C) Stearic acid.

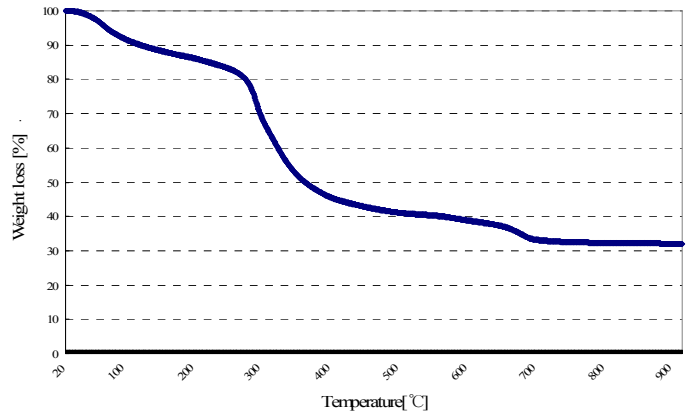

Figure 5-2. The TGA curve of a non-sintered calcium oxide pellet at a heating rate of 10°C /min in air

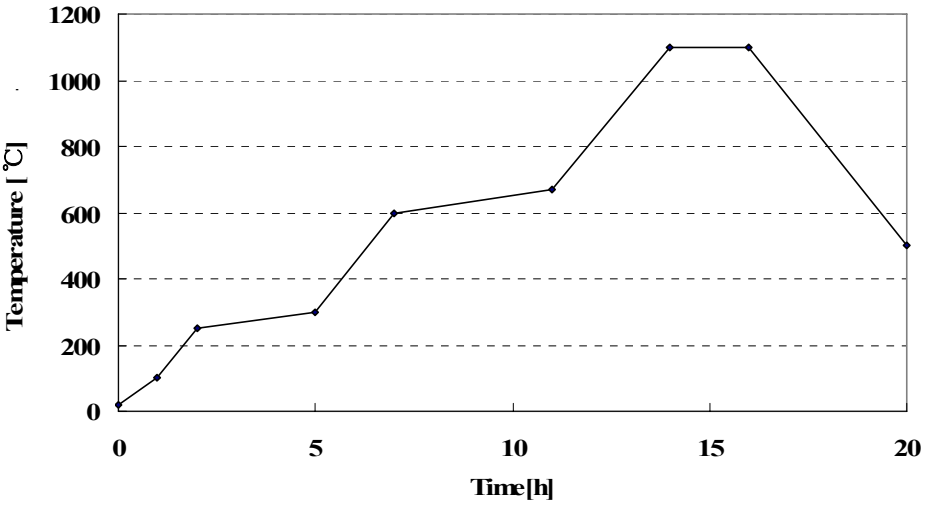

Figure 5-3. Sintering steps for Ca-pellets

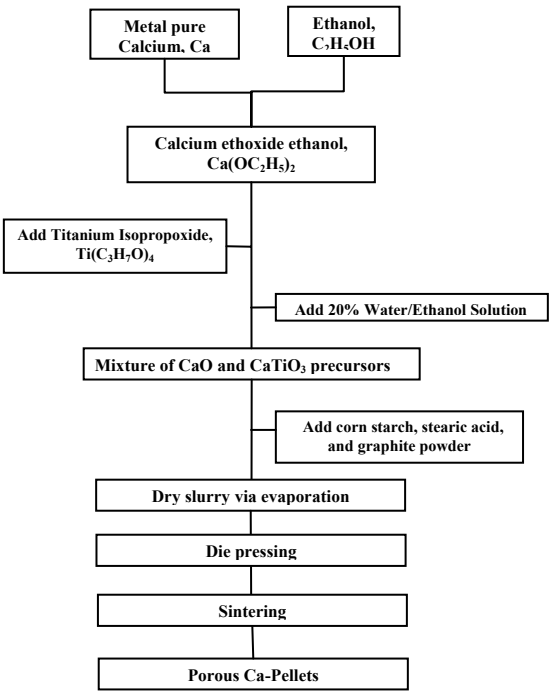

Figure 5-4. Flow diagram for the preparation of Ca-pellets

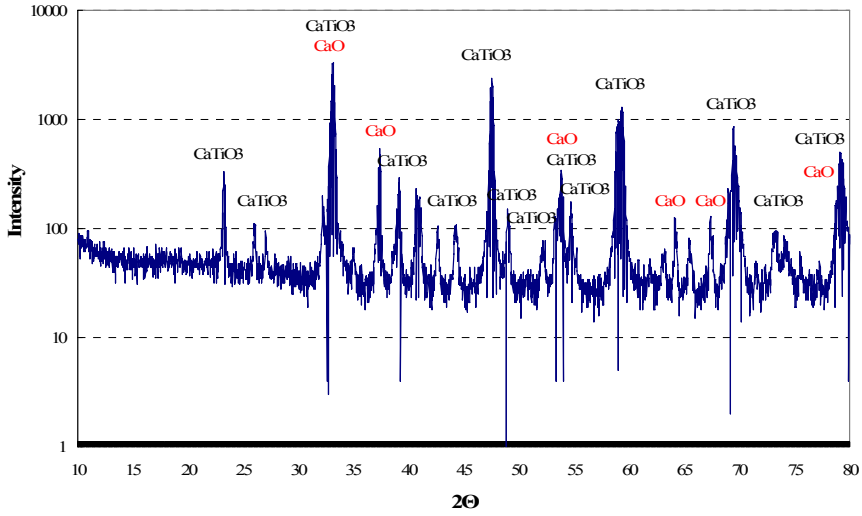

Figure 5-5. The XRD pattern of the fresh calcium oxide pellet

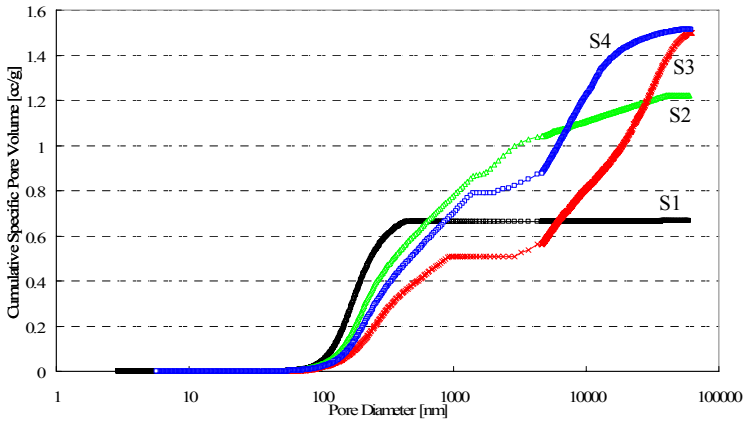

Figure 5-6. Pore size distributions of Ca-pellets (Sample 1-4) prepared with different pore forming agents

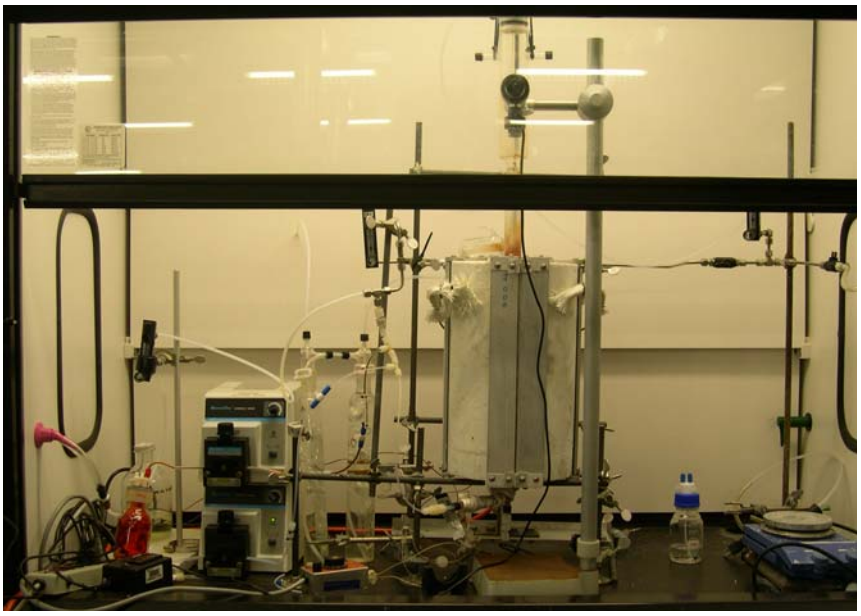

Figure 5-7. Laboratory Set-up

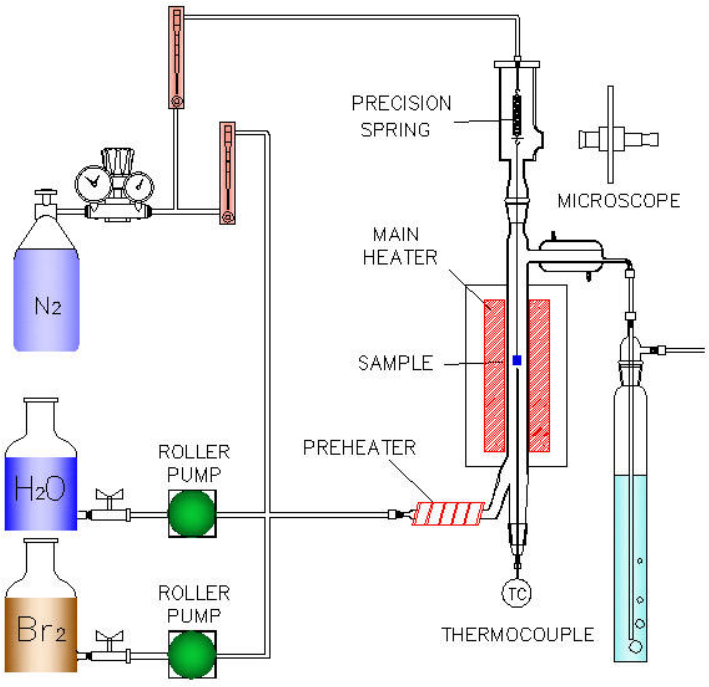

Figure 5-8. Schematic Diagram for Laboratory Set-up

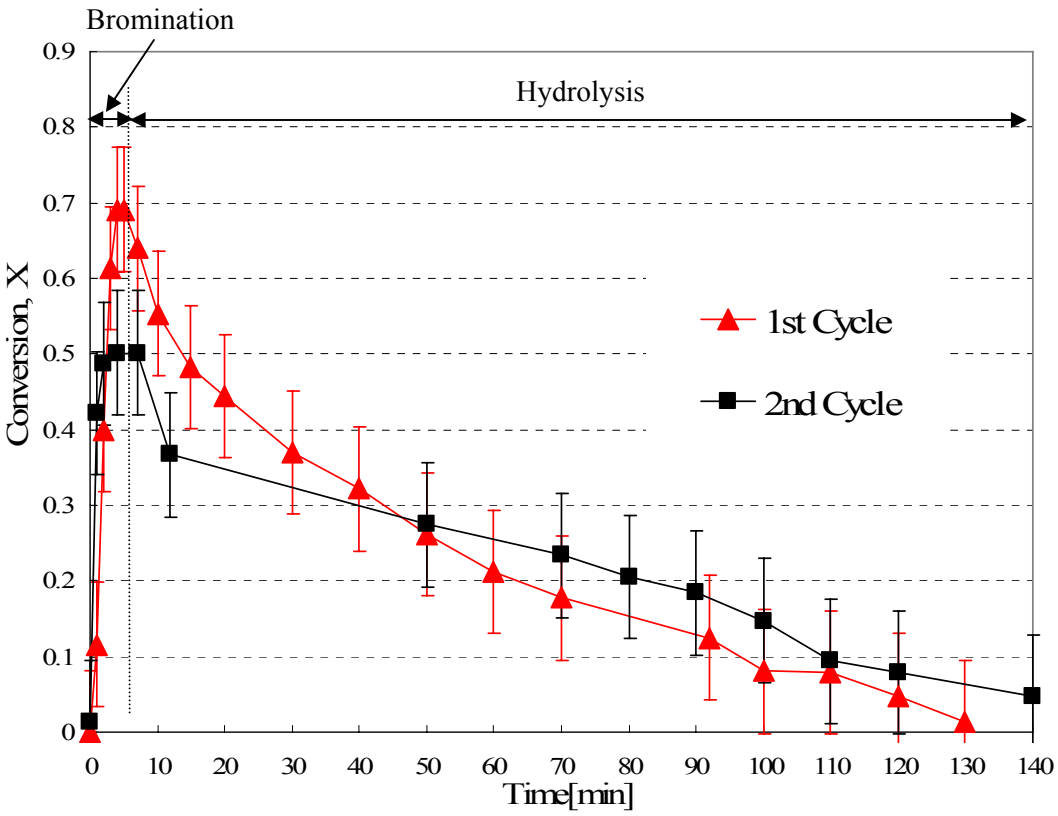

Figure 5-9. Cyclic conversion profiles of a calcium oxide pellet (Sample: S4)

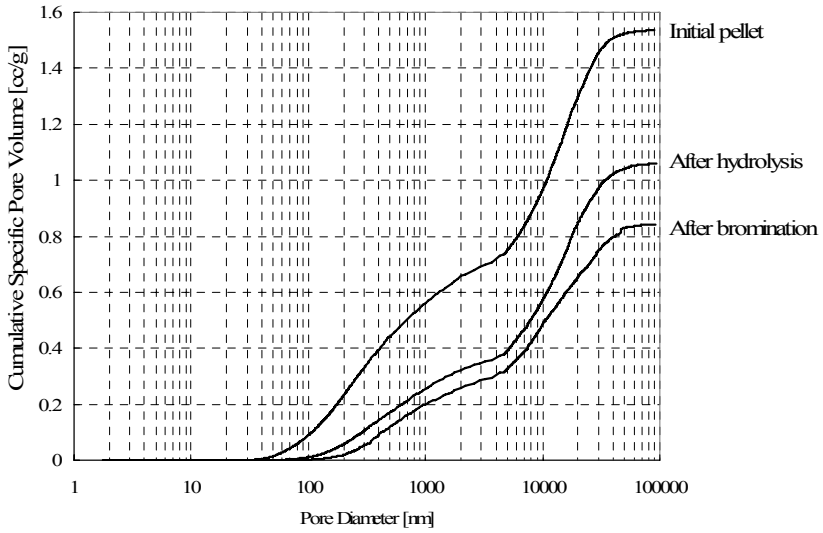

Figure 5-10. Changes of pore size distribution after bromination and hydrolysis in a calcium oxide pellet

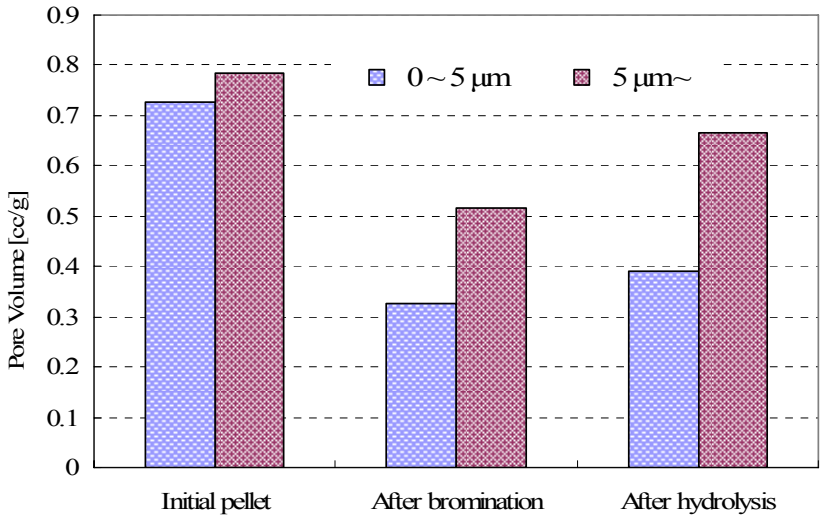

Figure 5-11. Comparison of pore volumes of initial, after bromination and after hydrolysis in a calcium oxide pellet

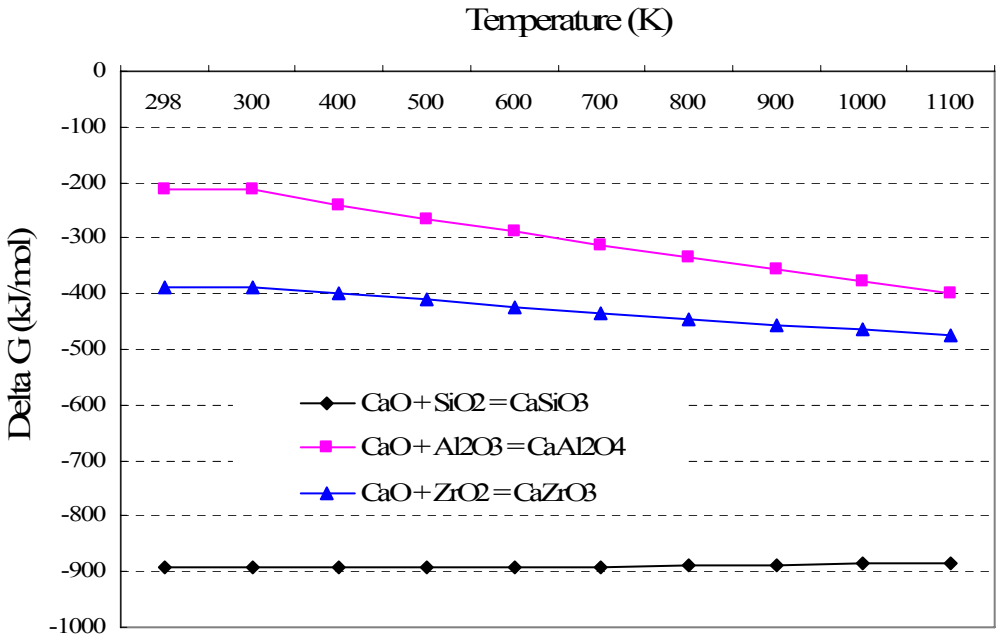

Figure 5-12. Changes of Gibbs free energy of reactions between calcium oxide and ceramic materials as a function of reaction temperature

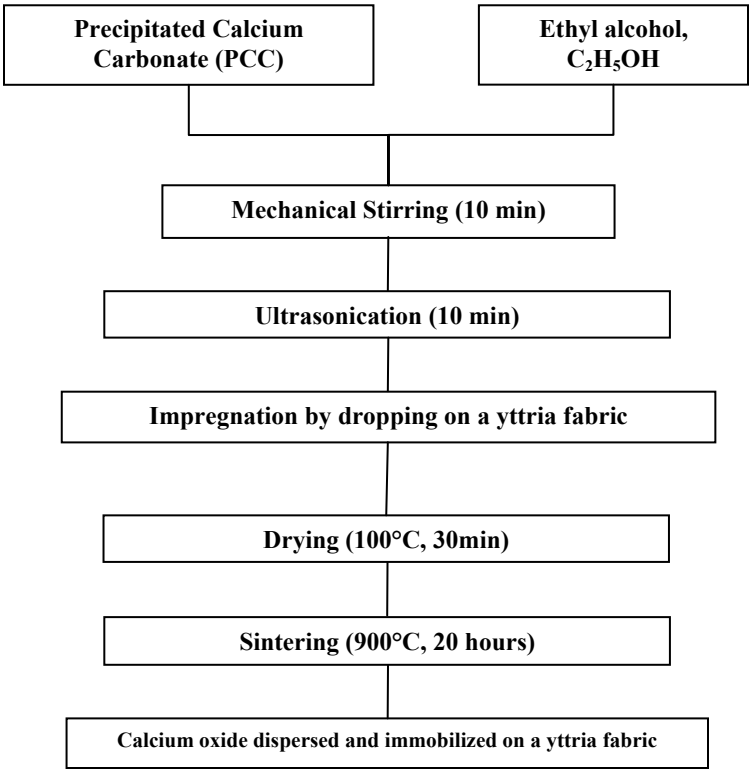

Figure 5-13. Preparation steps for impregnation of calcium oxide on a yttria fabric

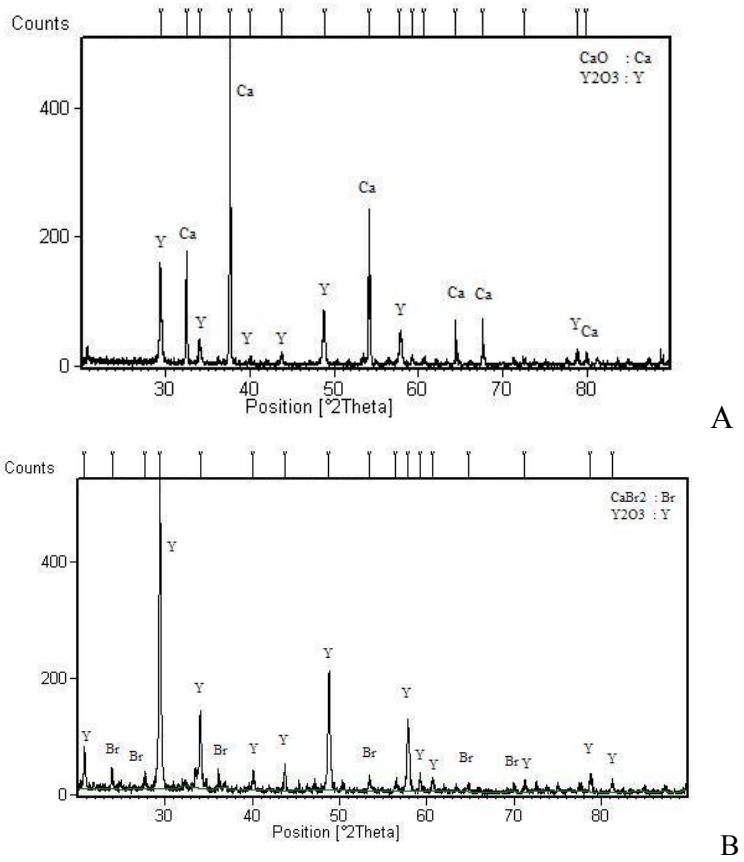

Figure 5-14. The XRD patterns of the samples. A) Fresh sintered. B) After bromination reaction.

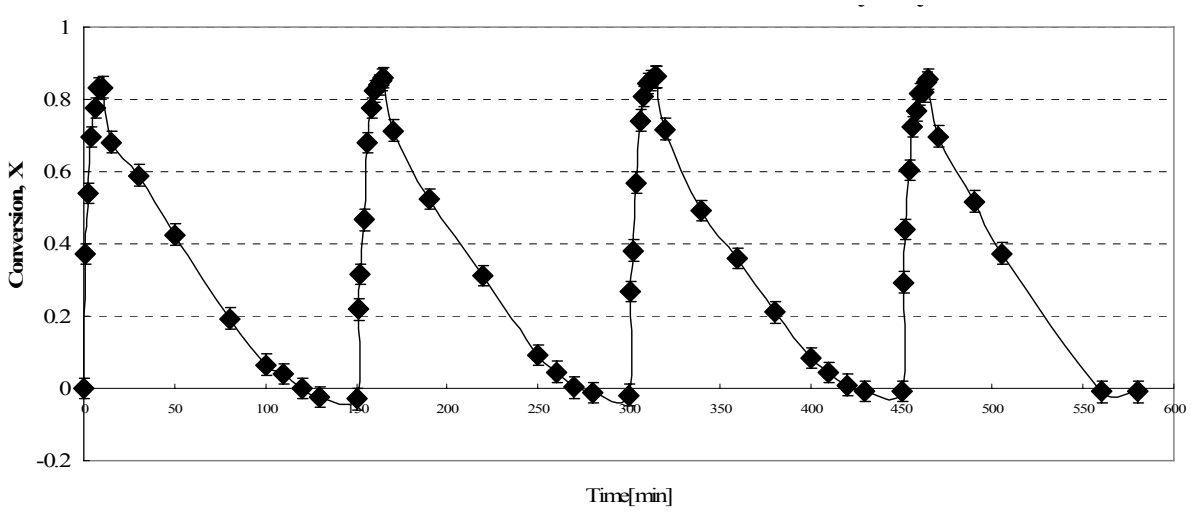

Figure 5-15. Conversion profiles of cyclic reactions, bromination and hydrolysis, of the calcium oxide fabric sample

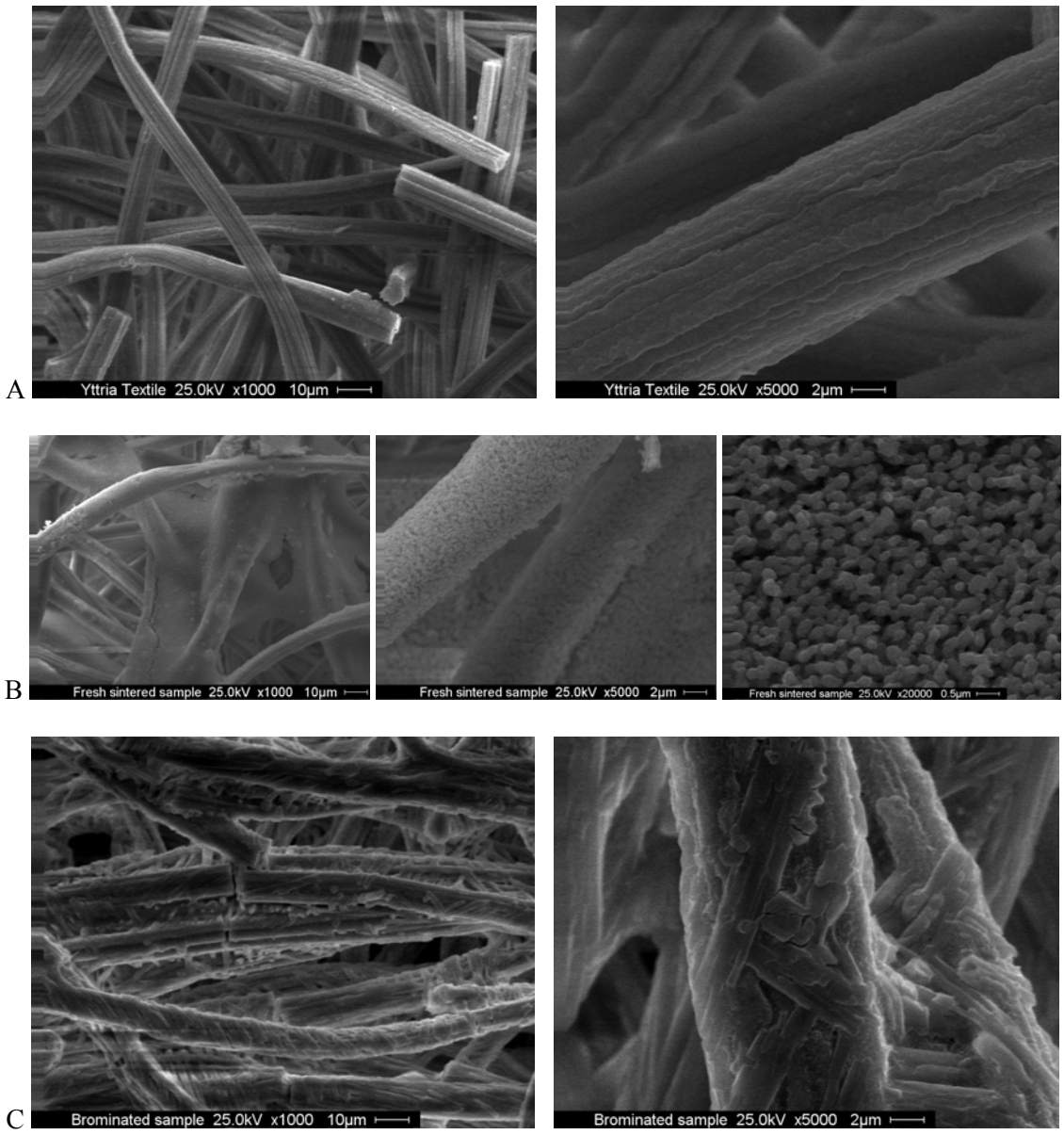

Figure 5-16. The SEM images of samples. A) Bare yttria fabric. B) Fresh calcium oxide fabric sample. C) Brominated sample.

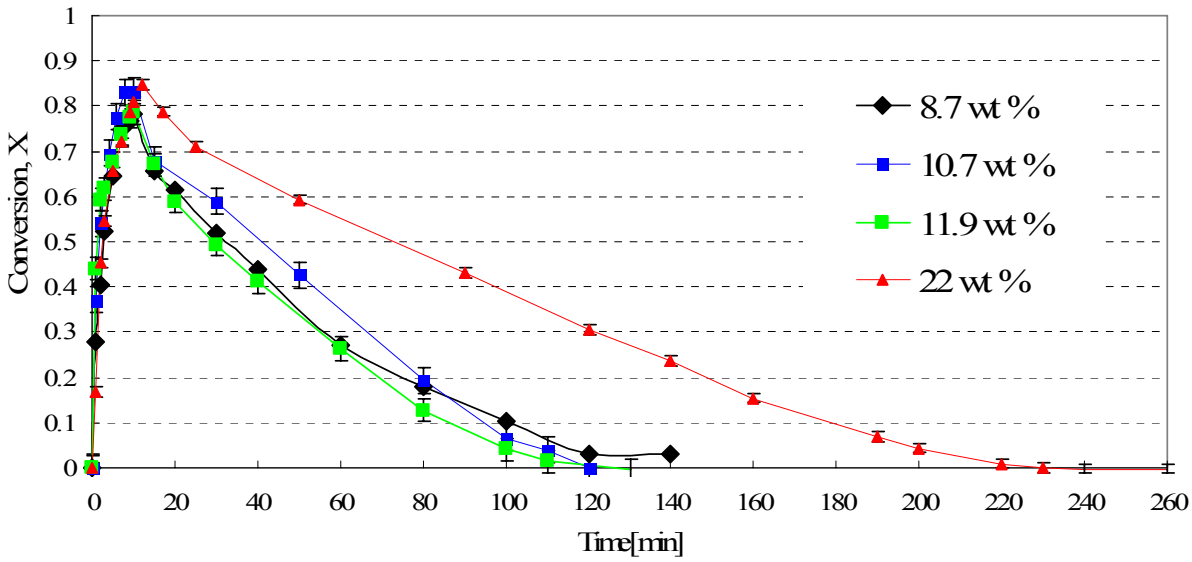

Figure 5-17. Comparison of the first cyclic reactions of calcium oxide fabric samples with various amounts of calcium oxide in the fabric sample

Table 5-1. Composition conditions for the pellets with different additives

Sample	Additives (wt %)		
	Corn [a] Starch	Stearic [b] acid	Graphite [b]
S1	0	0	0
S2	0	0	100
S3	0	100	100
S4	100	50	50

[a] The content of corn starch is expressed as weight percent of calcium. [b] The contents of stearic acid and graphite are expressed as weight percent of the sintered pellet.

Table 5-2. Characteristics and experimental data of Ca-pellets

Sample	Surface area (m^2/g)	Total pore volume (cc/g)	Max. Conversion	Hydrolysis time (min)
S1	7.61	0.6587	0.65	> 400
S2	6.69	1.213	-	-
S3	4.01	1.501	0.81	130
S4	5.58	1.508	0.71	120

CHAPTER 6
THERMAL EFFICIENCY OF UT-3 PROCESS

6.1 Analysis Description

The thermal efficiency of UT-3 cycle was evaluated thermodynamically. This parametric study focused on the effects of inert material amounts in the solid reactants, incomplete conversion and heat recovery on the efficiency. These parameters were not considered as a major factor for UT-3 process in great depth by other researchers, but the factors would have significant influence on the efficiency as well as the operation cost in the actual scale plants since the solid reactants contain considerable amounts of inert materials and all reactions were found to be fractionally completed according to the experiments in this and previous studies.

The thermal efficiencies (η) were calculated based on the higher heating value (HHV) of the produced hydrogen according to the following equation:

$$\eta = \frac{HHV\ of\ H_2}{H_{in}} \tag{6-1}$$

where, HHV of H_2 = 286kJ/mol and H_{in} = Total heat input per mole of hydrogen to the system.

In the analysis, one mole of hydrogen production was considered and operating pressure was 1 atm. Assumptions for this study are listed below:

- Negligible pressure drop, pumping work, and heat loss
- No excess water
- No separation work
- In pinch analysis, the minimum approach temperature (ΔT_{min}) is assumed to be 20K.

6.2 Pinch Analysis

In order to determine feasible heat recovery in the process, pinch analysis was employed in this thermodynamic analysis. The pinch analysis also known as pinch point analysis has been used as a simple and efficient means to improve energy saving and reduce initial capital cost via optimization of the heat exchanger network in the industrial applications (Ebrahim et al., 2000)

since introduced by Linnhoff and Flower (1978). In the pinch analysis, hot and cold composite curves which represent heat availability and demand in the process are plotted with a gap by the minimum approach temperature (ΔT_{min}) on a temperature-enthalpy diagram shown in Figure 6-1(A). The maximum amount of the possible heat recovery, the overlap region between the two composite curves, is indicated in Figure 6-1(B) (National Resources Canada, 2003).

6.3 Thermodynamic Analysis

The thermodynamic data for the four reactions in the UT-3 cycle were calculated using FactSage thermochemical software and databases (FactSage, Web version) and are summarized in Table 6-1. The optimized reaction temperatures determined in Chapter. 4 were employed. As shown in the Table 6-1, two bromination reactions, R1 and R3, are exothermic which release heat. On the other hand, the two hydrolysis reactions, R2 and R4, are endothermic which require thermal energy to drive the reactions. The total heat input for exothermic chemical reactions was 593.5kJ/mol and the total rejected heat from exothermic reactions was 345.95kJ/mol. The rejected heat from the exothermic reactions can be utilized for the endothermic reactions or heating of the reactant steam.

The material and heat flow sheet for the whole process is illustrated in Figure 6-2. The cooling and heating of all reactants and products for the following reactions are indicated and the inert materials and incompletion of the conversion are not taken into account in the figure. It was assumed that one mole of water is supplied and one mole of hydrogen and a half of oxygen were produced at ambient temperature.

6.3.1 Ideal Case (Case 1: Complete Conversion and No Inert Materials)

Ideally, UT-3 process may be operated as shown in Figure 6-2. One mole of hydrogen can be produced with the chemicals in the flowsheet provided all the reactions are completed and no inert materials are required in the solid reactants.

The enthalpy changes for the heating and cooling of the materials were calculated in consideration of the sensible and latent heats in the process. The sensible enthalpies were determined using a mean heat capacity over the temperature range. The required energy for heating was 261.3kJ and the rejected heat from cooling processes was 228kJ to produce one mole of hydrogen, respectively.

The amount of recovered heat from the cooling processes and exothermic reactions was calculated via pinch analysis. The hot composite curve represents heat available in the process and cold composite curve represents heat demand for the process are plotted in Figure 6-3(A) and (B), respectively. The combined composite curves with the minimum approach temperature (20K) are plotted in Figure 6-3(C). According to the pinch analysis, the maximum amount of recovered heat was 324kJ.

The thermal efficiencies were calculated with and without heat recovery. The calculated thermal efficiencies with and without heat recovery were 53.9 and 33.5% as shown in Table 6-3.

6.3.2 Effect of Inert Materials on Efficiency (Case 2: Complete Conversion and Including Inert Materials)

The solid reactants are integrated forms of actual reactants and inert materials in order to make the reactants reactive and durable in the cyclic transformation. Calcium titanate ($CaTiO_3$, Aihara et al., 1999) and iron titanate (Fe_2TiO_5, Sakurai et al., 2006) were used for calcium oxide pellets and iron oxide pellets as the inert material, respectively. In this study, yttria fibers play the role of supporting the calcium oxide reactant. The amount of the inert material was greater than the reactant in the final forms of pellets and fabrics. Hence, the inert materials incorporated in the solid reactants should also be included in the calculation of enthalpy changes for heating and cooling. The efficiency comparison of the pellets of Aihara et al. (1999) and Sakurai et al. (2006) and fabrics in this study is somewhat difficult since the types of inert material and the

molar ratios of the actual reactants to the inert materials are different. The molar ratios of actual reactants to inert materials and the additional energies for the other researchers (pellet) and this study (fabric) were calculated and are listed in the Tables 6-4 and 6-5, respectively. As shown in the tables, the absolute values of energies for heating and cooling of the inert material in each table were same because the inert materials were not consumed or generated during the processes. It was seen that there is a discrepancy of 121.9 kJ (=410.4kJ-288.5kJ) between the values of other researchers and this study because of the difference in the heat capacities of the inert materials and reactant/inert molar ratios.

For pinch analysis, the combined composite curves for pellet and fabric samples with inert materials are plotted in Figure 6-4(A) and (B), respectively.

The thermal efficiencies including the effect of the inert materials are shown in Table 6-6. The 33.5% efficiency without heat recovery dropped to 22.6% and 25% for the pellet type reactants and the fabric type reactants, respectively. With heat recovery, the 53.9% efficiency was slightly reduced to 52.0% and 52.6%, respectively because most of the rejected heat from the cooling of the inert material was recovered in the pinch analysis. However, the minimization of the inert materials is preferable even with heat recovery since the additional capital and operational costs for heat exchangers to recover the rejected heat is required. The reason of the somewhat greater drop in the efficiency for the pellets is mainly due to the higher heat capacities of the inert materials, $CaTiO_3$ and Fe_2TiO_5 compared to that of yttria.

6.3.3 Effect of Inert Material and Incomplete Conversion on Efficiency (Case 3: Including inert material and incomplete conversion (CaO: 85%, Fe_3O_4: 90%))

The effect of incomplete conversion as well as inert material on the thermal efficiency was evaluated. The experiments revealed incompletion of each bromination reaction possibly due to the diffusion limitation of gaseous reactants into the core of the solid reactant. The maximum

conversions of calcium oxide and iron oxide were observed to be 85% (this study) and 90% (Sakurai et al., 2006) in the bromination reaction, respectively. Hence, these values were employed in this calculation. Additional reactants were added to produce one mole of hydrogen due to the incomplete conversion. The energies required and rejected for heating and cooling of inert material, respectively, and the additional unreacted solid reactant are listed in Tables 6-7 and 6-8 for the pellet type reactants from other researchers and for fabric type reactants of this study, respectively.

For pinch analysis, the combined composite curves for pellet and fabric samples with inert materials and incompletion conversion are plotted in Figure 6-5(A) and (B), respectively.

The thermal efficiencies including the effects of inert material & incomplete conversion were calculated and are listed in Table 6-9. The effects of incomplete conversion on the efficiencies of pellets and fabrics were not great due to the high conversions employed in the calculation. The efficiencies dropped by about 1% without heat recovery and by 0.2% with heat recovery due to incomplete conversion.

6.4 Summary of Thermodynamic Analysis

The efficiencies of UT-3 cycle have been evaluated in the earlier studies; however, inert materials, incomplete conversion and heat recovery were not considered in those analyses. In this chapter, a thermodynamic analysis has been carried out in order to determine the effect of the inert materials, incomplete conversion and heat recovery on the efficiency. The analyses used the experimental data on the amounts of inert materials in the pellets and fabrics and the maximum bromination conversions of calcium oxide and iron oxide reactants. The results of the thermodynamic analysis are illustrated in Figure 6-6. Without heat recovery, the efficiency with complete conversion and no inert materials was 33.5% and the efficiencies for pellet and fabric reactants including inert materials were 22.6% and 25.0%, respectively. The efficiencies for

pellet and fabric reactants including inert materials and incomplete conversion were 21.6% and 24.1%, respectively, without heat recovery. With heat recovery, the efficiency with complete conversion and no inert materials was 53.9% and the efficiencies for pellet and fabric reactants including inert materials were 52.0% and 52.6%, respectively. The efficiencies for pellet and fabric reactants including inert materials and incomplete conversion were 51.8% and 52.4%, respectively, with heat recovery. The efficiency differences with and without heat recovery were in the range of 20.4-30.2%. The inert materials accounted for 10.9 and 8.5% reductions of the efficiency for the pellet and fabric reactants, respectively, without heat recovery. On the other hand, the effect of the inert materials on the efficiencies was not considerable with heat recovery since most of the rejected heat from the cooling of the inert material was found to be recovered in the pinch analysis. The efficiencies for the pellet and fabric reactants only dropped by 1.9 and 1.3%, respectively. The thermal efficiencies of the pellets were slightly lower than those of fabric type reactants in this study whether or not heat recovery was used, while the amounts of the inert materials are somewhat smaller. The reason of the lower efficiencies is higher heat capacities of inert materials, $CaTiO_3$ and Fe_2TiO_5, in the pellets compared to the yttria fabric. The influence of incomplete conversion was not significant because of the high conversions, 85% and 95%, used for this estimation. To sum up, it was found that the effect of heat recovery and inert materials cannot be underestimated in the calculation of thermal efficiency of the cycle. Thus, in order to increase the efficiency, heat recovery must be employed and the use of the inert materials should be minimized.

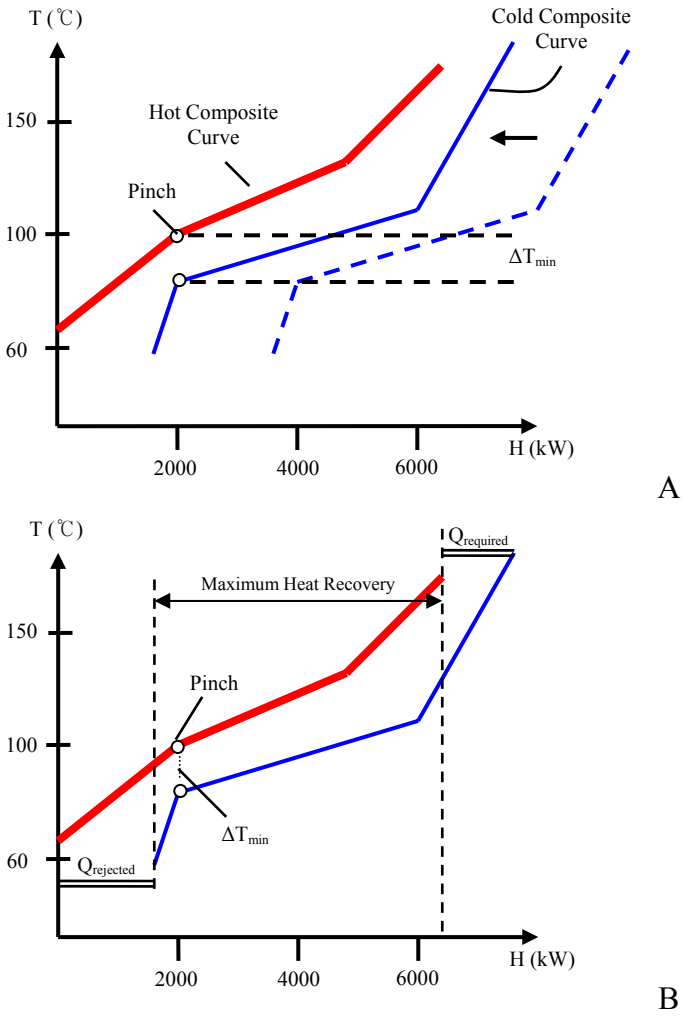

Figure 6-1. Temperature-enthalpy diagrams. A) Hot and cold composite curves and B) maximum heat recovery on temperature-enthalpy diagram. Adapted from National Resources Canada, 2003. *Pinch analysis: for the efficient use of energy, water & hydrogen*, CANMET Energy Technology Centre-Varennes. (Figure 3-5, page 25). Available at http://cetc-varennes.nrcan.gc.ca/fichier.php/codectec/En/2003-140/2003-140e.pdf

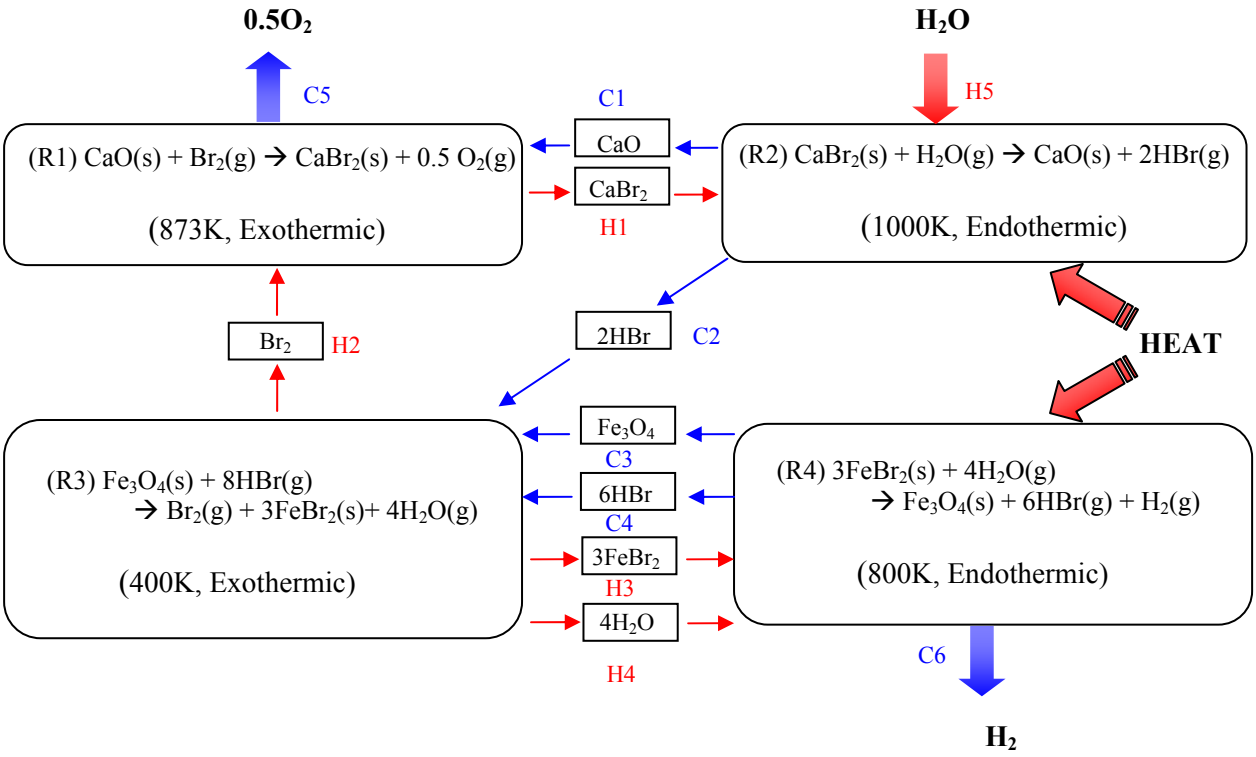

Figure 6-2. Process flowsheet of heat and material in the UT-3 cycle

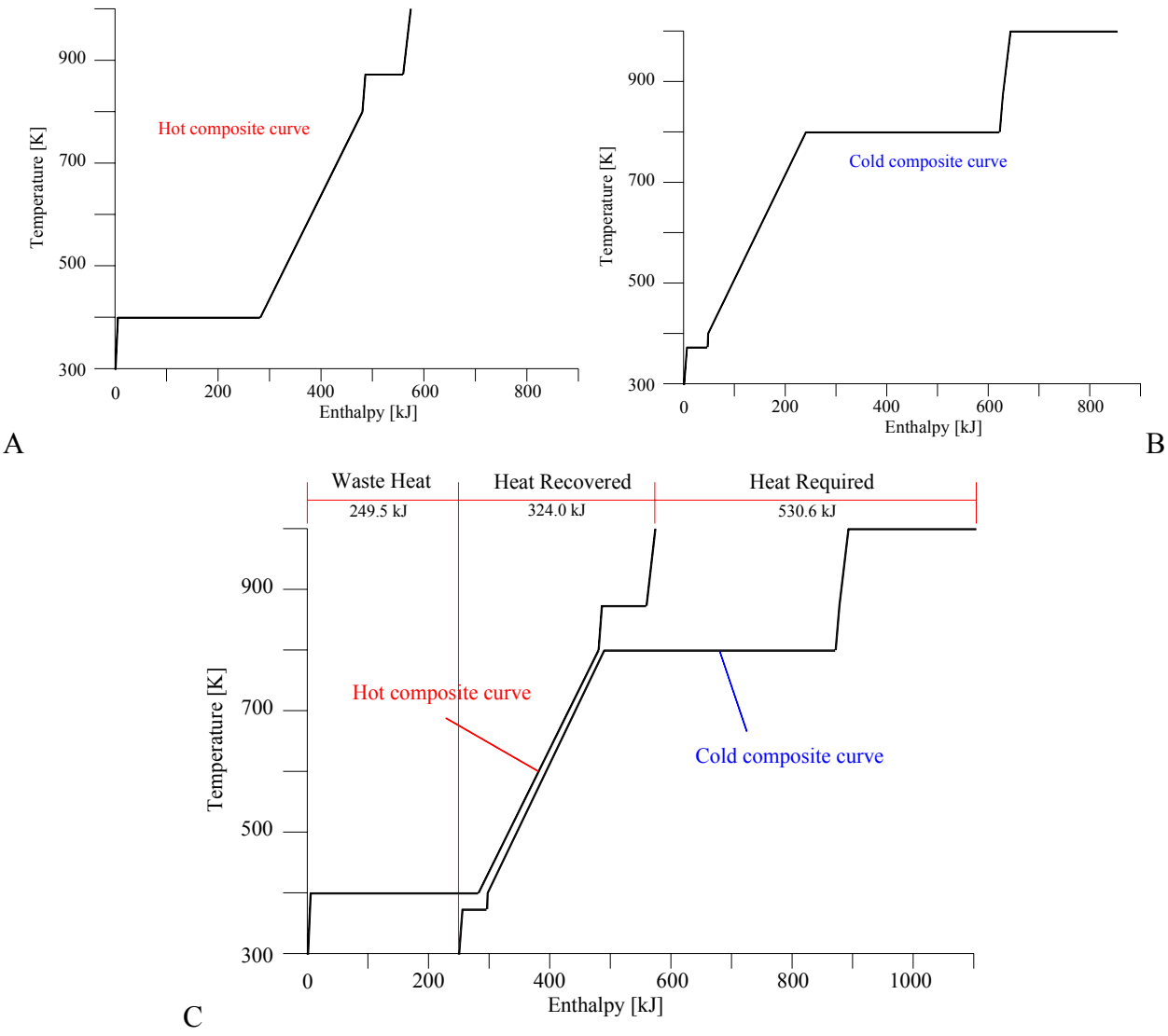

Figure 6-3. Temperature-enthalpy diagrams for Case 1. A) Hot composite curve. B) Cold composite curve. C) Combined composite curves for pinch analysis.

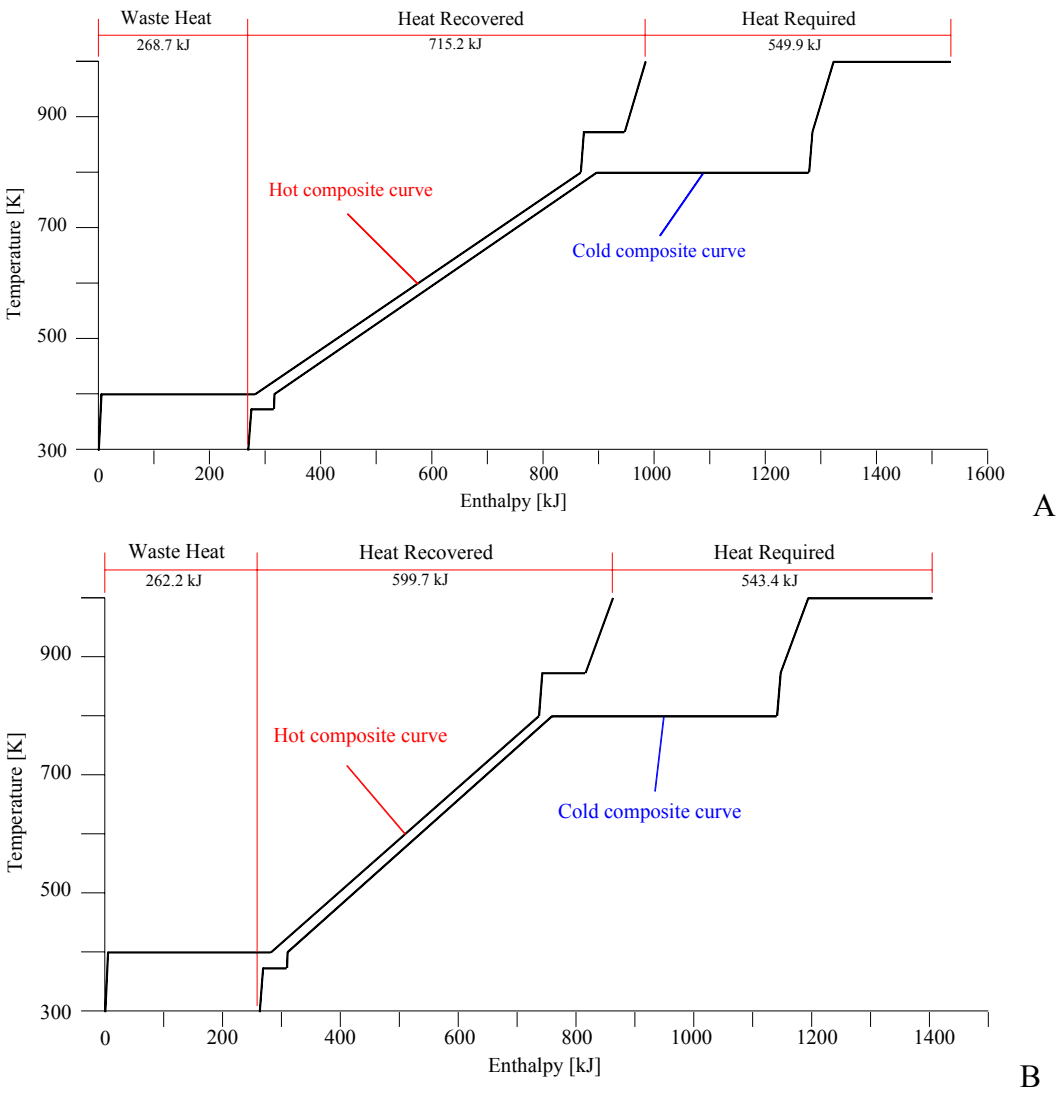

Figure 6-4. Combined composite curves (Case 2). A) Pellet and B) Fabric samples

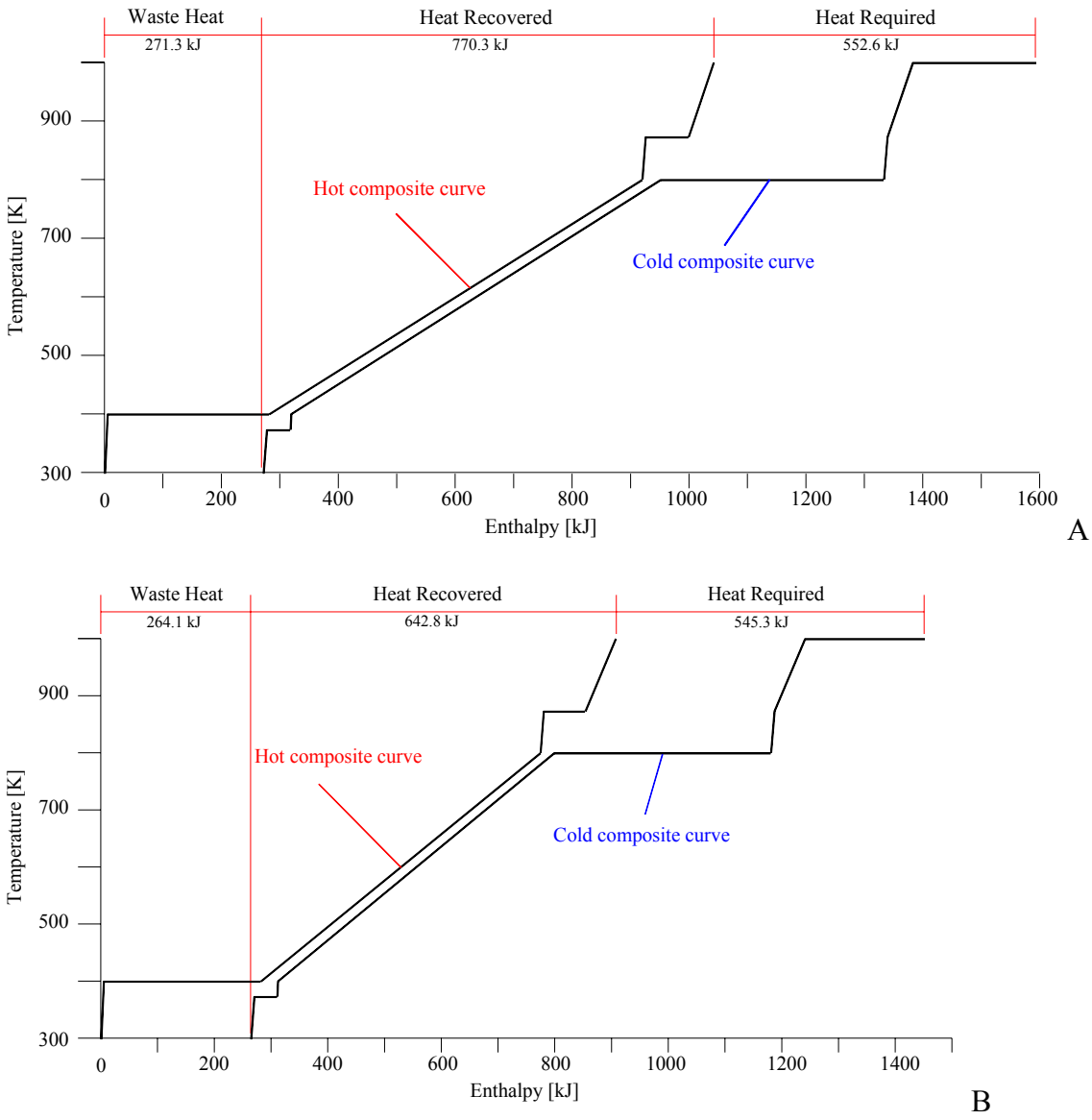

Figure 6-5. Combined composite curves (Case 3). A) Pellet and B) Fabric samples

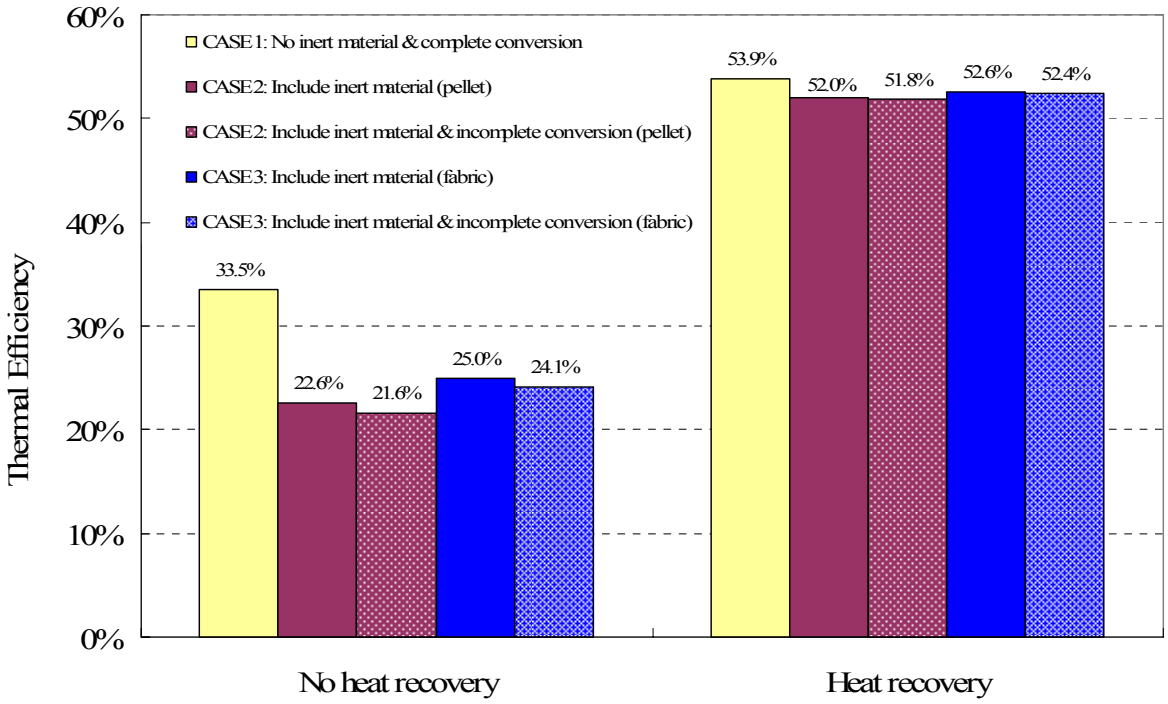

Figure 6-6. Comparison of thermal efficiency in various situations

Table 6-1. Thermodynamic data of the reactions in UT-3 cycle

No.	Reaction	Rx Temp.	ΔH [kJ/mol]	ΔG [kJ/mol]	Remarks
R1	$CaO(s) + Br_2(g) \rightarrow CaBr_2(s) + 0.5O_2(g)$	873K	-73.55	-38.22	Exothermic
R2	$CaBr_2(s) + H_2O(g) \rightarrow CaO(s) + 2HBr(g)$	1000K	211.7	104.3	Endothermic
R3	$Fe_3O_4(s) + 8HBr(g) \rightarrow Br_2(g) + 3FeBr_2(s) + 4H_2O(g)$	400K	-272.4	-149.6	Exothermic
R4	$3FeBr_2(s) + 4H_2O(g) \rightarrow Fe_3O_4(s) + 6HBr(g) + H_2(g)$	800K	381.8	146.3	Endothermic

Table 6-2. Energies required and rejected (Enthalpy change for heating and cooling based on latent heat and sensible heat)

	Heating or cooling	Temperature [K]		Cp [J/(K-mol)]		Enthalpy change [J]		Remark
		Initial	Final	Initial	Final	Latent	Sensible	
H1	$CaBr_2(s) \rightarrow CaBr_2(s)$	873	1000	85.15	88.61		11033.8	
H2	$Br_2(g) \rightarrow Br_2(g)$	400	873	36.67	37.66		17579.8	
H3	$3FeBr_2(s) \rightarrow 3FeBr_2(s)$	400	800	82.50	91.41		104343	3 mol
H4	$4H_2O(g) \rightarrow 4H_2O(g)$	400	800	34.27	38.73		58395.2	4 mol
H5	$H_2O(l) \rightarrow H_2O(g)$	298	373	75.38	76.00	40626.0	5676.64	
		373	1000	34.05	41.26		23609.7	
	Energy required for heating					261.3 kJ		
C1	$CaO(s) \rightarrow CaO(s)$	1000	873	53.51	52.89		-6756.59	
C2	$2HBr(g) \rightarrow 2HBr(g)$	1000	400	32.31	29.22		-36912.6	2 mol
C3	$Fe_3O_4(s) \rightarrow Fe_3O_4(s)$	800	400	266.7	174.0		-88144.6	
C4	$6HBr(g) \rightarrow 6HBr(g)$	800	400	31.07	29.22		-72340.8	6 mol
C5	$0.5O_2(g) \rightarrow 0.5O_2(g)$	873	298	34.20	29.38		-9139.34	0.5 mol
C6	$H_2(g) \rightarrow H_2(g)$	800	298	29.63	28.84		-14675.0	
	Rejected heat from cooling					-228 kJ		

Table 6-3. Thermal efficiencies with complete conversion and no inert materials (Case 1)

	No recovery	Heat recovery
Thermal energy for reactions	593.5 kJ/mol	593.5 kJ/mol
Total energy for heating	261.3 kJ./mol	261.3 kJ./mol
Recovered thermal energy	-	324 kJ/mol
Thermal efficiency	33.5%	53.9%

Table 6-4. Additional energies required and rejected for heating and cooling of inert material $CaO:CaTiO_3$=1:1.4*, $Fe_3O_4:Fe_2TiO_5$=1:5** (Pellet)

	Heating or cooling	Temperature [K]		Cp [J $K^{-1}mol^{-1}$]		Enthalpy change [J/mol]	Total enthalpy change [J]
		Initial	Final	Initial	Final	Sensible	
H6	$CaTiO_3(s)\rightarrow CaTiO_3(s)$	873	1000	128.8	130.4	16458.8	23042.3
H7	$Fe_2TiO_5(s)\rightarrow Fe_2TiO_5(s)$	400	800	182.0	205.4	77473.2	387366
				Energy required for heating			410.4 kJ
C7	$CaTiO_3(s)\rightarrow CaTiO_3(s)$	1000	873	130.4	128.8	-16458.8	-23042.3
C8	$Fe_2TiO_5(s)\rightarrow Fe_2TiO_5(s)$	800	400	205.4	182.0	-77473.2	-387366
				Rejected heat from cooling			-410.4 kJ

* Molar ratio of CaO to $CaTiO_3$ in calcium oxide pellets. (Aihara et al., 1999). ** Molar ratio of Fe_3O_4 to Fe_2TiO_5 in iron oxide pellets. (Sakurai et al., 2006).

Table 6-5. Additional energies required and rejected for heating and cooling of inert material $CaO:Y_2O_3$=1:2*, Fe_3O_4: Y_2O_3=1:5** (Fabric)

	Heating or cooling	Temperature [K]		Cp [J $K^{-1}mol^{-1}$]		Enthalpy change [J/mol]	Total enthalpy change [J]
		Initial	Final	Initial	Final	Sensible	
H6	$Y_2O_3(s)\rightarrow Y_2O_3(s)$	873	1000	124.6	126.9	15970.5	31941
H7	$Y_2O_3(s)\rightarrow Y_2O_3(s)$	400	800	131.8	124.7	51306.8	256534
				Energy required for heating			288.5 kJ
C7	$Y_2O_3(s)\rightarrow Y_2O_3(s)$	1000	873	126.9	124.6	-15970.5	-31941
C8	$Y_2O_3(s)\rightarrow Y_2O_3(s)$	800	400	124.7	131.8	-51306.8	-256534
				Rejected heat from cooling			-288.5 kJ

* Molar ratio of CaO to $CaTiO_3$ in calcium oxide fabrics. (this study). ** The molar ratio of Fe_3O_4 to Y_2O_3 was assumed same as the value of iron pellet. (Sakurai et al., 2006).

Table 6-6. Thermal efficiencies with complete conversion and inert material (Case 2)

	Pellets (other researches*)		Fabrics (this study)	
	No recovery	Heat recovery	No recovery	Heat recovery
Thermal energy for reactions	593.5 kJ/mol	593.5 kJ/mol	593.5 kJ/mol	593.5 kJ/mol
Total energy for heating	671.7 kJ./mol	671.7 kJ./mol	549.8 kJ./mol	549.8 kJ./mol
Recovered thermal energy	-	715.2 kJ/mol	-	599.7 kJ/mol
Thermal efficiency	22.6%	52.0%	25.0%	52.6%

* From Aihara et al., 1999 and Sakurai et al., 2006.

Table 6-7. Additional energies required and rejected for heating and cooling of inert material and unreacted solid reactant, $CaO:CaTiO_3=1:1.4^*$, $Fe_3O_4:Fe_2TiO_5=1:5^{**}$ (Pellet)

	Heating or cooling	Temperature [K]		Cp [J $K^{-1}mol^{-1}$]		Enthalpy change [J/mol]	Total enthalpy change [J]
		Initial	Final	Initial	Final	Sensible	
H6	$CaTiO_3(s)\rightarrow CaTiO_3(s)$	873	1000	128.8	130.4	16458.8	27189.9
H7	$Fe_2TiO_5(s)\rightarrow Fe_2TiO_5(s)$	400	800	182.0	205.4	77473.2	429976
H8	$0.18CaO(s)\rightarrow 0.18CaO(s)$	873	1000	52.89	53.51	6756.59	1216.19
H9	$0.11Fe_3O_4(s)\rightarrow 0.11Fe_3O_4(s)$	400	800	174.0	266.7	88144.6	9695.91
		Energy required for heating					468.1 kJ
C7	$CaTiO_3(s)\rightarrow CaTiO_3(s)$	1000	873	130.4	128.8	-16458.8	-27189.9
C8	$Fe_2TiO_5(s)\rightarrow Fe_2TiO_5(s)$	800	400	205.4	182.0	-77473.2	-429976
C9	$0.18CaO(s)\rightarrow 0.18CaO(s)$	1000	873	53.51	52.89	-6756.59	-1216.19
C10	$0.11Fe_3O_4(s)\rightarrow 0.11Fe_3O_4(s)$	800	400	266.7	174.0	-88144.6	-9695.91
		Rejected heat from cooling					-468.1 kJ

* Molar ratio of CaO to $CaTiO_3$ in calcium oxide pellets. (Aihara et al., 1999). ** Molar ratio of Fe_3O_4 to Fe_2TiO_5 in iron oxide pellets. (Sakurai et al., 2006).

Table 6-8. Additional energies required and rejected for heating and cooling of inert material and unreacted solid reactant, $CaO:Y_2O_3=1:2^*$, Fe_3O_4: $Y_2O_3=1:5^{**}$ (Fabric)

	Heating or cooling	Temperature [K]		Cp [J $K^{-1}mol^{-1}$]		Enthalpy change [J/mol]	Total enthalpy change [J]
		Initial	Final	Initial	Final	Sensible	
H6	$Y_2O_3(s)\rightarrow Y_2O_3(s)$	873	1000	124.6	126.9	15970.5	37690.4
H7	$Y_2O_3(s)\rightarrow Y_2O_3(s)$	400	800	131.8	124.7	51306.8	284753
H8	$0.18CaO(s)\rightarrow 0.18CaO(s)$	873	1000	52.89	53.51	6756.59	1216.19
H9	$0.11Fe_3O_4(s)\rightarrow 0.11Fe_3O_4$	400	800	174.0	266.7	88144.6	9695.91
		Energy required for heating					333.4kJ
C7	$Y_2O_3(s)\rightarrow Y_2O_3(s)$	1000	873	126.9	124.6	-15970.5	-37690.4
C8	$Y_2O_3(s)\rightarrow Y_2O_3(s)$	800	400	124.7	131.8	-51306.8	-284753
C9	$0.18CaO(s)\rightarrow 0.18CaO(s)$	1000	873	53.51	52.89	6756.59	-1216.19
C10	$0.11Fe_3O_4(s)\rightarrow 0.11Fe_3O_4(s)$	800	400	266.7	174.0	88144.6	-9695.91
		Rejected heat from cooling					-333.4kJ

* Molar ratio of CaO to Y_2O_3 in calcium oxide fabrics. (this study). ** The molar ratio of Fe_3O_4 to Y_2O_3 was assumed same as the value of iron pellet. (Sakurai et al., 2006).

Table 6-9. Thermal efficiencies including inert material & incomplete conversion (Case 3)

	Pellets (other researches*)		Fabrics (this study)	
	No recovery	Heat recovery	No recovery	Heat recovery
Thermal energy for reactions	593.5 kJ/mol	593.5 kJ/mol	593.5 kJ/mol	593.5 kJ/mol
Total energy for heating	729.4 kJ./mol	729.4 kJ./mol	594.7 kJ./mol	594.7 kJ./mol
Recovered thermal energy	-	770.3 kJ/mol	-	642.8 kJ/mol
Thermal efficiency	21.6%	51.8%	24.1%	52.4%

* From Aihara et al., 1999 and Sakurai et al., 2006.

CHAPTER 7
CALCIUM OXIDE ABSORBENT FOR HIGH TEMPERATURE CARBON DIOIXDE CAPTURE

7.1 Introduction

The emissions from fossil fuel power plants are one of the largest sources of anthropogenic carbon dioxide emissions in the atmosphere. The carbon dioxide from the power plants can be separated from the sources via the post-combustion, pre-combustion and oxyfuel combustion carbon dioxide capture processes (Metz et al., 2005). Among them, the pre-combustion process is considered as a feasible way to capture carbon dioxide in the coal gasification and the steam methane reforming (SMR) processes.

The conventional coal gasification and SMR consist of the following reformation and water-gas shift reactions:

Reformation $$CH_x + H_2O \longleftrightarrow CO + yH_2 \quad (7\text{-}1)$$

(coal gasification: x=0, y=1, SMR: x=4, y=3)

Water-Gas Shift reaction $$H_2O + CO \longleftrightarrow CO_2 + H_2 \quad (7\text{-}2)$$

Hydrogen yield from these processes can be increased using absorbents to react with or absorb carbon dioxide since the forward equilibrium shift would occur by removing carbon dioxide in the water-gas shift reaction (Balasubramanian et al., 1999; Lin et al., 2002). Various absorbents have been introduced and studied, but calcium oxide based absorbents seem very promising in consideration of the operating temperature, pressure and capture capacity (Gupta and Fan, 2002). The zero-emission coal (ZEC) process using the carbonation/calcination reactions for carbon dioxide sequestration and for higher hydrogen yield was introduced and discussed by Słowinski (2006). The author stated that the process is attractive because electricity can be generated with high efficiency and without emission of carbon dioxide, though improvement of stability and

cyclic kinetics of $CaO/CaCO_3$ bed are required. In the thermodynamic study of Mahishi et al. (2005), the heat duty for gasification was reduced by almost 42% via in-situ heat transfer since CO_2 absorption is exothermic, and the hydrogen yield increased by about 19% while production of carbon dioxide was reduced by 50.2%. Similarly, Satrio et al. (2005) reported that hydrogen yield was increased 20% with a combined catalyst and absorbent for methane reforming and Hanaoka et al. (2005) also found that hydrogen yield was significantly increased with the reduction of carbon dioxide and methane by the contact between the biomass and calcium oxide on gasification. For their study, the authors fabricated and experimentally tested core-in-shell spherical pellets which consist of calcium oxide core and alumina shell contains nickel catalyst.

The carbonation and calcination reactions are described as follows:

Carbonation: $CaO(s) + CO_2(g) \rightarrow CaCO_3(s)$, $H_{973K} = -169.7kJ/mol$ (exothermic) (7-3)

Calcination: $CaCO_3(s) \rightarrow CaO(s) + CO_2(g)$, $H_{1173K} = 166.3kJ/mol$ (endothermic) (7-4)

Carbon dioxide reacts with calcium oxide to form calcium carbonate in the carbonation reaction and the calcium oxide is regenerated and pure carbon dioxide can be obtained through the calcination reaction. However, substantial volume changes between carbonate (36.9 cm^3/mol) and oxide forms (16.9 cm^3/mol) are induced by these gas-solid reactions (Stanmore and Gilot, 2005). These structural and thermal stresses caused by the cyclic carbonation-carbonation reaction lead to the loss in active surface area, pore plugging and sintering of the particles in the absorbent. As a result, the performance of the absorbent was found to degrade seriously in the cyclic operation (Barker, 1973; Borgwardt, 1989). This degradation should be overcome or minimized for the calcium oxide absorbent to be practical.

For that reason, various structural forms of calcium oxide to capture carbon dioxide such as dolomite ($CaCO_3 \cdot MgCO_3$) (Curran et al., 1967; Dobner et al., 1977; Silaban et al., 1996),

calcium oxide dispersed in porous inert calcium titanate ($CaTiO_3$) matrix (Aihara et al., 2001), impregnated in porous alumina granules (Feng et al., 2006), or mixed with mayenite ($Ca_{12}Al_{14}O_{33}$) (Li et al., 2005 and 2006) or nano-sized alumina (Al_2O_3) particles (Wu et al., 2008) and core-in-shell catalysis/sorbent (Satrio et al., 2004, 2005 and 2007) have been introduced and investigated to improve the cyclic performance of the absorbents for carbon dioxide capture. Most of these attempts showed better cyclic performance than pure calcium oxide thanks to the inert materials, but those bring other drawbacks, complexity in preparation, high cost for the synthesis and low content of calcium oxide in the inert materials.

In this study, a relatively simple and cost effective immobilization procedure of nano-sized calcium oxide particles on a fibrous ceramic fabric which acts as a support of the calcium oxide particles was introduced to enhance its cyclic performance. The characteristics and cyclic performance of the proposed immobilized calcium oxide on the fabric were examined and compared with other results in the literature.

7.2 Experimental Procedure

7.2.1 Immobilization of Calcium Oxide on a Ceramic Fabric

A new procedure for the immobilization of calcium oxide in a ceramic fiber was developed. Calcium carbonate ($CaCO_3$) was selected as a starting material. The nano-sized calcium carbonate powder is readily available and inexpensive. In order to improve the homogeneity and dispersibility of the particles, precipitated nano-particulate calcium carbonate (PCC; average particle size = 70 nm) surface treated with stearic acid was procured from the manufacturer (Specialty Minerals, USA). The PCC was blended with ethyl alcohol under mechanical stirring and the suspension was ultrasonicated subsequently to improve dispersibility and reduce agglomeration of the powders. The resultant slurry was dropped onto a dried ceramic fabric

(alumina or yttria) using a transfer pipette. The impregnated fabric was dried at 100°C for 30 min and sintered at 800°C for 12 hours in air. The preparation steps are shown in brief in Figure 7-1.

7.2.2 Cyclic Reaction Experiment

The cyclic carbonation-calcination reactions were conducted in a Thermogravimetric (TG) Analyzer (Model: SDT-Q600). The cyclic experiments were performed in various conditions. The prepared samples were evaluated under the isothermal condition at 750°C and at different temperatures of 700°C and 850°C for carbonation and calcination, respectively. 20 vol. % of carbon dioxide in nitrogen was supplied for the severe calcination while pure nitrogen was supplied for the mild calcination. The reaction conditions for the mild and severe calcinations are summarized in Table 7-1.

The degree of carbonation conversion (X) of the calcium oxide in the sample was defined as moles of calcium oxide reacted with carbon dioxide over moles of calcium oxide initially present:

$$X = \frac{n\,(calcium\ oxide\ reacted\ with\ CO_2)}{n\,(initial\ calcium\ oxide)} \tag{7-5}$$

The moles of calcium oxide reacted with carbon dioxide were calculated from the weight change of the sample measured by the TG analyzer.

The trend of conversion of the carbonation reaction and the temperature for the calcium oxide fabric sample with respect to the reaction time are plotted in Figure 7-2. Alumina fabric was used as a substrate. There was a 2.5% weight loss as the furnace was heated at a rate of 20°C/min to 750°C under a pure nitrogen atmosphere. It was believed that the weight loss is possibly caused by the thermal decomposition of calcium hydroxide that might have formed by the reaction between calcium oxide and moisture. Once the temperature reached 750°C, 20 vol % CO_2 in nitrogen was delivered for the carbonation reaction. Like other trends in the literature, the

carbonation reaction was very rapid in the initial stage while it decreased as time passed since the calcium oxide particles are covered with a layer of calcium carbonate, which imposes a limitation of the reactant gas diffusion (Bhatia and Perlmutter, 1983; Mess et al., 1999). 60% conversion was attained within approximately 20 minutes while 80% conversion took two hours. Therefore 20 minute duration for the carbonation reaction was chosen for the cyclic experiment in consideration of the effectiveness.

The conversion and temperature profiles for cyclic carbonation/calcination reactions of the calcium oxide sample (alumina fabric) are illustrated in Figure 7-3. For calcination, pure nitrogen at 750°C was applied. The conversion began at comparatively low level (about 59%), but the value gradually increased in the first couple of cycles and seemed to stabilize at about 75%. The increase in the conversion in the early stage was possibly due to the increase in the surface area by the initial structural transformation that was caused by the volume change. Each profile consists of the first fast stage and the second sluggish stage of the carbonation reaction. It can be observed that the temperature fluctuated very slightly since the carbonation and calcination reactions are exothermic and endothermic, respectively. The calcination reactions were completed within at most 5 minutes. The degree of conversion of the sample was maintained at the same level after several cycles and showed no signs of decrease even after 13 cycles.

The absolute capacity of carbon dioxide capture based on the total sample weight is not high due to the low calcium oxide content in the samples, about 23 wt %. Therefore the impregnation step in Figure 7-1 was repeated for higher calcium oxide content. It was confirmed that the content of calcium oxide in the fabric increased in proportion to the number of the impregnation steps. The maximum carbonation conversions of two samples with different

calcium oxide contents, 23 wt % and 55 wt %, in the alumina fabric under the mild condition are plotted in Figure 7-4. The initial maximum carbonation conversions were comparatively low, but the value increased and maintained at the same level. The sample with 23 wt % calcium oxide content attained about 75% carbonation conversion after 13 carbonation-calcination cycles and the carbonation conversion of the sample with 55 wt% calcium oxide reached about 62% after 10 cycles. It is possible that the lower conversion of the sample with higher calcium oxide contents is caused by higher diffusion resistance in the absorbent.

The weight resolution of TGA instrument is 0.1 μg. Hence, the error due to the TGA instrument in measurement error was negligible compared to the amount of the weight change of the samples.

The maximum amounts of reacted calcium oxide in the two samples are measured against those in the pure calcium oxide forms from the previous researchers in Figure 7-5. Two empirical curve fits of the experimental test data for various types of calcium oxide under different conditions from previous studies (Barker, 1973; Curran et al., 1967; Aihara et al., 2001; Shimizu et al., 1999; Silaban et al., 1995) were developed (Abanades and Alvarez, 2003; Abanades, 2002). One of the curve fit equations is given below (Abanades and Alvarez, 2003), which is also reproduced in the figure without actual experimental data points in order to compare our results with previous studies in the literature.

$$X = 0.83 \times 0.77^{N} + 0.17 \tag{7-6}$$

The fitted curve from the literature dropped steeply with the number of cycles while the values of the samples in this study gradually increased for the first few cycles and remained stable. The absolute capacities of carbon dioxide capture of the sample with 55 wt % calcium oxide content exceeded that of the conventional pure calcium oxide after the sixth cycle. The amount of carbon

dioxide capture of the sample with 23 wt % calcium oxide is lower due to the lower calcium oxide content in samples but the value of the sample is also expected to exceed the fitted curve approximately after the 25th cycle.

7.2.3 Characterization

The structure of the impregnated sample was examined under SEM. The observation focused on the structural changes over the cyclic reactions. The composition of the sample was investigated by X-ray diffraction (XRD) experiments to confirm the conversion of calcium oxide into calcium carbonate during carbonation and the regeneration of calcium oxide after calcination.

The structure of the impregnated sample was examined under SEM. Figure 7-6 shows the SEM images of an unaltered alumina fabric and a fresh sintered calcium oxide mat.

The original alumina fabric consists of micron sized alumina fibers which have a diameter of about 2 to 5 μm (Figure 7-6(A)). It was observed that calcium oxide particles are supported by the alumina fibers and interconnected microstructures of the calcium oxide were formed between the alumina fibers in the mat as shown in Figure 7-6(B). Some threads are exposed, while most others are buried by the calcium oxide particulate aggregates.

It was observed that the PCC was converted into calcium oxide during the sintering process by XRD analysis. Figure 7-7 shows X-ray diffraction patterns of the sample (23 wt % CaO) (A) fresh sintered (B) after the 10th carbonation and (C) after the 10th calcination. The XRD data indicate that the samples after sintering and the 10th calcination contain only calcium oxide while calcium carbonate accounts for the major compound along with small quantities of unreacted calcium oxide after the 10th carbonation.

The changes in the surface area during cyclic operation of the sample were measured by nitrogen adsorption in an AUTOSORB-1 instrument from Quantachrome Instruments. The

surface areas of the sample with 23 wt % calcium oxide in the alumina fabric over several cyclic reactions are shown in Figure 7-8.

Considering the molar volumes of calcium oxide and calcium carbonate, it was expected that the surface area would diminish during the carbonation reaction and would be regenerated after the calcination reaction. The fresh sample began with a comparatively low surface area (9.2 m^2/g). It decreased to 5.3 (m^2/g) after carbonation due to the volume expansion of the particles as expected, but it increased drastically to about 18.3 m^2/g after one cycle. After that, values of the surface area of the sample after calcination remained in the range of 16-19 m^2/g. Based on the figure, one can conclude from the figure that the big jump of the surface area in the initial stage was caused by the permanent partial structural breakage and void generation owing to the volume contraction from carbonate to oxide form.

Figure 7-9 shows the magnified images of the freshly sintered sample (23 wt % CaO) and the sample after the 10^{th} carbonation and calcination reactions. From images (a) and (b), it was observed that the calcium oxide particles which have a diameter of about 150 nm, are dispersed in the alumina fabric. After the 10^{th} carbonation reaction (c and d), the structure was comparatively closed-packed with larger particles possibly due to the volume expansion of the particles. The structure after the 10^{th} calcination seems to consist of more interconnected agglomerates of the calcium oxide particles with a stabilized high surface area in the images (e) and (f).

7.2.4 Severe Calcination Condition

Practically, the severe condition for calcination reaction is preferable for carbon dioxide sequestration or utilization since higher concentration of carbon dioxide from carbonated absorbents can be obtained. However, it was observed that the severe calcination under higher temperature and presence of carbon dioxide pulled down the performance of the calcium oxide

absorbents significantly (Li et al., 2005 and 2006; Wu et al., 2008; Silaban et al., 1995; Grasa et al., 2007). Under high temperature, it was proved that the mixture of calcium oxide and alumina react to form a new compound, $Ca_{12}Al_{14}O_{33}$ (Wu et al., 2008), in the composite of calcium oxide and alumina. This new inert materials could be a reason for the degradation under the severe calcination condition.

For this reason, a yttria fabric was also introduced as a substrate in place of the alumina fabric. The cyclic carbonation-calcination experiments of the two samples using different fabric materials, alumina and yttria, were conducted under the severe calcination condition in Table 7-1 and the maximum conversion trends of the samples are illustrated in Figure 7-10. As shown in the figure, the maximum carbonation conversions (about 55%) of the sample using yttria fabric as a substrate showed no sign of degradation over the 12 cycles while those of the sample using alumina dropped by about eight percent after 12 cycles from the maximum of 59%,. Li et al. (2005) observed the decline of the carbonation conversion due to the presence of 14 wt % CO_2 in calcination process at 850°C because the sintering rate of calcium oxide particles at a given temperature was accelerated by the presence of CO_2 (Borgwardt, 1989). Judging from these experimental results and the previous literature, it was concluded that the yttria fabric is superior to the alumina fabric as a substrate for calcium oxide absorbent at the severe calcinations condition due to the possibility of the formation of $Ca_{12}Al_{14}O_{33}$ by the reaction between calcium oxide and alumina under the high temperature over 800°C. Also this new proposed calcium oxide reactant using yttria was found to be better than the Ca-based CO_2 absorbent, (CaO/ $Ca_{12}Al_{14}O_{33}$), proposed by Li et al. (2005) since the cyclic performance was maintained even with 20% CO_2 at 850°C.

7.3 Summary

In order to minimize the degradation of the absorption capacity in cyclic operation due to the pore plugging and sintering of particles, the calcium oxide on fibrous ceramic fabricated via a simple and effective immobilization process developed for the UT-3 cycle was applied to carbon dioxide capture at high temperature. The prepared samples were characterized and evaluated by various analytical and experimental tools comprehensively. Two samples with 23 wt% and 55 wt% calcium oxide contents in the alumina fabric achieved continuous cyclic carbonation conversions, about 75% and 62% over 13 and 10 carbonation-calcination cycles under the mild calcinations condition at 750°C in N_2. Under the more severe calcination condition at 850°C and 20 wt% CO_2 in N_2, it was confirmed that the yttria fabric was superior to the alumina as a substrate for carbon dioxide capture. The reactivity of the calcium oxide absorbent using the yttria fabric was maintained at the same level in 12 cycles. The stabilized conversion was about 55%. On the other hand, the sample using the alumina fabric showed degradation by about eight percent from the maximum, 59%, after 12 cycles possibly due to the formation of $Ca_{12}Al_{14}O_{33}$.

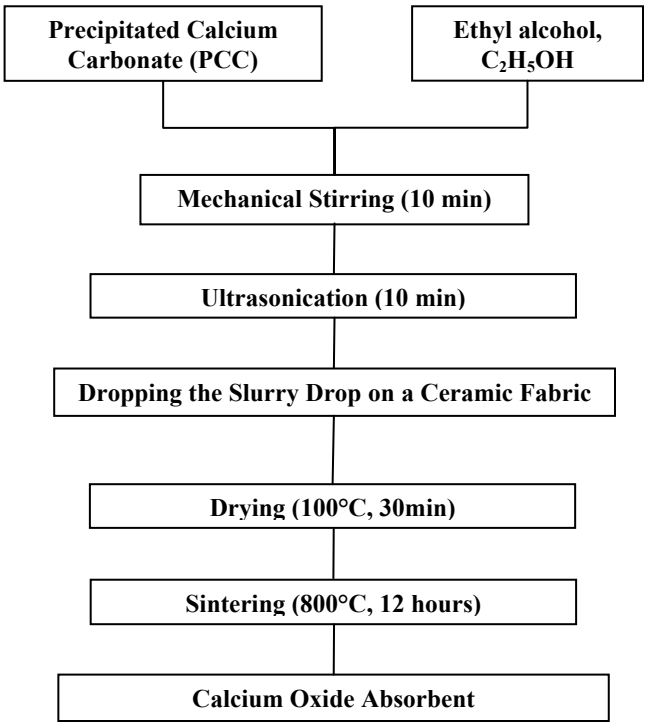

Figure 7-1. Preparation steps for immobilization of calcium oxide on a ceramic fabric

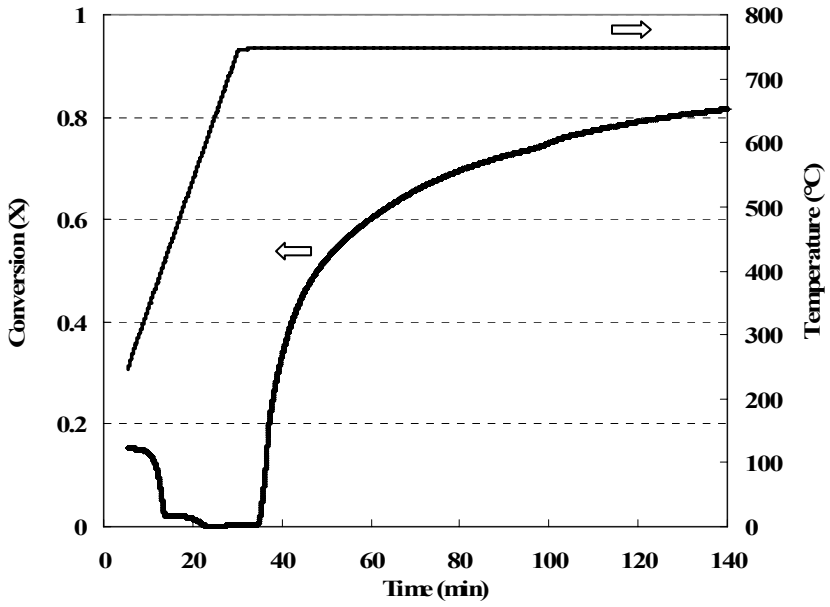

Figure 7-2. Carbonation conversion of the prepared sample

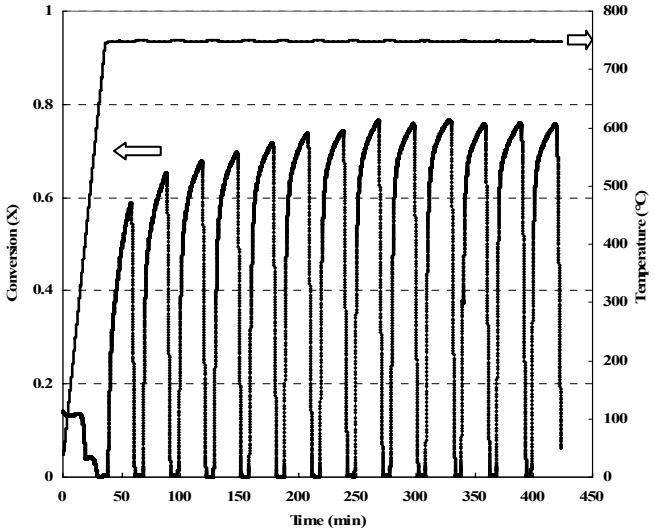

Figure 7-3. Conversion profiles of cyclic reactions

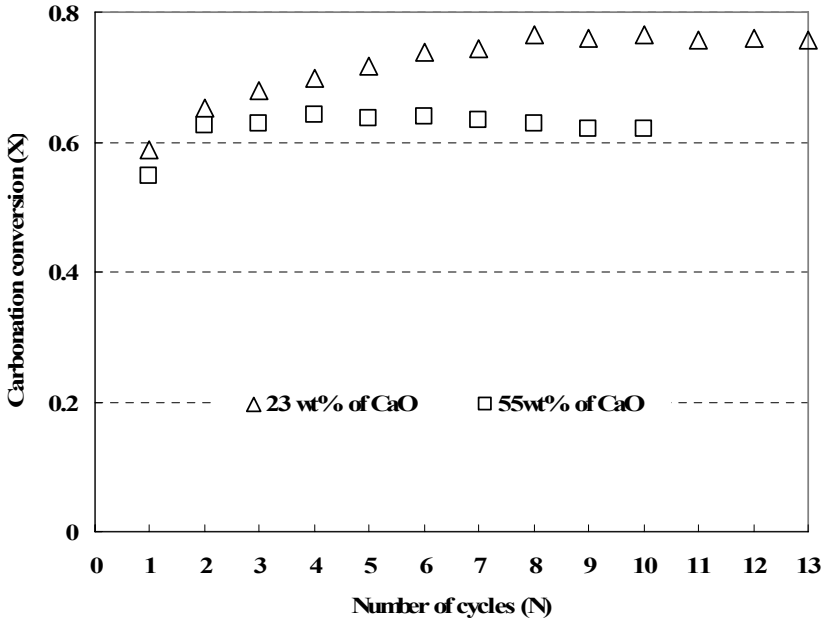

Figure 7-4. Maximum conversions of carbonation reaction of two samples loaded different calcium oxide contents, 23 wt % and 55 wt %, with the number of cycles

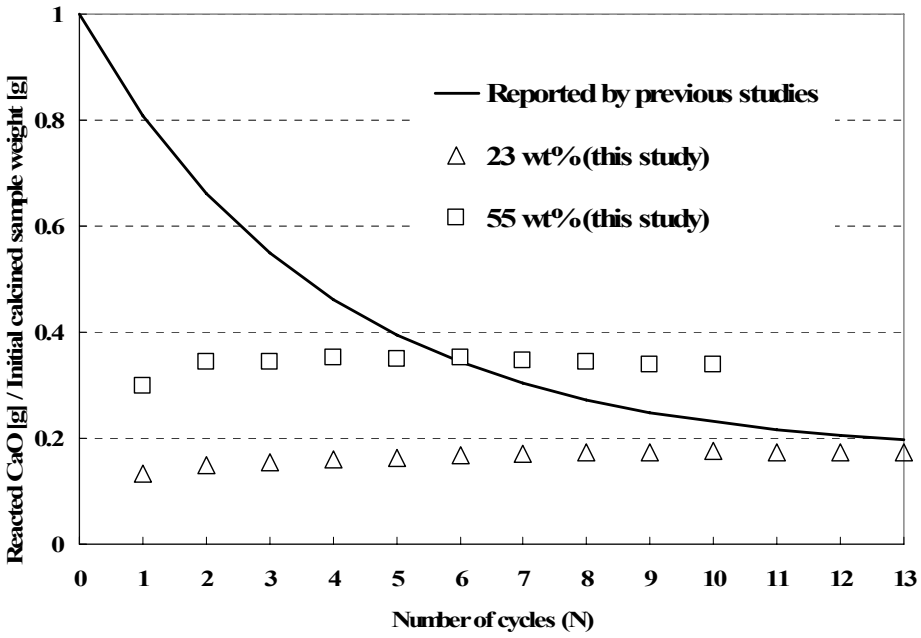

Figure 7-5. Maximum amounts of reacted calcium oxide in the carbonation reactions based on initial sample weight with the number of cycles

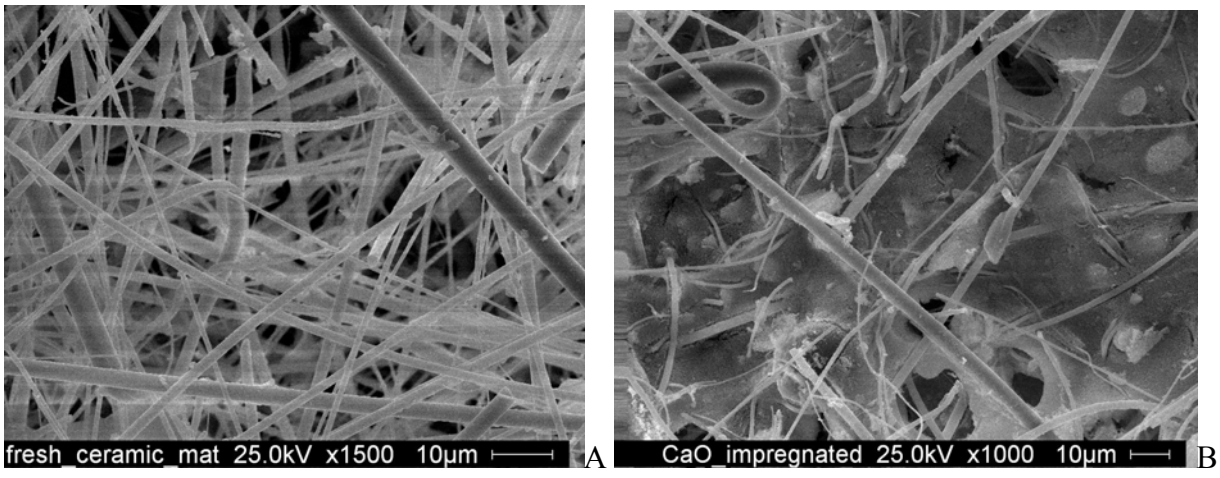

Figure 7-6. The SEM images of a fabric sample. A) An original alumina fabric. B) Fresh sintered sample.

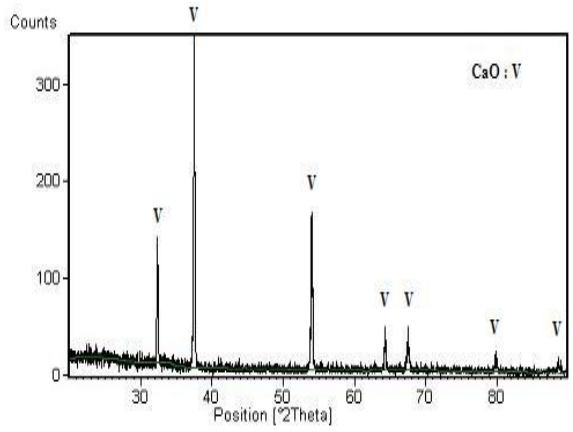

A

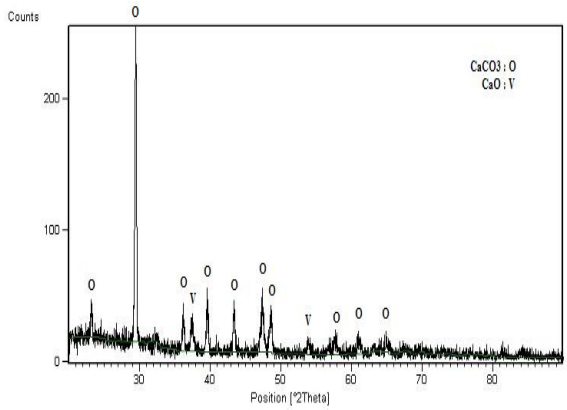

B

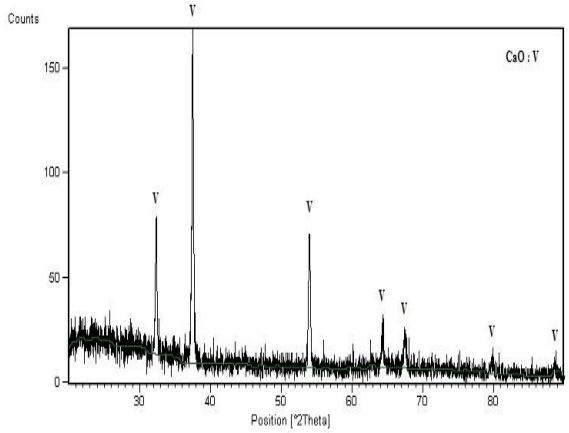

C

Figure 7-7. The XRD patterns of the samples. A) Fresh. B) After 10th carbonation. C) After 10th calcination (10 cycles).

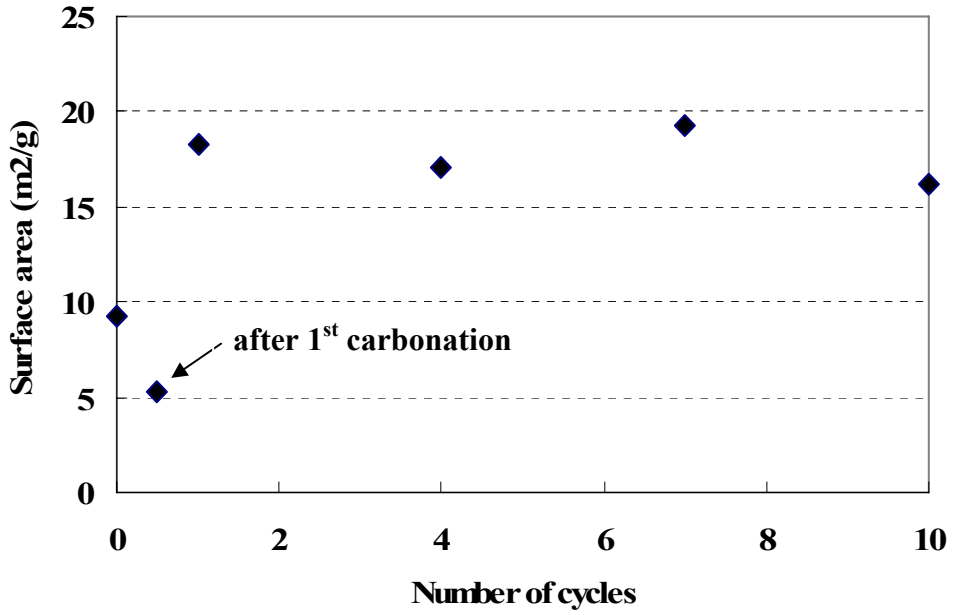

Figure 7-8. Change of surface area in the sample over the several cyclic reactions

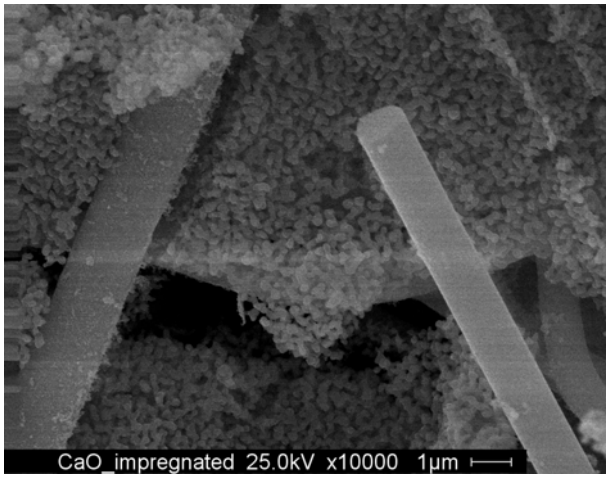

A

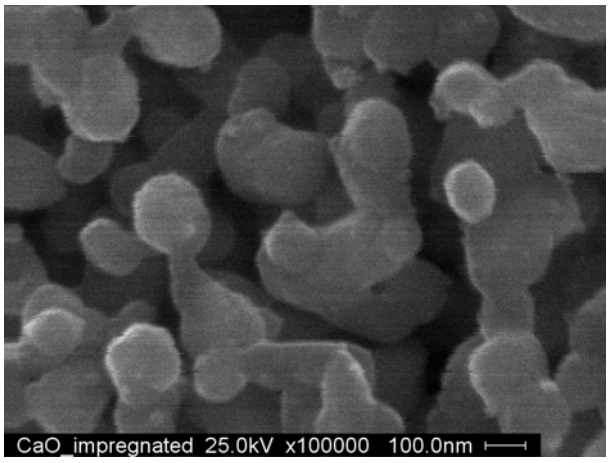

B

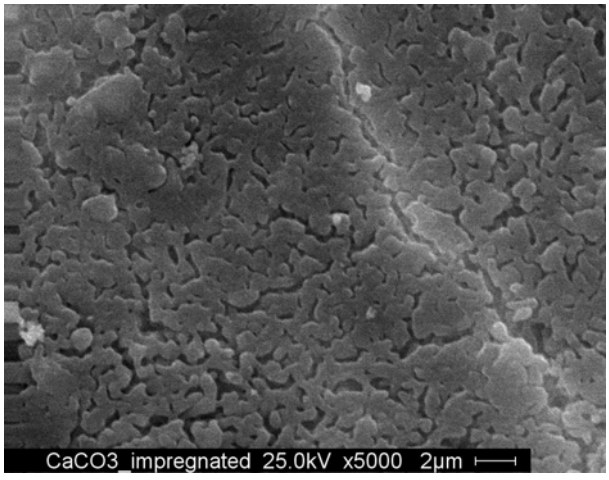

C

Figure 7-9. The SEM pictures for the sample. (A and B) Fresh. (C and D) After 10th carbonation. (E and F) After 10th calcination (10 cycles).

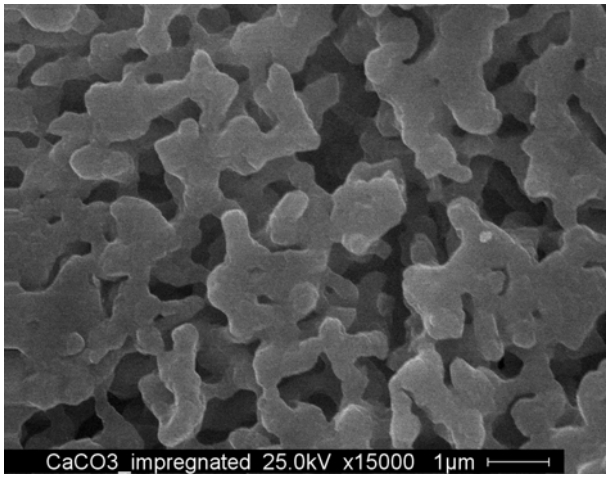

D

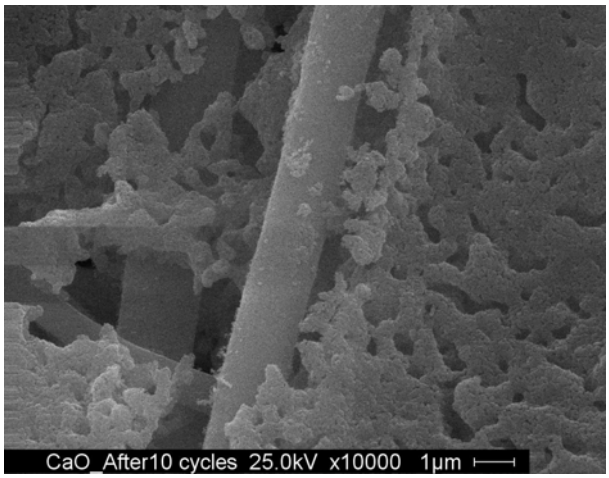

E

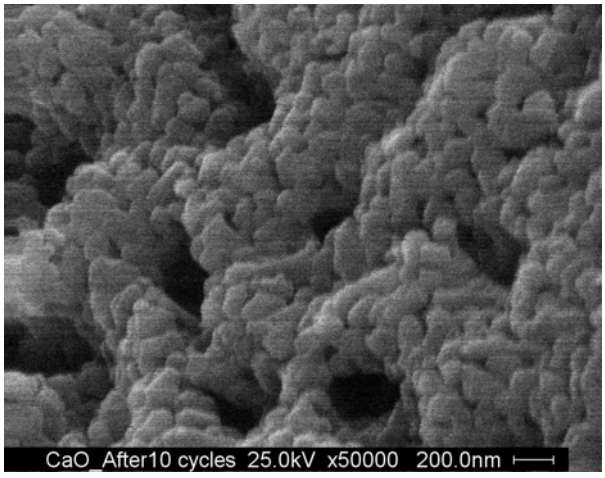

F

Figure 7-9. Continued

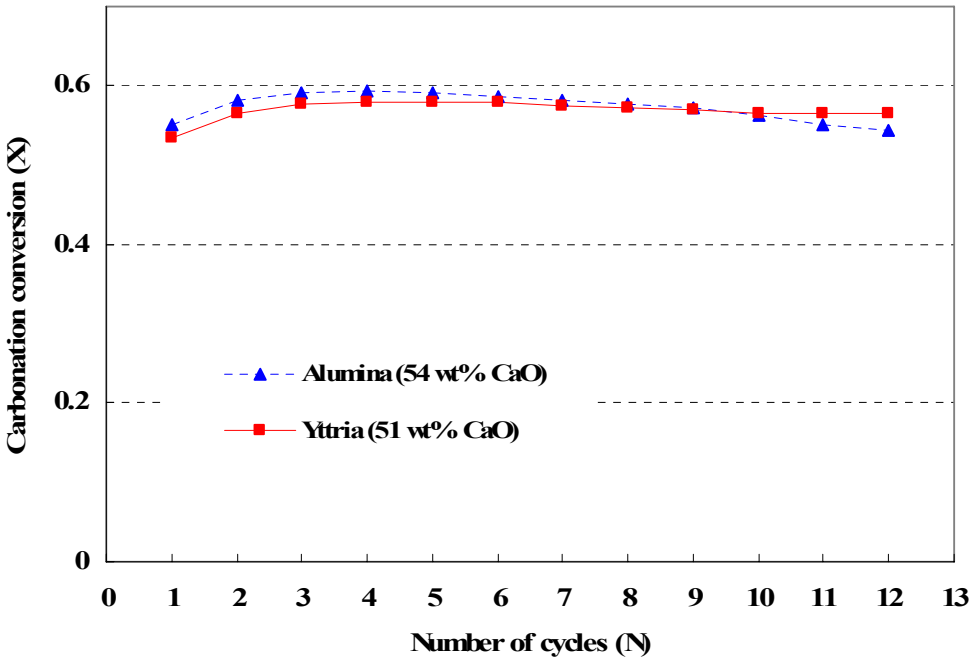

Figure 7-10. The cyclic maximum carbonation conversions of the samples using yttria and alumina as a substrate under the severe calcination condition at 850°C and 20 wt % CO_2

Table 7-1. Mild and severe calcination conditions

	Carbonation			Calcination		
	Temperature	Gas feed	Duration	Temperature	Gas feed	Duration
Mild condition	750°C	20 vol. % of CO_2 in N_2	20 min	750°C	Pure N_2	10 min
Severe condition	700°C	20 vol. % of CO_2 in N_2	30 min	Ramp 15°C/min from 700°C to 850°C	20 vol. % of CO_2 in N_2	10 min

CHAPTER 8
CONCLUSIONS AND FUTURE WORK

8.1 Conclusions

This study began with the goal of thermodynamic feasibility investigation of UT-3 cycle and the development of calcium oxide reactant with better characteristics and performance. The feasibility of each reaction in the UT-3 cycle was examined via theoretical thermodynamic approaches in order to determine the optimal operating conditions for high reaction rate as well as high conversion. The effects of excess steam, temperature and pressure on the conversion and chemical compositions at the equilibrium state were investigated. The major findings were:

- Thermodynamically, the two hydrolysis reactions are unfavorable while the two bromination reactions are favorable in the UT-3 cycle.
- The excess steam enhanced the hydrolysis reactions of calcium bromide and iron bromide significantly while no serious adverse effect of the excess steam on the bromination was observed.
- The temperature for hydrolysis reaction of calcium bromide is limited by the melting temperature of 1000K for calcium bromide.
- The conversion of the hydrolysis reaction of calcium bromide is expected to be complete by continuously removing the product gas, HBr, from the equilibrium state even at atmospheric pressure.

Porous calcium oxide pellets for the UT-3 cycle were prepared and characterized experimentally. The effects of pore forming agents on the characteristics and performance of pellets were investigated. From the characterization and kinetic studies, it was ascertained that the amount and type of additives had an important effect on the pore volume and increasing the volume of pores greater than 5μm speeded up the hydrolysis rate of calcium bromide in the pellets. Subsequently, an inexpensive and straightforward calcium oxide immobilization process on yttria fibrous fabric was developed. The performance was evaluated in cyclic bromination and hydrolysis reactions experimentally. Based on the experimental results in the cyclic reactions, the

calcium oxide dispersed and immobilized on the fibrous yttria fabric had continuous higher reactivity (~ 85%) in four bromination reactions and the rate of hydrolysis reaction was comparable to that of calcium oxide pellets.

The thermodynamic efficiency of UT-3 cycle was investigated considering inert materials, heat recovery and incomplete conversion. The effect of heat recovery on the efficiency was considerable, which accounted for 20.4-30.2% efficiency discrepancy. The inert materials accounted for 10.9 and 8.5% reductions of the efficiency for the pellet and fabric reactants, respectively, without heat recovery. However, the influence of incomplete conversion was not significant. Also it was found that the fabric type reactant was somewhat better than the pellet type reactant for thermal efficiency.

The developed calcium oxide fabrics were used for carbon dioxide capture in coal or biomass gasification, SMR process and conventional coal power plants. A new type calcium oxide absorbent was fabricated on fibrous alumina and the cyclic carbonation conversion was maintained over ten carbonation-calcination cycles under mild calcinations condition. Under the severe calcination condition, the carbonation conversion of the calcium oxide sample using yttria fabric was maintained at 56% through 12 cycles while those of the sample using alumina dropped by about eight percent after 12 cycles from the maximum of 59%, possibly due to the formation of $Ca_{12}Al_{14}O_{33}$ by the reaction between calcium oxide and alumina.

8.2 Recommendations for Future Work

The newly developed calcium oxide reactant for the UT-3 cycle was tested in four cyclic bromination and hydrolysis reactions. In order to make the process commercially feasible, however, several thousands cycles are needed without severe degradation of the solid reactant. A new preparation method for iron oxide is also needed to be developed because the existing iron pellet is also made through an expensive and complicated process.

The process efficiency should be estimated by including the hydrogen and oxygen separation work, pumping work, actual process pressure, excess water and realistic heat match in the calculations. Heat recovery and reduction of the inert material should be investigated in order to increase the efficiency.

The excess steam was found to enhance hydrolysis reactions of calcium bromide and iron bromide significantly in this study. However, there may be economic penalty associated with the use of excess steam. It is recommended that economic and technical considerations of the excess steam must be studied with regard to the cost and size of the building and the separation efficiency of the high temperature membrane.

The prepared calcium oxide absorbent for high temperature carbon dioxide capture showed continuous high reactivity in the cyclic carbonation-calcination cycle even under severe calcinations condition. However, in order to obtain pure carbon dioxide for sequestration from the calcination reaction, cyclic experiments under the more severe calcination condition at higher temperature of at least 950°C under 100% concentration of carbon dioxide would be needed. Future work must also consider the economics of the calcium oxide absorbent as compared with other type of carbon dioxide absorbents.

APPENDIX
CYCLIC CONVERSION PROFILES (ALUMINA, SILICA, ZIRCONIA)

Several ceramic materials such as alumina (Al_2O_3), silica (SiO_2), zirconia (ZrO_2) and yttria (Y_2O_3) were considered as a substrate of calcium oxide reactant for UT-3 cycle. Among them, the yttria fabric was selected as the substrate for the calcium oxide reactant through preliminarily experiments. The cyclic bromination and hydrolysis profiles of calcium oxide samples immobilized on alumina, silica and zirconia fabrics are shown in Figure A-1, A-2 and A-3, respectively. It was observed that the performance of all samples severely degraded at the second cycle, which is possibly due to the formation of inert materials such as calcium aluminate, calcium silicate and calcium zirconate due to reactions between calcium oxide and the substrate materials.

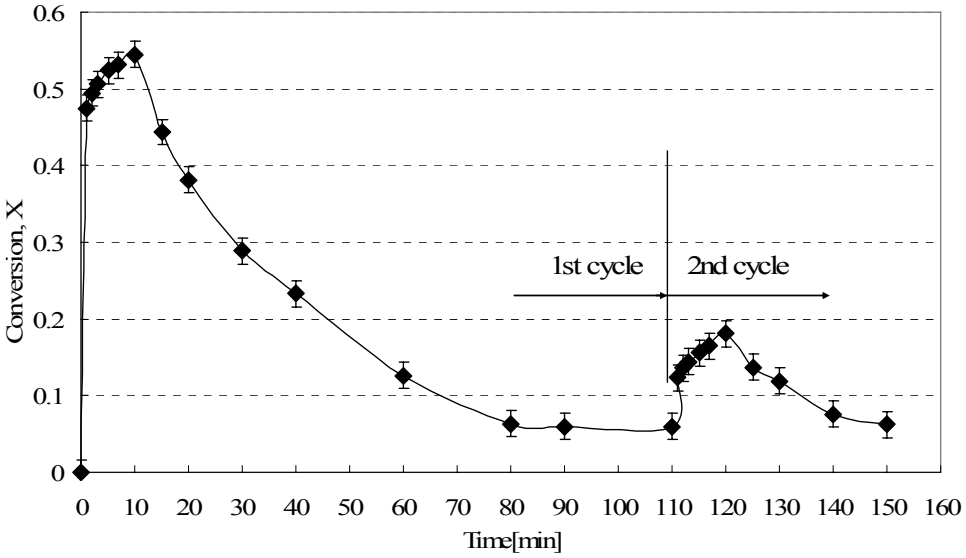

Figure A-1. Cyclic conversion profiles of a calcium oxide sample immobilized on an alumina fabric

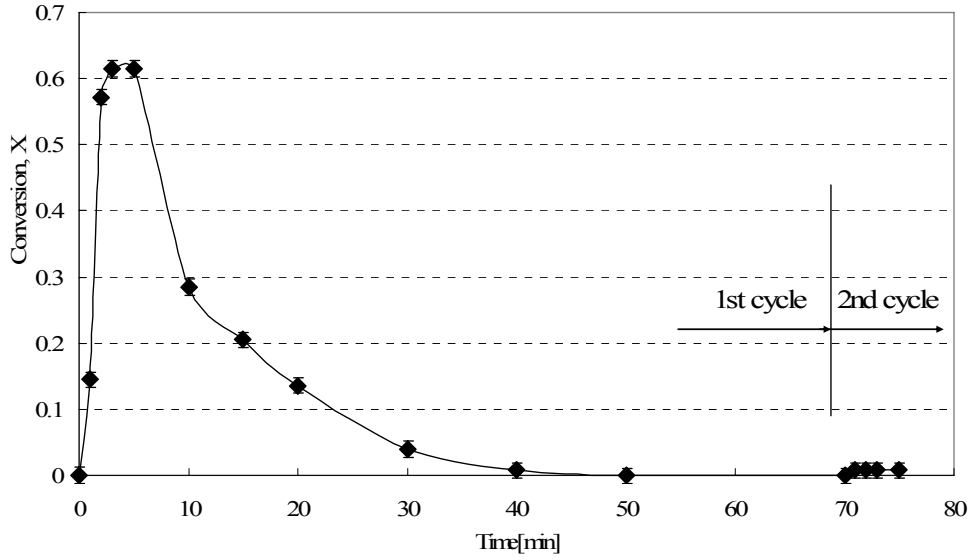

Figure A-2. Cyclic conversion profiles of a calcium oxide sample immobilized on a silica fabric

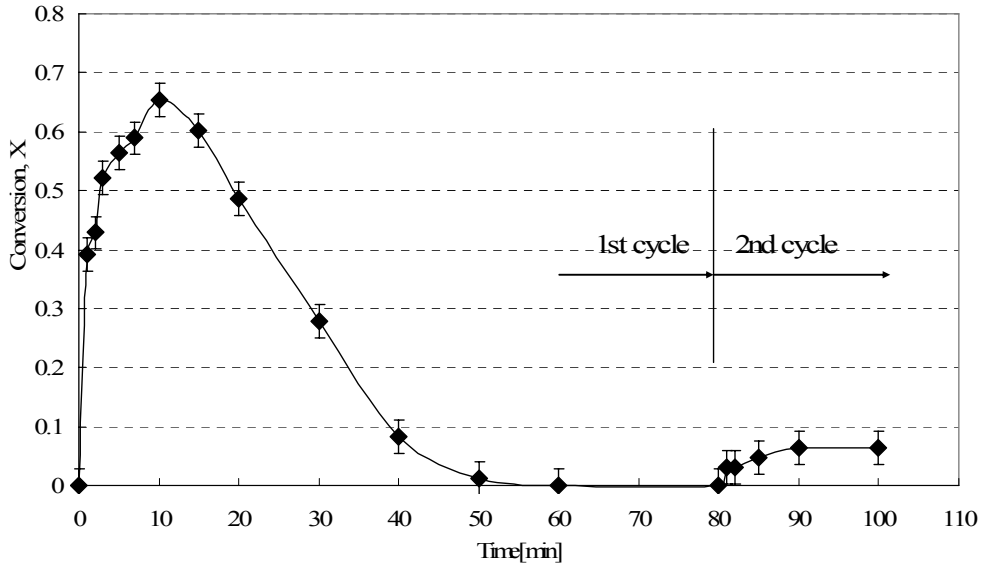

Figure A-3. Cyclic conversion profiles of a calcium oxide sample immobilized on a zirconia fabric

LIST OF REFERENCES

Abanades, J. C., 2002. The maximum capture efficiency of CO_2 using a carbonation/calcination cycle of $CaO/CaCO_3$. Chemical Engineering Journal 90, 303-306.

Abanades, J. C., Alvarez, D., 2003. Conversion limits in the reaction of CO_2 with lime. Energy & Fuels 17, 308-315.

Aihara, M., Umida, H., Tsutsumi, A., Yoshida, K., 1990. Kinetic study of UT-3 thermochemical hydrogen production process. International Journal of Hydrogen Energy 15, 7-11.

Aihara, M., Sakurai, M., Tsutsumi, A., Yoshida, K., 1992. Reactivity improvement in the UT-3 thermochemical hydrogen production process. International Journal of Hydrogen Energy 17, 719-723.

Aihara, M., Nagai, T., Matsushita, J., Negishi, Y., Ohya, H., 2001. Development of porous solid reactant for thermal-energy storage and temperature upgrade using carbonation/decarbonation reaction. Applied Energy 69, 225-238.

Amir, R., Sato, T., Yoko Yamamoto, K., Kabe, T., Kameyama, H., 1992. Design of solid reactants and reaction kinetics concerning the iron compounds in the UT-3 thermochemical cycle. International Journal of Hydrogen Energy 17, 783-788.

Amir, R., Shiizaki, Yamamoto, K., Kabe, T., Kameyama, H., 1993. Design development of iron solid reactants in the UT-3 water decomposition cycle based on ceramic support materials. International Journal of Hydrogen Energy 18, 283-286.

Aochi, A., Tadokoro, T., Yoshida, K., Kameyama, H., Nobue, M., Yamaguchi, T., 1989. Economical and technical evaluation of UT-3 thermochemical hydrogen production process for an industrial scale plant. International Journal of Hydrogen Energy 14, 421-429.

Argonne National Laboratory, 2003. Basic research needs for the hydrogen economy. Report on the Basic Energy Sciences Workshop on Hydrogen Production, Storage, and Use, available at http://www.sc.doe.gov/bes/hydrogen.pdf

Balasubramanian, B., Ortiz, A. L., Kaytakoglu, S., Harrison, D. P., 1999. Hydrogen from methane in a single-step process. Chem Eng Sci 54, 3543-3552.

Barker, R., 1973. The reversibility of the reaction $CaCO_3 = CaO + CO_2$. J. Appl. Chem. Biotechnol 23, 733-742.

Beghi, G. E., 1986. A decade of research on thermochemical hydrogen at the joint research center, Ispra. International Journal of Hydrogen Energy 11, 761-771.

Bennett, J. E., 1980. Electrodes for generation of hydrogen and oxygen from seawater. International Journal of Hydrogen Energy 5, 401-408.

Bhatia, S. K., Perlmutter, D. D., 1983. Effect of the product layer on the kinetics of the CO_2-lime reaction. AIChE Journal 29, 79-86.

Bilgen, E., Joels, R. K., 1985. An assessment of solar hydrogen production using the mark 13 hybrid process. International Journal of Hydrogen Energy 10, 143-155.

Borgwardt, R. H., 1989. Calcium oxide sintering in atmospheres containing water and carbon dioxide. Ind. Eng. Chem. Res. 28, 493-500.

Bockris, J. O. M., 1975. *Energy: the Solar Hydrogen Alternative*, John Wiley & Sons, New York.

Brecher, L. E., Spewock, S., Warde, C. J., 1977. The westinghouse sulfur cycle for the thermochemical decomposition of water. International Journal of Hydrogen Energy 2, 7-15.

Bromine Statistics and Information, 2008. Available at http://minerals.usgs.gov/minerals/pubs/commodity/bromine/mcs-2008-bromi.pdf

Brown, L. C., Besenbruch, G. E., Lentsch, R. D., Schultz, K. R., Funk, J. F., Pickard, P. S., et al., 2003. High efficiency generation of hydrogen fuels using nuclear power. GA-A24285. Prepared under the Nuclear Energy Research Initiative Program for the US Department of Energy.

Casper, M. S., ed., 1978. *Hydrogen Manufacture by Electrolysis, Thermal Decomposition and Unusual Techniques*, Noyes Data Corporation.

Chase, M. W. Jr., Davies, C. A., Downey, Jr., Frurip, D. J., McDonald, R. A., Syverud, A. N., 1985. JANAF Thermochemical Tables, 3rd ed., Journal of Physical and Chemical Refercence Data 14, Supplement No. 1.

Cox, K. E., Williamson, K. D., 1977. *Hydrogen: Its technology and implication, Vol. 1 Hydrogen Production Technology,* CRC PRESS, Inc.

Curran, G. P., Fink, C. E., Gorin, E., 1967. Carbon dioxide-acceptor gasification process: studies of acceptor properties. Adv. Chem. Ser. 69, 141-165.

Dobner, S., Sterns, L., Graff, R. A., Squires, A. M., 1977. Cyclic calcinations and recarbonation of calcined dolomite. Ind. Eng. Chem., Process Des. Dev. 16, 479-486.

Doctor, R. D., Marshall, C. L., Wade, D. C., 2002. Hydrogen cycle employing calcium-bromine and electrolysis. ACS Division of Fuel Chemistry, Preprints 47, 755-756.

Ebrahim, M., Kawari, A., 2000. Pinch technology: an efficient tool for chemical-plant energy and capital-cost saving. Applied Energy 65, 45-49.

FactSage, Web version, Thermo-chemical database software, Thermfact, GTT Technologies, Germany, Available at http//www.factsage.com/

Feng, B., Liu, W., Li, X., An, H., 2006. Overcoming the problem of loss-in-capacity of calcium oxide in CO_2 capture. Energy & Fuels 20, 2417-2420.

Funk, J. E., Reinstrom, R. M., 1964. Final report energy depot electrolysis study. TID 20441(EDR3714), Vol. 2, Supplement A.

Funk, J. E., Reinstrom, R. M., 1966. Energy requirements in the production of hydrogen from water. Industrial and Engineering Chemistry Process Design and Development 5, 336-342.

Funk, J. E., 2001. Thermochemical hydrogen production: past and present. International Journal of Hydrogen Energy 26, 185-190.

Goel, N., Mirabel, S., Ingley, S., Goswami, Y., 2003. Solar hydrogen production. Advanced in Solar Energy.

Grasa, G., Gonzalez, B., Alonso, M., Abanades, J. C., 2007. Comparison of CaO-based synthetic CO_2 sorbents under realistic calcination conditions. Energy & Fuels 21, 3560-3562.

Gupta, H., Fan, L., 2002. Carbonation-calcination cycle using high reactivity calcium oxide for carbon dioxide separation from flue gas. Ind. Eng. Chem. Res. 41, 4035-4042.

Hanaoka, T., Yoshida, T., Fujimoto, S., Kamei, K., Harada, M., Suzuki, Y., Hatano, H., Yokoyama, S.-Y., Minowa, T., 2005. Hydrogen production from woody biomass by steam gasification using a CO_2 sorbent. Biomass and Bioenergy 28, 63-68.

Haueter, P, Moeller, S, Palumbo, R, Steinfeld, A., 1999. The production of zinc by thermal dissociation of zinc oxide-solar chemical reactor design. Solar Energy 67, 161-167.

Iodine Statistics and Information, 2008, Available at http://minerals.usgs.gov/minerals/pubs/commodity/iodine/mcs-2008-iodin.pdf

Kameyama, H., Yoshida, K., 1978. Br-Ca-Fe water-decomposition cycles for hydrogen production. Proc. of the 2nd World Hydrogen Energy Conf., Zurich, Switzerland, 829-850.

Kameyama, H., Yoshida, K., 1981. Reactor design for the UT-3 thermochemical hydrogen production process. International Journal of Hydrogen Energy 6, 567-575.

Kameyama, H., Tomino,Y., Sato, T., Amir, R., Orihara, A., Aihara, M., Yoshida, K., 1989. Process simulation of "MASCOT" plant using the UT-3 thermochemical cycle for hydrogen production. International Journal of Hydrogen Energy 14, 323-330.

Lee, M. S., Goswami, Y., Hettinger, B., Vijayaraghavan, S., 2006. Preparation and characteristics of calcium oxide pellets for UT-3 thermochemical cycle. Proceedings in 2006 ASME International Mechanical Engineering Congress and Exposition.

Lee, M. S., Goswami, Y., Kothurkar, N., Stefanakos, E. K., 2007. Fabrication of porous calcium oxide film for UT-3 thermochemical hydrogen production cycle. Proceedings in Energy Sustainability 2007, ASME.

Lemort, F., Lafon, C., Dedryvère, R., Gonbeau, D., 2006. Physicochemical and thermodynamic investigation of the UT-3 hydrogen production cycle: A new technological assessment. International Journal of Hydrogen Energy 31, 906-918.

Li, Z.-S., Cai, N.-S., Huang, Y.-Y., Han, H.-J., 2005. Synthesis, experimental studies, and analysis of a new calcium-based carbon dioxide absorbent. Energy & Fuels 19, 1447-1452.

Li, Z.-S., Cai, N.-S., Huang, Y.-Y., 2006. Effect of preparation temperature on cyclic CO_2 capture and multiple carbonation-calcination cycles for a new ca-based CO_2 sorbent. Ind. Eng. Chem. Res. 45, 1911-1917.

Lin, S., Harada, M., Suzuki, Y., Hatano, H., 2002. Hydrogen production from coal by separating carbon dioxide during gasification. Fuel 81, 2079-2085.

Lin, S.-Y., Suzuki, Y., Hatano, H., Harada, M., 2002. Developing an innovative method, HyPr-RING, to produce hydrogen from hydrocarbons. Energy Conservation and Management 43, 1283-1290.

Linnhoff, B., Flower, J. R., 1978. Synthesis of heat exchanger networks: Part I and II. AIChE Journal 24, 633-642.

Mahishi, M. R., Sadrameli, M. S., Vijayaraghavan, S., Goswami, D. Y., 2005. Hydrogen production from ethanol: A thermodynamic analysis of a novel sorbent enhanced gasification process. American Society of Mechanical Engineers, Advanced Energy Systems AES 45, 455-463.

Meites, L., 1981. *An Introduction to Chemical Equilibrium and Kinetics*, Pergamon Series in Analytical Chemistry, Vol. 1, Pergamon Press.

Mess, D., Sarofim, A. F., Longwell, J. P., 1999. Product layer diffusion during the reaction of calcium oxide with carbon dioxide. Energy & Fuels 13, 999-1005.

Metz, B., Davidson, O., Coninck, H., Loos, M., Meyer, L. (Eds.), 2005. *IPCC special report on carbon dioxide capture and storage*. Cambridge University Press.

Morooka, S., Kim, S. S., Yan, S., Kusakabe, K., Watanabe, M., 1996. Separation of hydrogen from an H_2-H_2O-HBr system with a SiO_2 membrane formed in macropores of an α-Alumina support tube. International Journal of Hydrogen Energy 21, 183-188.

Nakajima, R., Kikuchi, R., Tsutsumi, A., 2000. Improvement of the Fe-pellet reactivity in the UT-3 thermochemical hydrogen production cycle. Hydrogen energy progress XIII: Proceedings of the 13th World Hydrogen Energy Conference, Beijing, China.

Nakayama, T., Yoshioka, H., Furutani, H., Kameyama, H., Yoshida, K., 1984. MASCOT- a bench-scale plant for producing hydrogen by the UT-3 thermochemical decomposition cycle. International Journal of Hydrogen Energy 9, 187-190.

National Research Council and National Academy of Engineering, 2004. *The Hydrogen Economy: Opportunities, Costs, Barriers, and R&D Needs*, The National Academies Press.

National Resources Canada, 2003. Pinch analysis: for the efficient use of energy, water & hydrogen, CANMET Energy Technology Centre-Varennes, available at http://cetc-varennes.nrcan.gc.ca/fichier.php/codectec/En/2003-140/2003-140e.pdf

Ogawa, M., Nishihara, T., 2004. Present status of energy in Japan and HTTR project. Nuclear Engineering and Design 233, 5-10.

Ohya, H., Nakajima, H., Togami, N., Aihara, M., Negishi, Y., 1994. Separation of hydrogen from thermochemical processes using zirconia-silica composite membrane. International Journal of Hydrogen Energy 97, 91-98.

Ohya, H., Nakajima, H., Togami, N., Ohashi, H., Aihara, M., Tanisho, S., Negishi, Y., 1997. Hydrogen purification using zirconia-silica composite membranes for thermochemical process. International Journal of Hydrogen Energy 22, 509-515.

Ohta, T., ed., 1979. *Solar-Hydrogen Energy Systems*, Oxford and New York, Pergamon Press.

Onuki, K., Inagaki, Y., Hino, R., Tachibana, Y., 2005. Research and development on nuclear hydrogen production using HTGR at JAERI. Progress in Nuclear Energy 47, 496-503.

Riis, T., Hagen, E. F., Vie, P. J. S., Ulleberg, O., 2006. Hydrogen production R&D: priorities and gaps. International Energy Agency (IEA).

Rosen, M. A., 1996. Thermodynamic comparison of hydrogen production process. International Journal of Hydrogen Energy 21, 349-365.

Sakurai, M., Aihara, M., Miyake, N., Tsutsumi, A., Yoshida, K., 1992. Test of one-loop flow scheme for the UT-3 thermochemical hydrogen production process. International Journal of Hydrogen Energy 17, 587-592.

Sakurai, M., Tsutsumi, A., Yoshida, K., 1995. Improvement of Ca-pellet reactivity in UT-3 thermo-chemical hydrogen production cycle. International Journal of Hydrogen Energy 20, 297-301.

Sakurai, M., Bilgen, E., Tsutsumi, A., Yoshida, K., 1996a. Adiabatic UT-3 thermochemical process for hydrogen production. International Journal of Hydrogen Energy 21, 865-870.

Sakurai, M., Bilgen, E., Tsutsumi, A., Yoshida, K., 1996b. Solar UT-3 thermochemical cycle for hydrogen production. Solar Energy 57, 51-58.

Sakurai, M., Ogiwara, J., Kameyama, H., 2006. Reactivity improvement of Fe-compounds for the UT-3 thermochemical hydrogen production process. Journal of Chemical Engineering of Japan 39, 553-558.

Satrio, J. A., Shanks, B. H., Wheelock, T. D., 2004. Application of combined catalyst/sorbent on hydrogen generation from biomass gasification. AIChE Annual Meeting Conference Proceedings, November 7-12, Austin, TX.

Satrio, J. A., Shanks, B. H., Wheelock, T. D., 2005. Development of a novel combined catalyst and sorbent for hydrocarbon reforming. Industrial & Engineering Chemistry Research 44, 3901-3911.

Satrio, J. A.,Shanks, B. H., Wheelock, T. D., 2007. A combined catalysis and sorbent for enhancing hydrogen production from coal or biomass. Energy & Fuels 21, 322-326.

Shimizu, T., Hirama, T., Hosoda, H., Kitano, K., Inagaki, M., Tejima, K., 1999. A twin fluid-bed reactor for removal of CO_2 from combustion processes. Trans. IChemE 77 (Part A), 62-68.

Simpson, M. F., Utgikar, V., Sachdev, P., McGrady, C., 2007. A novel method for producing hydrogen based on the Ca–Br cycle. International Journal of Hydrogen Energy 32, 505-509.

Silaban, A., Harrison, D. P., 1995. High temperature capture of carbon dioxide: Characteristics of the reversible reaction between CaO(s) and CO_2(g). Chem. Eng. Comm. 137, 177-190.

Silaban, A., Narcida, M., Harrison, D. P., 1996. Characteristics of the reversible reaction between CO_2(g) and calcined dolomite. Chem. Eng. Comm. 146, 149-162.

Słowinski, G., 2006. Some technical issues of zero-emission coal technology. International Journal of Hydrogen Energy 31, 1091-1102.

Spath, P. L., Mann, M. K., 2001. Life Cycle Assessment of Hydrogen Production via National Gas Steam Reforming. National Renewable Energy Laboratory.

Stanmore, B.R., Gilot, P., 2005. Review-calcination and carbonation of limestone during thermal cycling for CO_2 sequestration. Fuel Processing Technology 86, 1707-1743.

Steinfeld, A., 2002. Solar hydrogen production via a two-step water-splitting thermochemical cycle based on Zn/ZnO redox reactions. International Journal of Hydrogen Energy 27, 611-619.

Stiegel, G. J., Ramezan, M., 2006. Hydrogen from coal gasification: an economical pathway to a sustainable energy future. International Journal of Coal Geology 65, 173-190.

Teo, E. D., Brandon, N. P., Vos, E., Kramer, G. J., 2005. A critical pathway energy efficiency analysis of the thermochemical UT-3 cycle. International Journal of Hydrogen Energy 30, 559-564.

T-Raissi, A., 2005. Technoeconomic analysis of area II hydrogen production. DOE final report to U.S. DOE under DEFC3600GO10603.

U. S. DOE, 2002. A national Vision of america's transition to a hydrogen economy-to 2030 and beyond. United States Department of Energy, available at http://www1.eere.energy.gov/hydrogenandfuelcells/pdfs/vision_doc.pdf

Velzen, D. V., Langenkamp, H., Schütz, G., Lalonde, Flamm, D. J., Fiebelmann, P., 1980. Development and design of a continuous laboratory-scale plant for hydrogen production by the Mark-13 cycle. International Journal of Hydrogen Energy 5, 131-139.

Vitart, X., Carles, P., Anzieu, P., 2008. A general survey of the potential and main issues associated with the sulfur-iodine thermochemical cycle for hydrogen production using unclear heat. Progress in Nuclear Energy 50, 402-410.

Webber, M. E., 2007. The water intensity of the transitional hydrogen economy. Environmental Research Letters 2, 034007 (7pp).

Weidenkaff, A., Reller, A. W., Wokaun, A., Steinfeld, A., 2000. Thermogravimetric analysis of the ZnO/Zn water splitting cycle**.** Thermochimica Acta 359, 69-75.

Wendt, H., ed. 1990. *Electrochemical Hydrogen Technologies: Electrochemical Production and Combustion of Hydrogen*, Elsevier, Amsterdam.

Williams, L.O., 1975. Electrolysis of sea-water. *Hydrogen Energy* (T.N. Veziroglu, Ed.), Plenum, New York, 417–425.

Wu, S. F., Li, Q. H., Kim, J. N., Yi, K. B., 2008. Properties of a nano CaO/Al_2O_3 CO_2 sorbent. Ind. Eng. Chem. Res 47, 180-184.

Yoshida, K., Kameyama, H., Aochi, T., Nobue, M., Aihara, M., Amir, R., Kondo, H., Sato, T., Tadokoro, Y., Yamaguchi, T., Sakai, N., 1990. A simulation study of the UT-3 thermochemical hydrogen production process. International Journal of Hydrogen Energy 15, 171-178.

BIOGRAPHICAL SKETCH

Man Su Lee was born in 1974 in Gokseong, a small town in South Korea. He was raised primarily in Seoul, South Korea. He received his Bachelor of Engineering and Master of Engineering in mechanical engineering from Chung-Ang University, Seoul, South Korea, in 1997 and 1999, respectively. He worked for R&D Institute of Unisem, Osan, South Korea, as a development researcher for 3 years. Then he moved to Daewoo Electronics Co. and worked there for 2 years as a researcher. In August 2004 he enrolled in the doctoral program in mechanical engineering at University of Florida. He joined Dr. Goswami's Solar Energy and Energy Conservation Laboratory and has been working on the thermochemical hydrogen production and high temperature carbon dioxide capture. Upon graduation, he would like to pursue a career in the field of clean energy research.